ชั้นกั้นการแพร่ระหว่างโลหะฐานเซอร์โคเนียมสำหรับแพลเลเดียมเมมเบรนบนตัวรองรับเหล็กกล้าไร้สนิม

นางสาวมัสลิน โชติรัตน์

วิทยานิพนธ์นี้เป็นส่วนหนึ่งของการศึกษาตามหลักสูตรปริญญาวิทยาศาสตรมหาบัณฑิต
สาขาวิชาปิโตรเคมีและวิทยาศาสตร์พอลิเมอร์
คณะวิทยาศาสตร์ จุฬาลงกรณ์มหาวิทยาลัย
ปีการศึกษา 2552

Zr-BASED INTERMETALLIC DIFFUSION BARRIER FOR STAINLESS STEEL SUPPORTED PALLADIUM MEMBRANE

Ms. Maslin Chotirach

A Thesis Submitted in Partial Fulfillment of the Requirements
for the Degree of Master of Science Program in Petrochemistry and Polymer Science
Faculty of Science
Chulalongkorn University
Academic Year 2009

Thesis Title	Zr-BASED INTERMETALLIC DIFFUSION BARRIER FOR STAINLESS STEEL SUPPORTED PALLADIUM MEMBRANE
By	Miss Maslin Cotirach
Field of Study	Petrochemistry and Polymer Science
Thesis Advisor	Assistant Professor Korbratna Kriausakul, Ph.D.
Thesis Co-Advisor	Assistant Professor Sukkaneste Tungasmita, Ph.D.

Accepted by the Faculty of Science, Chulalongkorn University in Partial Fulfillment of the Requirements for the Master's Degree

…….. Dean of the Faculty of Science
(Professor Supot Hannongbua, Dr.rer.nat.)

THESIS COMMITTEE

…….. Chairman
(Associate Professor Supawan Tantayanon, Ph.D.)

…….. Thesis Advisor
(Assistant Professor Korbratna Kriausakul, Ph.D.)

…….. Thesis Co-Advisor
(Assistant Professor Sukkaneste Tungasmita, Ph.D.)

…….. Examiner
(Associate Professor Wimonrat Trakarnpruk, Ph.D.)

…….. External Examiner
(Karuna Tuchinda, Ph.D.)

มัสลิน โชติรัตน์ : ชั้นกั้นการแพร่ระหว่างโลหะฐานเซอร์โคเนียมสำหรับแพลเลเดียมเมมเบรนบนตัวรองรับเหล็กกล้าไร้สนิม. (ZR-BASED INTERMETALLIC DIFFUSION BARRIER FOR STAINLESS STEEL SUPPORTED PALLADIUM MEMBRANE) อ.ที่ปรึกษาวิทยานิพนธ์หลัก: ผศ.ดร.กอบรัตน์ เกรียวสกุล, อ.ที่ปรึกษาวิทยานิพนธ์ร่วม: ผศ.ดร.สุคคเณศ ตุงคะสมิต, 90 หน้า.

แพลเลเดียมเมมเบรน เตรียม โดยเทคนิคการเคลือบแบบไม่ใช้กระแสไฟฟ้าบนเหล็ก กล้าไร้สนิมที่มีชั้นกั้นการแพร่ระหว่างโลหะฐานเซอร์โคเนียมได้แก่ เซอร์โคเนียม เซอร์โคเนียมออกไซด์ และเซอร์โคเนียมไนไตรด์ ฟิล์มบางเซอร์โคเนียม เคลือบด้ว ยเทคนิคดีซีแมกนีตรอนสปัตเ ทอร์ริง ออกซิไดซ์ฟิล์มบางเซอร์โคเนียมในอากาศ ที่อุณหภูมิ 500 องศาเซลเซียส เป็นเวลา 1 ชั่วโมงเพื่อให้ได้ฟิล์มบาง เซอร์โคเนียมออกไซด์ ฟิล์มบางเซอร์โคเนียมไนไตรด์ปลูกโดยเทคนิครีแอกทีฟ ดีซีแมกนีตรอนสปัตเทอร์ริงที่อัตราการไหลของไนโตรเจน 2 เอ็สซีซีเอ็ม เพื่อให้ได้องค์ประกอบ เชิงสตอยชิโอเมทรี พิสูจน์เอกลักษณ์ฟิล์มที่เตรียมได้ ได้แก่โครงสร้างของเฟส องค์ประกอบธาตุ และลักษณะของพื้นผิว ด้วยเทคนิคการเลี้ยวเบนรังสีเอ็กซ์ อีดีเอ็ส และ เอ็สอีเอ็ม ตามลำดับ ใช้ เอ็สอีเอ็ม-อีดีเอ็ส เพื่อตรวจสอบ ชั้นแพลเ ลเดียม เมมเบรนที่มีและไม่มีชั้นกั้นการแพร่ภายใต้บรรยากาศไฮโดรเจนที่ 400 ถึง 600 องศาเซลเซียสเป็นเวลา 24 ชั่วโมง พบว่า ชั้นกั้นการแพร่เซอร์โคเนียมออกไซด์มีประสิทธิภาพมากกว่าเซอร์โคเนียมไนไตรด์ และเซอร์โคเนียม ค่าการแพร่ผ่านของไฮโดรเจนที่ได้จากการใช้แพลเลเดียม เมมเบรนที่มีชั้นกั้นการแพร่มากกว่าแพลเลเดียมเมมเบรนที่ไม่มีชั้นกั้นการแพร่ โดยที่มีค่าเพิ่มขึ้นดังนี้ เซอร์โคเนียม หนา 0.5 ไมโครเมตร < เซอร์โคเนียม ไนไตรด์หนา 0.5 ไมโครเมตร < เซอร์โคเนียมออกไซด์ หนา 0.17 ไมโครเมตร < เซอร์โคเนียมออกไซด์ หนา 0.5 ไมโครเมตร ดังนั้นฟิล์มบางเซอร์โคเนียมออกไซด์เป็นชั้นกั้นการแพร่ระหว่างโลหะที่เหมาะสมที่สุด เนื่องจากไม่เพียงแต่ป้องกันการแพร่ของโลหะเข้าไปในชั้นแพเลเดียมเมมเบรนเท่านั้น แต่ยังให้ค่าการแพร่ผ่านของไฮโดรเจนที่สูงอีกด้วย

สาขาวิชา ปิโตรเคมีและวิทยาศาสตร์พอลิเมอร์ ลายมือชื่อนิสิต .....

ปีการศึกษา 2552 ลายมือชื่ออ.ที่ปรึกษาวิทยานิพนธ์หลัก .....

ลายมือชื่ออ.ที่ปรึกษาวิทยานิพนธ์ร่วม .....

5072426023 : MAJOR PETROCHEMISTRY AND POLYMER SCIENCE
KEY WORDS : PALLADIUM MEMBRANE/ INTERMETALLIC DIFFUSION/ ZIRCONIUM/ ZIRCONIUM OXIDE/ ZIRCONIUM NITRIDE

MASLIN CHOTIRACH: ZR-BASED INTERMETALLIC DIFFUSION BARRIER FOR STAINLESS STEEL SUPPORTED PALLADIUM MEMBRANE. THESIS ADVISOR: ASST. PROF. KORBRATNA KRIAUSAKUL, Ph.D., THESIS CO-ADVISOR: ASST. PROF. SUKKANESTE TUNGASMITA, Ph.D., 90 pp.

Electroless-plated palladium membranes were prepared on 316L stainless steel supports with Zr-based intermetallic diffusion barriers, i.e., Zr, ZrO_2 and ZrN. A dc magnetron sputtering method was used to deposit Zr films. The ZrO_2 thin films were obtained from oxidation of Zr thin films in air at 500°C for 1 hour. The ZrN thin films were grown by dc reactive magnetron sputtering at nitrogen flow rate of 2 sccm to obtain stoichiometric composition. The prepared films were characterized by XRD, EDS and SEM for phase structure, elemental composition, and surface morphology, respectively. SEM-EDS line scan was used to investigate palladium membranes with and without the diffusion barriers under hydrogen atmosphere at 400-600°C for 24 hours. It was found that ZrO_2 intermetallic diffusion barrier was more effective than ZrN and Zr. The hydrogen permeation flux obtained from palladium membranes with the diffusion barriers was higher than that without, with increasing order, Zr 0.5 μm < ZrN 0.5 μm < ZrO_2 0.17 μm < ZrO_2 0.5 μm. Thus, ZrO_2 thin film is the most suitable intermetallic diffusion barrier due not only to prevent the metal migration into palladium membranes but also giving high hydrogen permeance.

Field of Study : Petrochemistry and Polymer Science Student's Signature .....
Academic Year: 2009 Advisor's Signature .....
Co-Advisor's Signature .....

ACKNOWLEDGEMENTS

I would like to express my greatest gratitude and sincere thank to my advisor, Assistant Professor Dr. Korbratna Kriausakul and Assistant Professor Sukkaneste Tungasmita, for guidance, supervision and helpful suggestion throughout this research. I am also grateful to Associate Professor Dr. Supawan Tantayanon, Associate Professor Dr. Wimonrat Trakarnpruk, and Dr. Kaurna Tuchinda for serving as chairman and members of thesis committee, respectively and for their comments and suggestions.

This work cannot be completed without kindness and helps of many people. I would like to thank Dr.Pongpan Jindaudom and Dr.Noppadon Nuntawong for giving a big opportunity to the use of sputter equipment in Photonic Technology Laboratory (PTL), which is supported by the National Electronics and Computer Technology Center (NECTEC), Thailand. Special thank to Dr.Mati Horprathum, Dr. Pitak Eiamchai, Mr.Viyapol Patthanasettakul, Mr.Yongyut Inritsapong and Mrs. Puenisara Limnonthakul for their help and suggestion in the growth of films. I also thank Mr. Sathaporn Janhom and Mr.Taveesak Janduang for all help with the instrument and machinery.

I would like to extend my deepest gratitude to Mrs. Thitinat Sukonkate for her help and guidance throughout this work. Many thanks are going to my friends and colleagues for their friendship and encouragement. I gratefully acknowledge the materials support from Bangkok Industrial Gas Co., Ltd. and funding support from Program of Petrochemistry and Polymer Science, and National Center of Excellence for Petroleum, Petrochemicals, and Advanced Materials (NCE-PPAM).

Finally, I would like to express my gratitude to my family for their love, understanding, encouragement and great support throughout my study.

CONTENTS

PAGE

PAGE

LIST OF TABLES

LIST OF FIGURE

FIGURE PAGE

FIGURE PAGE

FIGURE PAGE

LIST OF ABBREVIATIONS

°C	: Degree Celsius
cm	: Centimeter
min	: minute
h	: Hour
l	: Liter
ml	: Milliliter
nm	: Nanometer
µm	: Micrometer

CHAPTER I

INTRODUCTION

1.1 Introduction

In recent years, the demand for hydrogen as clean energy has increased rapidly due to its basic role in many industrial processes. Hydrogen is mainly used in the petrochemical industry and a small amount in fuel cell operation. Approximately 80 percent of industrial hydrogen is generated from natural gas and other hydrocarbons through steam reforming, dry reforming, partial oxidation, gasification and hydrolysis. Hydrogen purification is an essential step in industrial hydrogen production. Palladium-based membranes have a potential to be used in hydrogen separation and membrane reactor applications because of their high hydrogen permeability and chemical resistance. In general, palladium membrane is prepared by electroless plating technique on a porous substrate such as porous stainless steel, ceramic and vycor glass.

Porous stainless steel (PSS) is usually adopted as a support for palladium membrane due to its better mechanical strength, resistance to cracking, ease of sealing and module fabrication [1]. However, when porous stainless steel supports were used at temperatures above 400°C, interdiffusion of atomic metals between palladium-based membranes and substrate materials occurred [2]. The important factor of intermetallic diffusion between palladium membranes and integral element of porous stainless steel supports is Tamman temperature. The Tamman temperature is temperature of a metal which equals to one half of its melting point and the temperature at or above which its atomic vibration starts to be considerable. If the temperature was increased to 650°C or 923 K, a temperature higher than the Tamman temperature of 316 L stainless steel (550–560°C 833K) and palladium (640°C or 913 K), intermetallic diffusion significantly took place with an apparent and continuous

decline of hydrogen permeance, poor-selectivity and shorter-life palladium membrane. [3] Nonetheless, intermetallic diffusion could be prevented by using a barrier to avoid direct contact of the palladium membranes with the stainless steel supports. The intermediate layer serving as a diffusion barrier is required to have the Tamman temperature higher than those of palladium membranes and stainless steel supports, good mechanical and thermal stabilities, good adhesion and allowing hydrogen transports.

In this work, Zr-based thin films were prepared and used as intermetallic diffusion barriers owing to their prominent properties such as higher Tamman temperature than those of palladium membranes and stainless steel supports (i.e., Tamman temperatures of zirconium, zirconium oxide, and zirconium nitride are 927°C (1200 K), 1350°C (1623 K), and 1491°C (1764 K), respectively), good thermal stability, corrosion resistance, compatible thermal expansion coefficient to palladium membranes and the stainless steel support [2] (i.e., palladium, 1.20 x 10^{-5}; 316L, 1.73 x 10^{-5}; Zr, 2.35 x 10^{-5}; ZrO_2, 1.0 x 10^{-5}, and ZrN 1.98 x 10^{-5} K^{-1}), high hydrogen permeability [4] and its access ability with low costs.

1.2 Objectives of the Research Work

This study aims to develop suitable conditions for the preparation of Zr-based intermetallic diffusion barriers for the palladium membranes on the stainless steel support and determine their efficiencies in reducing the intermetallic diffusion for the use of palladium membranes in hydrogen permeation.

1.3 Scope of the Research Work

1. Develop suitable conditions for the preparation of Zr-based intermetallic diffusion barriers, i.e. Zr, ZrO_2 and ZrN by sputter deposition technique.

2. Prepare the palladium membranes on the stainless steel substrate coated with Zr-based intermetallic diffusion barriers.

3. Determine the efficiencies in reducing intermetallic diffusion of the Zr-based intermetallic diffusion barriers for palladium membranes.

4. Test the capacity of hydrogen permeation through the palladium membranes with Zr-based intermetallic diffusion barriers.

CHAPTER II

THEORY AND LITERATURE REVIEWS

2.1 Palladium Membranes

Recently many efforts in hydrogen separation for fuel cell application have been devoted to development of pure palladium and Pd-alloyed composite membrane.[5] Palladium holds a unique position among the metallic elements in being able to take into solution large quantities of hydrogen while simultaneously retaining a high degree of ductility. These attributes coupled with the high mobility or rate of diffusion of hydrogen in the lattice have been exploited in the use of palladium and subsequently of palladium based alloys as hydrogen diffusion membranes.

Palladium membrane hydrogen purifiers operate via pressure driven diffusion across palladium membranes as shown in Figure 2.1. Only hydrogen can diffuse through palladium membrane. The hydrogen gas molecule coming into contact with the palladium membrane surface, then dissociates into hydrogen atoms and diffuses through the membrane. On the other surface of the palladium membrane, the hydrogen atoms are recombined into molecular hydrogen to produce the ultrapure hydrogen as shown in the following equation.

$$H_2 \text{ (gas)} \rightleftharpoons 2H \text{ (surface)} \quad [6] \qquad (2.1)$$

The hydrogen permeation process is influenced by the surface topography, the purity of the metal and its defect structure (e.g., grain boundaries and dislocations). [7]. Pure palladium has mainly been restricted because of phase transition from α to β form. The phase transition occurs generally at temperatures below 300°C and pressure below 2×10^6 Pa, depending on the hydrogen concentration in the metal. Since the lattice constant of the β-phase is larger than that of the α-phase, the phase transition

leads to lattice strain and distortion of the metal lattice, known as embrittlement. Thus, it is necessary to operate a pure palladium membrane at temperature above 300°C to avoid this phenomenon. In order to minimize the hydrogen embrittlement problem, alloying palladium with other metal such as Ag or Cu will lower the critical temperature for the phase transformation.

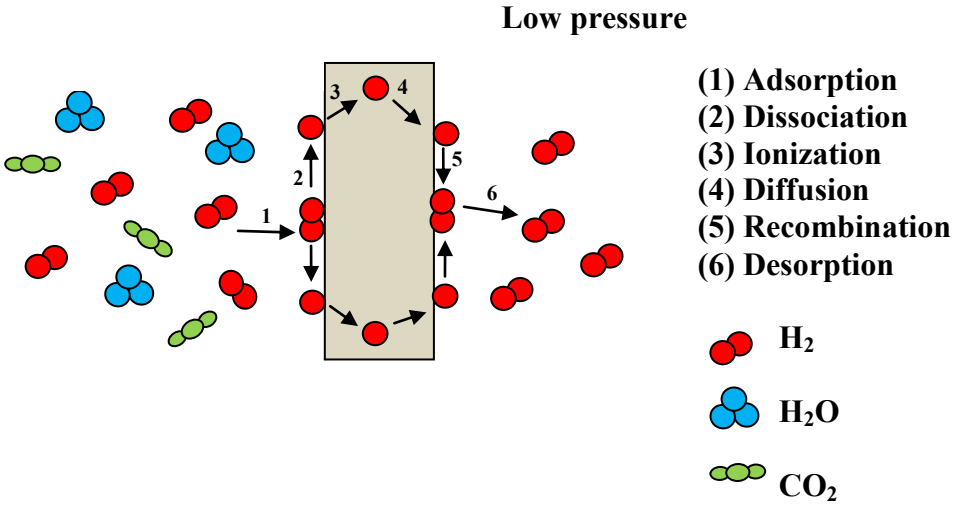

Figure 2.1 Schematic hydrogen permeation in palladium membranes. [8]

Assuming that the rate limiting step of hydrogen permeation is controlled by the hydrogen diffusion through the bulk palladium layer, the hydrogen flux can be expressed by the Fick's first law,

$$J = -D\frac{dc}{dl} = \frac{D}{l}(C_{HP} - C_{LP}) \quad [7] \qquad (2.2)$$

In equation 2.2, J is the hydrogen permeation flux, $m^3/m^2.s$ or $mol/m^2.s^{-1}$. D is the diffusivity of the hydrogen in the palladium membrane (m^2/s^1). l is the thickness of the membrane (m). C is the hydrogen concentrations. Subscripts HP and LP designate the high and low pressure sides of the membrane (mol/m^3). The hydrogen concentrations can be expressed as,

$$C = k\eta \quad [9] \tag{2.3}$$

where k is the hydrogen concentration constant (mol/m^3) and η is the atomic *H/Pd* ratio. At very low concentrations of hydrogen, η is linearly dependent on the square root of the partial pressure of hydrogen, $C = kp^{1/2}$, a good approximation outside the immiscibility region. Equation 2.1 then reduces to

$$J = \frac{kD}{l}(P_{HP}^{1/2} - P_{LP}^{1/2}) \quad [6] \tag{2.4}$$

Both k and D are functions of temperature and kD is the permeability. It is often difficult to accurately determine the membrane thickness (l). P = kD/l (k.mole/m^{2}s.Pa$^{1/2}$) defined as the permeance is frequently used. However, the exponent of the pressure is not 1/2 due to factors such as the non-linearity of the $P^{1/2}$-C isotherm, surface reaction and existence of significant mass transfer resistances and diffusion through the palladium bulk. Therefore, Equation 2.4 can be expressed in a general form as,

$$J = P(P_{HP}^{n} - P_{LP}^{n}) \quad [6] \tag{2.5}$$

where $1 \geq n \leq 1/2$, For the Sieverts' law, n = 1/2.

2.2 Diffusion in Solids

Diffusion is the phenomenon of material transport by atomic motion. The atoms move from one lattice site to another in a stepwise manner. Two conditions are to be met: first, an empty adjacent site and second, sufficient energy to break bonds and cause lattice distortions during displacement. If two pieces of different metals are joined together for example, Cu and Ni in Figure 2.2, which illustrates the schematic atom positions and composition across the interface when the Cu/Ni composite is heated for a long time (but below their melting points). The results

indicated that Cu atoms have migrated or diffused into Ni, and that Ni has diffused into Cu.

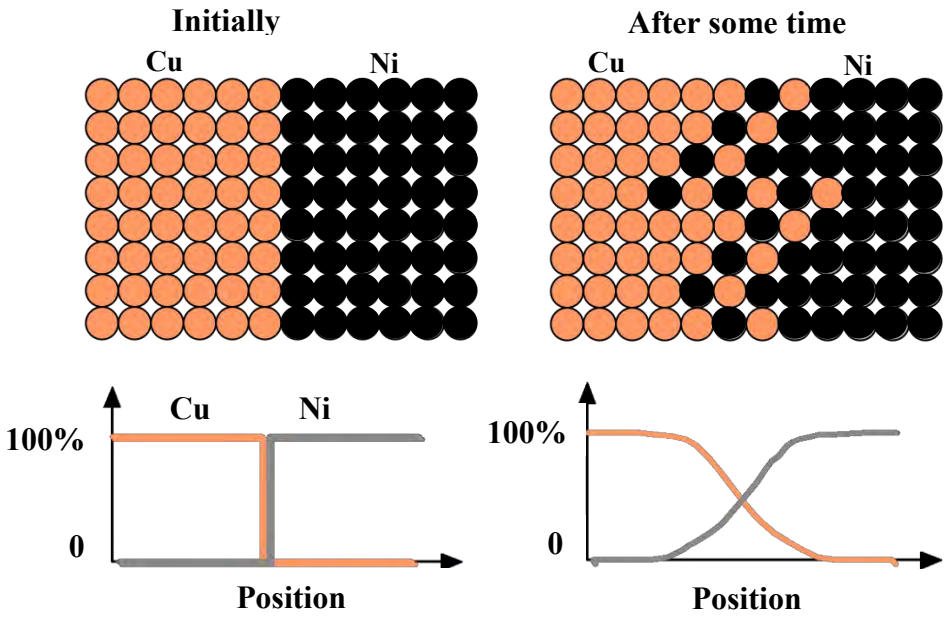

Figure 2.2 Cu-Ni diffusion before and after a high temperature heat treatment. [10]

2.2.1 Mechanisms of diffusion

One type of diffusion involves the exchange of an atom from its normal lattice position to an adjacent vacant lattice site or vacancy. This is known as "substitutional" or "vacancy diffusion" as shown in Figure 2.3. This process requires the presence of vacancies, and vacancy diffusion depends on the extent of vacancies in the material.

The second type of diffusion involves atoms that migrate from an "interstitial" or "in-between" position to a neighboring one that is empty. This occurs with the infusion of impurities such as hydrogen or carbon, which have atoms that are small enough to fit into the interstitial positions as shown in Figure 2.4. Typically, interstitial diffusion is much faster than vacancy diffusion.

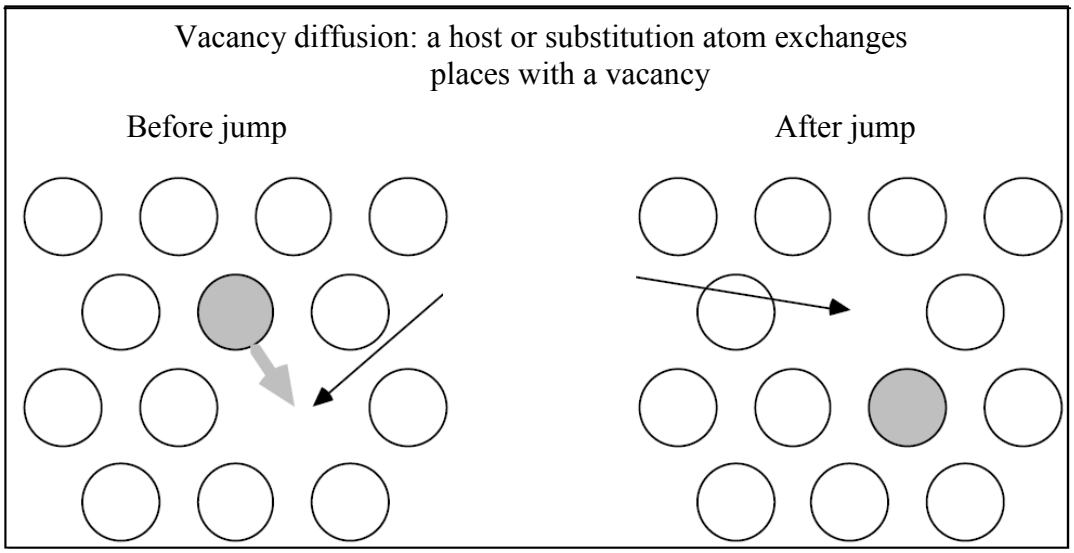

Figure 2.3 Schematic illustration of vacancy diffusion. [11]

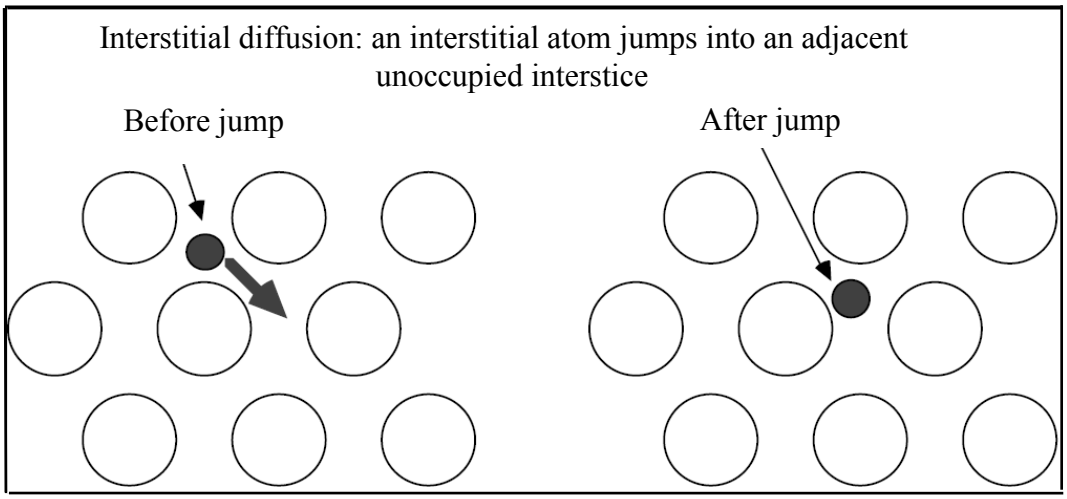

Figure 2.4 Schematic illustration of interstitial diffusion. [11]

2.2.2 Steady-state diffusion

Diffusion is a time-dependent process; the quantity of an element that is transported within another is a function of time. It is necessary to know how fast it occurs, or the rate of mass transfer. This rate is known as the diffusion flux (J) and is defined as the mass (M) diffusing through a unit cross-sectional area of solid per unit of time. This may be represented as [12],

$$J = \frac{M}{AT} \tag{2.6}$$

where A is the area across which diffusion is occurring, and T is the elapsed diffusion time. In Figure 2.5, the diffusion flux (J_x) does not change with time, a steady state condition exists, and this is called “steady-state diffusion".

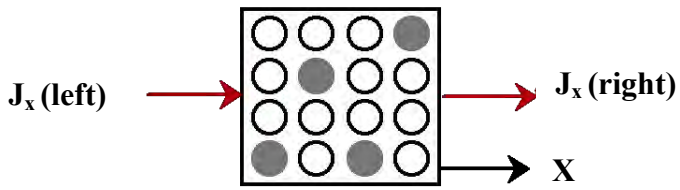

Figure 2.5 Schematic illustration of steady state diffusion. [12]

2.2.3 Non-steady state diffusion

Generally, most diffusion situations are non-steady state. The diffusion flux and concentration gradient varies with time. This is illustrated in Figure 2.6, which shows the concentration profiles at three different diffusion times, the following assumptions are,

- Atoms in the solid are uniformly distributed with the concentration of C_0 before diffusion.

- The value of x at the surface is zero and increases with the distance into the solid.
- Before the diffusion process begins, the time is taken to be zero.

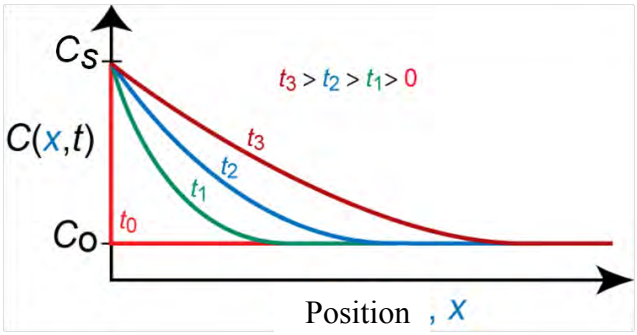

Fig. 2.6 Concentration profiles for nonsteady-state diffusion taken at three different times. [13]

This means that the last equation we used is no longer valid. In these situations an equation known as Fick's First Law is used. The law states that the rate of diffusion, or flux (J) of a species is proportional to the concentration gradient, $\partial C/\partial x$:

$$J = -D\frac{\partial C}{\partial X} \quad [11] \qquad (2.7)$$

where D is the diffusivity or coefficient of diffusion. For atomic diffusion the units are,

J (atoms $m^{-2}s^{-1}$)

D (m^2s^{-1})

$\partial C/\partial x$ (atoms m^{-4})

and the Fick's second Law is used [11]:

$$\frac{\partial C}{\partial t} = D\frac{\partial^2 C}{\partial x^2} \qquad (2.8)$$

2.3 Zr-based Intermetallic Diffusion Barriers

2.3.1 Zirconium

Zirconium (Zr) is a transition metal that resembles titanium. It has two stable crystal structures, hexagonal at T < 860°C and body-centered cubic at T > 860°C. These two structures are shown in Figure 2.7. The melting point of zirconium is 1,855°C [14]. Zirconium can easily react with oxygen forming a thin coating of zirconium oxide on its surface [15]. This coating protects the metal from further oxidation because zirconium is an excellent resistance to corrosion by acids and other chemicals. Due to its resistant quality, Zr is typically used as an alloying agent in materials which are exposed to corrosive agents i.e., surgical appliances, filaments and explosive primers.

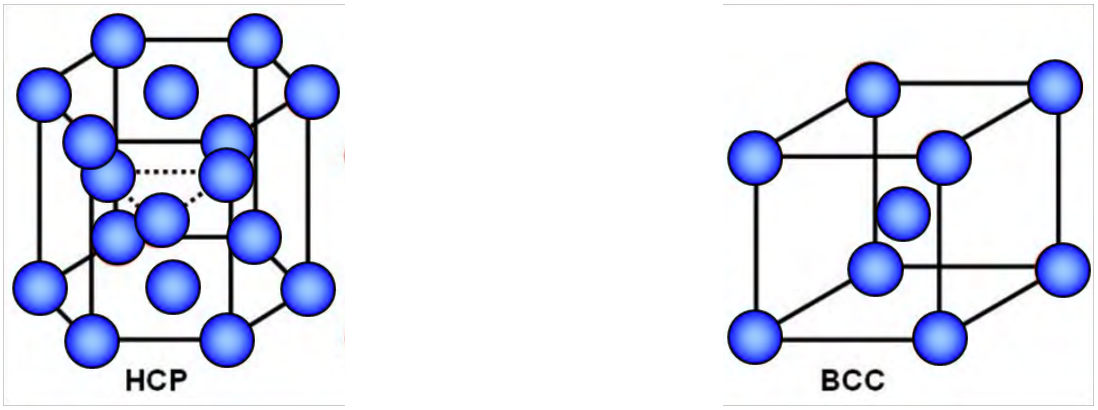

Figure 2.7 Schematic Zr crystal structures (a) hexagonal and (b) body-centered cubic. [16]

2.3.2 Zirconium oxide (ZrO_2)

Zirconium oxide (ZrO_2) has a monoclinic crystal structure at room temperature and undergoes transition to tetragonal and cubic at increasing temperatures. These three structures are shown in Figure 2.8. [17] It has a high melting point of 2700° C.

Zirconia films exhibit low thermal conductivity, relatively high dielectric constant, high refractive index, high transparency in the visible and near-infrared region [18], extreme chemical inertness, and a high laser damage threshold. It has been used in a variety of applications, such as: thermal barrier coatings, optical filters, laser mirrors, and alternative gate dielectrics in microelectronics [19]. Moreover, the stabilized cubic zirconia is a good oxygen conductor and has been used for high temperature oxygen separation, oxygen sensors, and fuel cells.

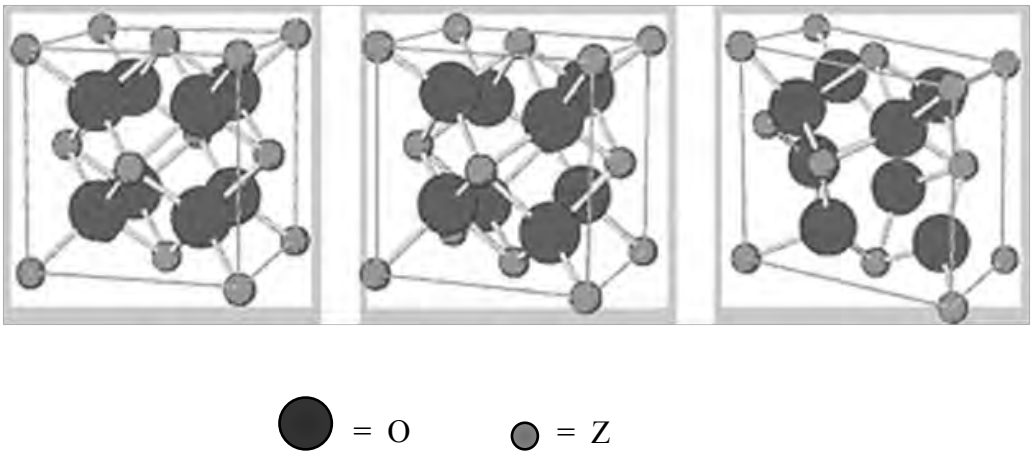

Figure 2.8 Schematic ZrO_2 crystal structures (a) cubic (b) tetragonal and (c) monoclinic. [20]

2.3.3 Zirconium nitride (ZrN)

Zirconium nitride belongs to the fourth-column transition metal mononitride, which includes titanium and hafnium nitride. The only stable compound is ZrN of NaCl structure and stoichiometric ratio of nearly 1:1 with gold-like color. The crystal structure is shown in Figure 2.9. [21] It has various applications such as hard coating, diffusion barriers in semiconductor technology, decorative coatings and protective coatings in cutting tools due to its excellent properties such as high hardness, chemical stability, thermal stability and high melting point of 2982°C [22].

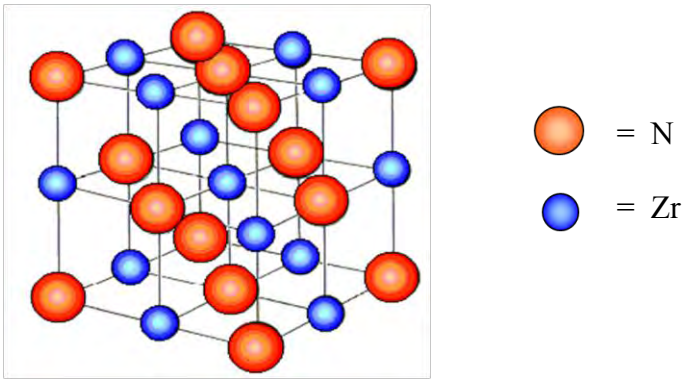

Figure 2.9 Schematic NaCl type structure of ZrN. [23]

2.4 Deposition Techniques

2.4.1 Sputter deposition technique

Sputtering is one of the commonly utilized depositions of thin films. It is a physical vapor deposition where material is physically removed by energetic ion bombardment. If the bombarding energy overcomes the surface binding energy, the material atoms are ejected to form a film on a substrate. There are simply energy and momentum exchange between ions and atoms of materials.

2.4.2 Dc magnetron sputtering

Direct current (dc) sputtering has become a preferred method for metal deposition. It provides high deposition rate and uniform coverage. A typical dc magnetron sputtering system is shown in Figure 2.10. In the operation, target is termed as the source of coating material, connected to the negative side of the direct current power supply, referred to as the cathode. The target is mounted opposite the substrate in a vacuum chamber which is evacuated to low base pressure and then energetic particle or sputtering gas, typically Ar gas is introduced into the chamber. To initiate positive ion bombardment, a negative potential is applied to the target while the substrate is grounded and Ar gas is continued to flow to establish a glow

discharge. [24] When the ions collide with surface of the target, the phenomena in Figure 2.11 may occur.

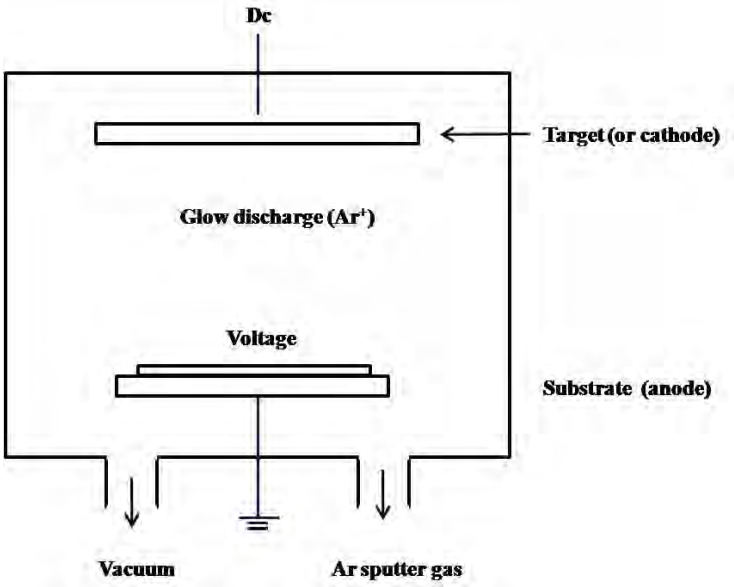

Figure 2.10 Basic features of a dc sputter deposition system. [25]

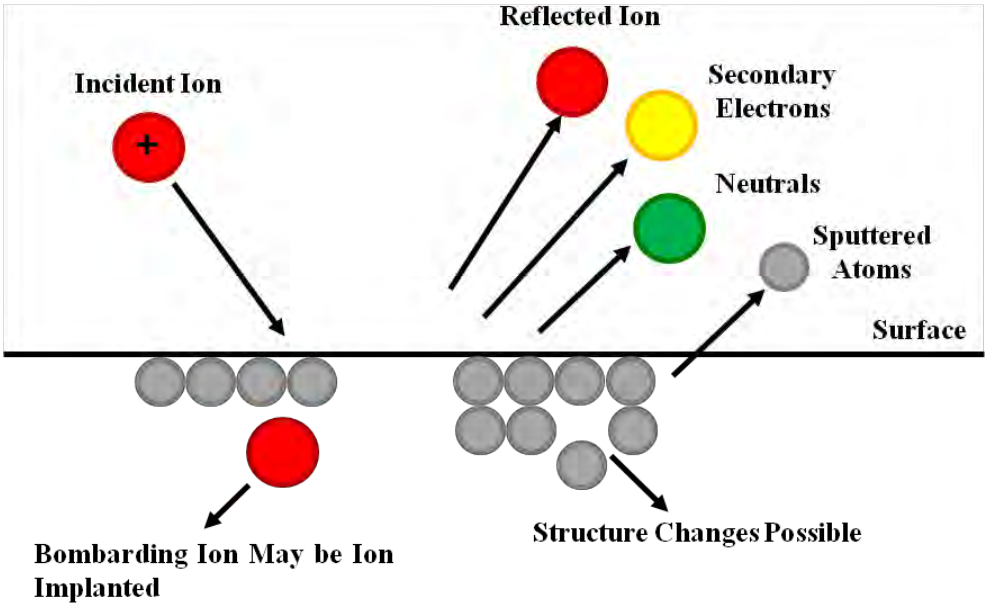

Figure 2.11 Interactions of ions with surfaces. [26]

a) The ion may be reflected, probably being neutralized in the process.

b) The impact of the ions may cause the target to eject an electron, usually referred to as a secondary electron.

c) The ion may become buried in the target. This is the phenomenon of ion implantation.

d) The ion impact may also be responsible for some structural rearrangements in the target material.

e) The ion impact may set up a series of collisions between atoms of the target, possibly leading to the ejection of one of these atoms. [26]

The average number of the atoms ejected from the surface per incident ion is called the sputtering yield (S). It depends on many factors, such as the mass and the energy of the incident particles, the mass and the binding energy of the sputtered atoms, the crystallinity of the target, etc.

To increase the ionization rate even further by emission of secondary electrons, a ring magnet below the target is used in the dc magnetron sputtering. The electrons in its field are trapped in cycloids and circulate over the targets surface. By the longer dwell time in the gas, they cause a higher ionization probability and hence form a plasma ignition at pressures, which can be up to one hundred times smaller than for conventional sputtering. On the other hand, less collision occurs for the sputtered material on the way to the substrate because of the lower pressure and hence the kinetic energy at the impact on the substrate is higher. The electron density resulted in the number highest of generated ions, where the magnetic field is parallel to the substrate surface. The highest sputter yield happens on the target area right below this region. An erosion zone is formed which follows the form of the magnetic field. The bombardment of a non-conducting target with positive ions would lead to charging of the surface and subsequently to a shielding of the electrical field. The ion current would die off. [24] Therefore, the dc-sputtering is restricted to conducting materials like metals or doped semiconductors.

2.4.3 Reactive sputtering

Reactive sputtering is the method in which thin films of compounds are deposited on substrates by sputtering from metallic targets using both the inert working gas and a reactive gas. The sputtering gases are required to be able to form such a film. Generally, a mixture between an inert gas and a reactive gas, such as N_2, O_2 and H_2S, can be used in the process. [27] The reactive gas could combine with the metal by chemical reactions in three ways (a) at the surface of the target, (b) in the space between the target and the substrate or (c) on the surface of the substrate, as shown in Figure 2.12.

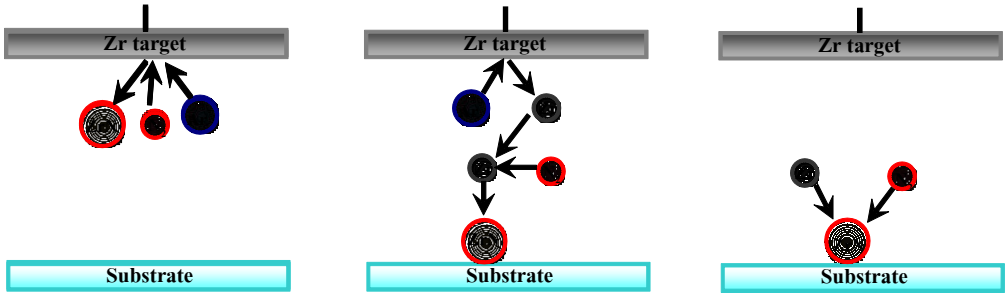

Figure 2.12 Three mechanisms for reactive sputter deposition: (a) at the target, (b) in the plasma volume, and (c) at the substrate.

The first mechanism gives the possibility to alter compound stoichiometry in sputtering from a compound target or to deposit a compound film from a metallic target. A typical behavior of reactive sputtering upon increasing the content of reactive gas in the gas mixture is the increasing compound coverage of the active target surface. The compound material on the surface is then sputtered away from the surface instead of the pure metal. This will change the deposition process and require an optimization of the process parameters since the compound usually have low sputtering rate.

2.4.4 Electroless plating

Electroless plating is a chemical reduction process in an aqueous solution, also known as chemical or auto-catalytic plating. Electroless deposition differs from electrolytic deposition in that no external supply of electrons (such as from a rectifier) are required. Electrolytic deposition requires the use of an externally connected DC rectifier, which supplies electrons for metal reduction at the cathode surface. Electroless deposition utilizes a chemical reducing agent that supplies electrons for metal deposition at a catalytic surface. The method consists of the spontaneous reduction of a metal (for example copper or silver) from a solution of its salt, e.g. Cu(II) or Ag(I). A reducing agent, a chemical which acts as the source of the electrons is required. The electroless deposition is particularly useful because a surface that clearly acts as a catalyst to allow the deposition to proceed is also necessary. This means that deposition is specific and, to some extent, can be controlled. The technique is used to deposit metallic coatings on various types of surface. The advantages of electroless plating are uniformity of the deposits, even on complex shapes. The most common electroless plating method is electroless nickel plating.

2.5 Characterization of Thin Films

2.5.1 X-Ray Diffraction (XRD)

X-ray diffraction (XRD) techniques are well developed for the characterization of crystallinity in materials such as metals, ceramics, polymers and other inorganic and organic compounds. This method reveals a sample's crystallinity through characteristic interference patterns obtained from the phase difference between the X-ray photons scattered at each individual lattice plane. The position, shape and intensity of these reflection peaks provide detailed information about the structural properties of the sample on an atomic scale. Figure 2.13 shows the condition for constructive interference from two parallel beams diffracted elastically by parallel crystal planes with distance d_{hkl} apart and is given by [28]

$$n\lambda = 2d\sin\theta \tag{2.8}$$

where θ is the angle of the lattice planes with respect to the incident X-ray beam of wavelength λ. Equation 2.8 is referred as Bragg's equation after W.L. Bragg. Thus, only planes parallel to the thin film surface can be detected. In order to detect a family of crystal planes (hkl), the line perpendicular to them and the incident and reflected X-ray beams must be on the same plane, thus satisfying equation (2.9) for cubic crystal structure. Therefore, θ is the experimental diffraction angle and d is the distance between the planes of the (hkl) family. Specifically, the d-spacing can be found from the relation [28],

$$d_{hkl} = \frac{a}{\sqrt{\left(h^2 + k^2 + l^2\right)}} \tag{2.9}$$

where a is the lattice constant.

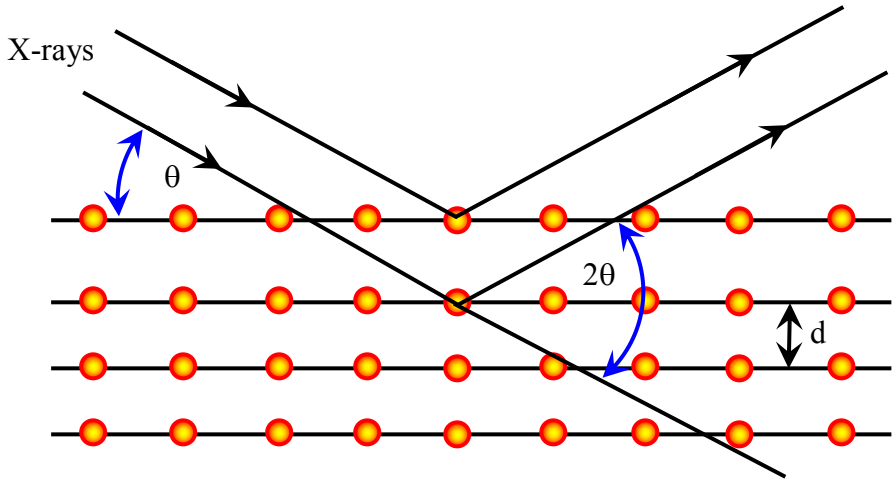

Figure 2.13 A schematic representation of Bragg diffraction at crystal planes with inner planar spacing d_{hkl}. [28]

2.5.2 Scanning electron microscopy with energy dispersive x-ray analysis

Scanning Electron Microscopy (SEM) is a high resolution imaging microscopic technique that uses electrons instead of light to form an image. It has many advantages over traditional microscopes such as a large depth of field, which allows more of a specimen to be in focus at one time, higher resolution, so that closely spaced specimens can be magnified at much higher levels. All of these advantages, as well as the actual strikingly clear images, make the scanning electron microscope one of the most useful instruments in research today.

For analytical electron microscope, a solid specimen is bombarded in vacuum by a primary electron beam. Once the beam hits the sample and then creates various signals, for example, secondary electrons, backscattered electrons, transmitted electrons, X-rays and Auger electrons, as shown in Figure 2.14. Detectors collect these X-rays, backscattered electrons, and secondary electrons and convert them into a signal that is sent to a screen. This produces the final image.

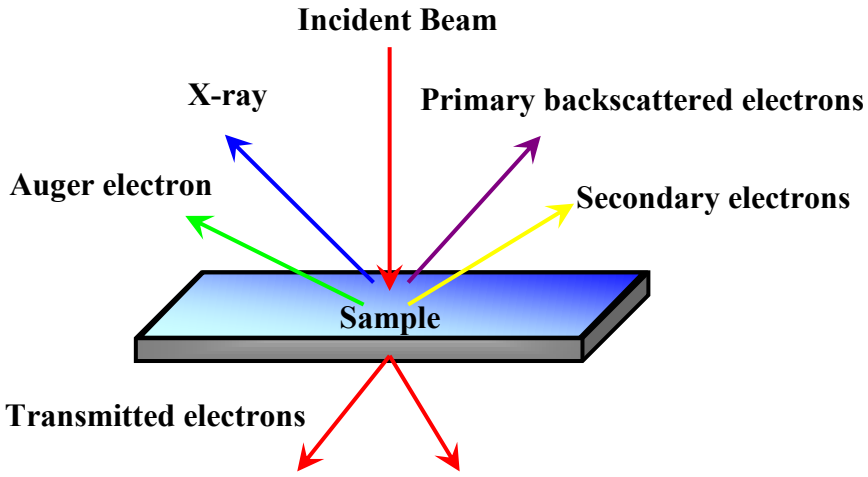

Figure 2.14 Photon and charged particle emission from an electron-bombarded surface. [29]

Energy dispersive X-ray analysis (EDS or EDX) is an analytical technique used to determine the composition of the specimens. EDS system works as an

integrated feature of the SEM technique which utilizes X-rays that are emitted from the specimen when bombarded by the electron beam.

During EDX analysis, the specimen is bombarded with an electron beam inside the SEM. Those electrons collide with the specimen's own electrons, knocking some of them from the atoms on the specimens' surface. A resulting electron vacancy is filled by an electron from a higher shell. When the electron is displaced, it gives up some of its energy by emitting an X-ray. Each element releases X-rays with unique amounts of energy during the transfer process. The EDS X-ray detector measures the relative abundance of emitted x-rays versus their energy.

2.6 Literature Survey

In 2007, Deshin Gan *et al*. [30] deposited nanocrystalline Zr thin films by radio frequency (rf) ion beam sputtering on the surface of NaCl single crystal slabs and glass substrate for subsequent annealing in air at 100, 150, 250, 350, 450, 500, and 750 ◦C for 1 h. The phases present were identified by Transmission electron mircroscopy (TEM) and the chemical composition was determined by Energy dispersive X-ray (EDX) analysis. The as-deposited films were nanometer-size (α-Zr+ZrO, α-Zr+ZrO, c-ZrO_2, c-ZrO_2, c-+t-ZrO_2, t-ZrO_2, and t-+m-ZrO_2) assemblages and the optimized temperature for the formation of t-ZrO_2 is between 350 and 500 °C for 1 h in air. They indicated that the thin films had a drastic change from dark to opal translucent color when annealing temperature was increased from 300 to 350 °C. When annealing above 350°C for 1 hour the film became translucent because oxygen deficient c-ZrO_2 undergoes transition to stoichiometric c- and/or t-ZrO_2.

In 2008, Lin *et al*. [31] prepared palladium membrane via electroless plating technique on porous stainless steel (PSS) disks with two intermediate layers. Metal oxide layer was formed by oxidizing the PSS surface and Yttria-stabilized zirconia (YSZ) layer was formed by sol-gel method. They reported that the effectiveness of intermediate layer to prevent intermetallic diffusion was a key factor for application of palladium membranes on PSS support. The results indicated that the PSS support

with oxide layer had a high permeation resistance and a rougher surface, leading to a thicker of palladium layer. Thus, palladium membrane on the PSS support with an oxide layer had lower hydrogen permeance than the YSZ layer. Both intermetallic diffusion barriers are effective at high temperature range of 773-873 K. At temperature above 873 K, only YSZ intermediate layer was effective in terms of preventing intermetallic diffusion and yielded a stable palladium membrane. While palladium membrane on PSS support with oxide layer was less effective due to the reduction of metal oxides in hydrogen ambient.

In 2008, Huang *et al*. [32] studied the effects of nitrogen flow rate on the microstructure, composition and electrical properties of ZrN_x. In their work, ZrN_x thin films were deposited onto Si wafer which coated with SiO_2 layer by DC magnetron sputtering from a Zr target (99.7%). The nitrogen flow rate was varied from 0 to 5 SCCM. The working pressure and a flow rate of Ar were maintained at 0.27 Pa and 40 SCCM, respectively. The substrate was not heated during the deposition process. The results indicated that the ZrN_x films were crystallized in NaCl type structure and showed near-stoichiometric composition at nitrogen flow rate of 3 SCCM. In addition, they found that the residual oxygen atoms in the ZrN_x films may possibly substitute the nitrogen atoms or occupy the interstitial positions in the ZrN lattice, causing the near-stoichiometric composition.

In 2006, Huang *et al*. [33] studied the effect of nitrogen flow rate (ranging from 5 to 35 SCCM) on the N/Zr ratio, structure and mechanical properties of the ZrN films. They found that the nitrogen flow rate had direct effects on N/Zr ratio, packing factor and grain size of the ZrN film. The N/Zr ratio and grain size increased with increasing nitrogen flow rate. The films were deposited on 304 stainless steel and Si substrate. Atomic force microscopy (AFM) indicated that the surface of the deposited film on 304 stainless steel substrate is rougher than that on the Si substrate. The 304 stainless steel substrate attracts more Zr ions than Si substrate, owing to higher electrical conductivity and surface rougher. This lead to higher deposition rate for the ZrN deposited film on 304 stainless steel.

In 2002, Takeyama *et al*. [34] prepared a thin nano-crystalline ZrN film using a thermally stable thin diffusion barrier in Cu/Si contacts. A ZrN layer was deposited onto Si(100) wafer by reactive sputtering of a Zr target in the mixture gas of Ar and (30%) N_2, and substrate temperature of 400°C. The Cu/ZrN/Si contacts with a 100 nm thick barrier tolerated annealing at 800°C for 1 h without structure change. The barrier was thermally stable at temperature up to 600°C or higher.

In 2006, Devia *et al*. [22] reported that thin films of TiN and ZrN were grown on 316L stainless steel substrate using the pulsed cathodic arc technique with different number of discharges (one to five discharges). The coatings were characterized in terms of crystalline structure, microstructure, elementary chemical composition and stoichiometry by X-ray diffraction (XRD), atomic force microscopy (AFM) and X-ray photoelectron spectroscopy for chemical analyses (XPS), respectively. The XRD results showed that for both TiN and ZrN, the preferential direction occurred in the (200) plane and this observation still remained even when the number of discharges was increased. The grain size was increased with increasing the number of discharges for both nitrides. The TiN film was rougher than the ZrN film. XPS analysis showed that there was higher percentage of nitrogen present in the ZrN film than in the TiN film.

In 2005, Lee *et al*. [35] fabricated pinhole-free Pd/Ni alloy composite membrane with a diffusion barrier on porous stainless steel supports by vacuum electrodeposition. To improve the structural stability of Pd alloy/Ni 316L stainless steel composite membrane, they prepared a thin intermediate layer of TiN by a sputtering method. The TiN thin film was introduced as a diffusion barrier between the Pd/Ni layer and stainless steel substrate. The results suggested that the Pd/Ni layer and alloy composite membrane with a diffusion barrier of TiN yielded a high separation performance for hydrogen and showed very good stability under the mixture gas of 50% H_2 and 50% N_2 for an operation time of more than 60 days.

In 2009, Zahedi *et al*. [36] prepared a palladium membrane by electroless plating on the surface of a porous stainless steel disk. They modified the disk surface with WO_3 to prevent metal penetration into palladium layer and obtain a membrane with nano-sized pores. The prepared membrane has very smooth, flat and dense with a thickness of about 12 μm. For hydrogen permeation behavior they measured the permeability at the temperatures of 723, 773 and 823 K. The composite membrane was found to be stable and yielded high hydrogen permeability at high temperature.

In 2005, Lin *et al*. [37] studied electoless plating synthesis of Pd-Cu alloy films on PSS support modified with palladium seeded ZrO_2 layer. This intermediate layer served as an intermetallic diffusion barrier that improved the membrane stability. For electroless plating process, they found that the excessive amount of hydrazine hydrate resulted in precipitation of a great deal of palladium powders in the plating bath. To prevent this phenomenon, several divided hydrazine hydrate batches was added into the plating bath during electroless plating. $Pd_{46}Cu_{54}/ZrO_2$ PSS composite membranes were found to exhibit no nitrogen permeation flux with H_2 permeation of 1.1 x 10^{-7} mol/m^2s Pa at 753 K.

CHAPTER III

EXPERIMENTAL

3.1 Materials, Equipments and Instruments

3.1.1 Materials

1. Porous and non-porous stainless steel grade 316L, Mott Corporation
2. Quartz wool, Alltech
3. Argon gas, 99.999%, Bangkok Industrial Gas
4. Nitrogen gas, 99.999%, Bangkok Industrial Gas
5. Helium gas, 99.99%, Bangkok Industrial Gas
6. Hydrogen gas 99.95% , Bangkok Industrial Gas
7. Zr-Target, Kurt J. Lesker

3.1.2 Chemicals

3.1.2.1 Chemicals for cleaning process

1. Detergent
2. Trichloroethylene (C_2HCl_3), Ajax Finechem
3. Iso-propanol (C_3H_7OH), Carlo Erba
4. Acetone ($OC(CH3)_2$), from J.T Baker

3.1.2.2 Chemicals for surface activation

1. Tin (II) chloride dehydrate ($SnCl_2.2H_2O$), 98% , Carlo Erba
2. Hydrocloric (HCl, 37% concentrated), JT. Baker
3. Palladium (II) chloride ($PdCl_2$), 99.9% , Alfa Aesar

3.1.2.3 Chemicals for electroless deposition

1. Tetra ammine palladium (II) chloride monohydrate ($Pd(NH_3)_4Cl_2.H2O$, (98%), Alfa Aesar
2. Disodium ethylenediaminetetraacetrate (Na_2EDTA), 99.5%, Carlo Erba
3. Hydrazine anhydrous (N_2H_4), 99.5% , Aldrich

3.1.3 Equipments

1. Furnace reactor, Lenton
2. Digital flow meter, Altech
3. Plasma sputtering chamber, in-house Photonic Technology Laboratory

3.1.4 Instruments

1. Scanning electron microscope (SEM), JEOL model JSM-5800LV with Energy Dispersive Spectrometer (EDS)
2. X-ray diffractometer (XRD), Bruker AXS, Germany Model D8 Advance

3.2 Experimental Procedures

3.2.1 Preparation of stainless steel supports

316L stainless steel sheets, 1cm x 1 cm x 0.1 cm, were used as support materials in this work, compose of (wt %): Fe 62.0-72.0%, Cr 16.0-18.0%, Ni 10.0-14.0% , Si 0.75%, Mn 2.0%, P 0.045%, S 0.03%, Mo 2.0-3.0% and N 0.10%. The supports were mechanical polished with silicon carbide papers and ultrasonically cleaned in 25 ml of trichloroethylene (TCE), acetone, isopropanol and DI water, respectively. Then, the supports were blow dried before positioned into a vacuum chamber.

3.2.2 Preparation of intermetallic diffusion barriers

High purity Zr disk with 3 inch diameter was used as a target to deposit Zr and ZrN thin films on 316L stainless steel supports by dc magnetron sputter deposition. Before deposition, the chamber was evacuated to low base pressure by a turbomolecular pump to avoid contamination during deposition process. The distance between target and substrate was 7 cm for both films. The supports were pre-sputtered in order to remove the oxide layer on the surface before growing films. The deposition was done at room temperature without using additional heater. For Zr thin film, the working pressure of Ar was maintained at 3 $x10^{-3}$ mbar with flow rate of 4.0 sccm. The as-deposited Zr film was annealed in air with varying temperature from 400-600°C for 1 hour to find the suitable condition to form ZrO_2 film. ZrN thin film was produced by reactive dc magnetron sputtering in a gas mixture of N_2(g) and Ar(g). To optimize N_2 flow rate, the Ar flow rate was fixed at 4 sccm and the N_2 flow rate was varied from 1-3 sccm. Normally, the sputter deposition of pure metal can be done by using an inert gas, such as argon (Ar). For a compound thin film, as in this work; ZrN, chemical reaction between the target material and the sputtering gas are required to be able to form such a film. This process in sputtering is called reactive sputter deposition [38]. Thus, the deposition conditions for both films are different. The coatings of Zr-based films were characterized by XRD and SEM for phase

structure and surface morphology, respectively. The deposition parameters used in the process are summarized in table 3.1 and the schematic dc magnetron sputter deposition system is shown in Figure 3.1.

Table 3.1 Deposition condition [40]

Parameter	Zr film	ZrN film
Substrate to target distance	7 cm	7 cm
Base pressure	1 x 10^{-5} mbar	6 x 10^{-6} mbar
Total gas pressure	3 x10^{-3} mbar	2.7 x10^{-3} mbar
Argon flow rate	4 sccm	4 sccm
Nitrogen flow rate	-	1-3 sccm
Magnetron Voltage	350 V	415 V
Magnetron Current	350 mA	700 mA
Power consumption	122.5 W	290.5 W
Deposition time	5-60 min	7.5-60 min

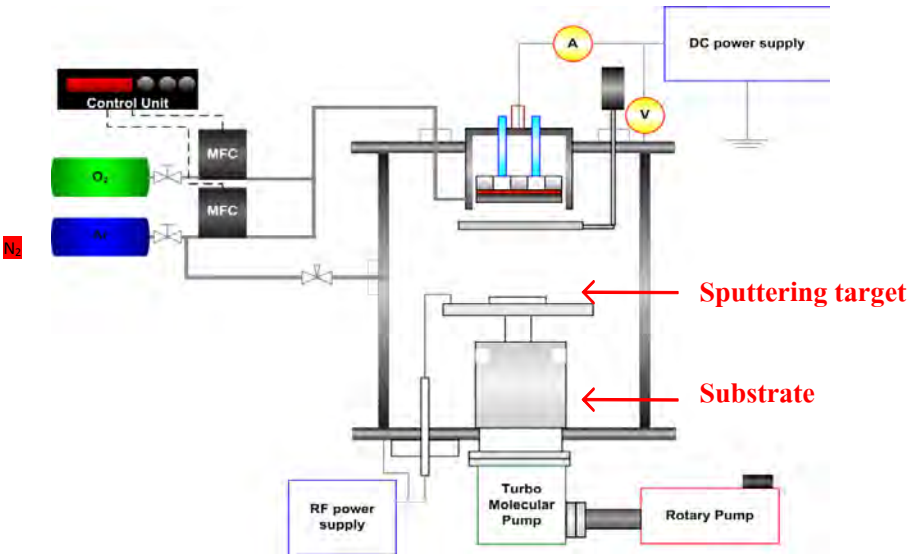

(a)

(b)

Figure 3.1 DC magnetron sputter deposition system (a) and Single-head Magnetron sputtering system (b).

3.2.3 Preparation of palladium membrane

Prior to electroless plating deposition, the prepared support was cleaned (section 3.2.1) and dried at 120°C for 3 hours. After the cleaning step, the surface of the support was first activated to seed palladium nuclei, initiating the autocatalytic process during electroless plating.

3.2.3.1 Surface activation

Surface activation solutions, including tin chloride ($SnCl_2$) solution, palladium chloride ($PdCl_2$) solution and hydrochloric solution 0.01 M (HCl) were prepared as follow,

- Preparation of $SnCl_2$ solution

In to 1 L volumetric flask, add approximately 200 mL DI, 1 mL 10 M (concentrated,~37%) HCl, 1 g $SnCl_2.H_2O$ and shake gently to dissolve. Then, make up to 1 L with DI water.

- Preparation of $PdCl_2$ solution

In to 1 L volumetric flask, add approximately 200 mL DI water, 1 mL 10 M (concentrated,~37%) HCl, 0.1 g $PdCl_2$, and heat up to ~ 60°C, stirring until dissolved (usually for approximately half an hour). Then, make up to 1 L with DI water.

- Preparation of 0.01 M HCl solution

In to 250 mL volumetric flask, add approximately 250 mL DI water, 1 mL 10 M (concentrated,~37%) HCl and make up to 1 L with DI water.

The surface activation process includes immersing the prepared support in $SnCl_2$ solution, DI water and $PdCl_2$ solution. Then, rinsing the activated support with 0.01 M to remove any trace amount of tin compounds on the surface and finally, rinsing in DI water. This cycle was repeated at least six times. After activation, the surface activated supports were dried at 120°C for 3 hours. A perfectly activated surface was smooth and dark-brown in color. The process of surface activation steps were summarized as follow,

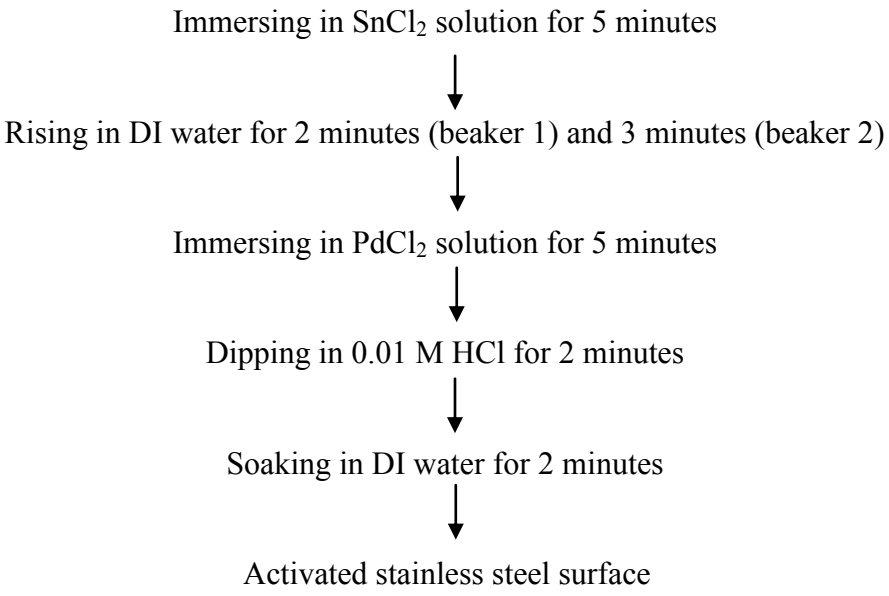

3.2.3.2 Palladium electroless plating

Following the surface activation, the supports were plated with palladium membrane by the electroless plating deposition as shown in Figure 3.2. The plating solution and 1 M hydrazine (N_2H_4) solution were prepared as follow,

- Preparation of plating solution

In to 200 mL volumetric flask, add approximately 200 mL DI water, 198 mL NH_4OH, 4 g $Pd(NH_3)_4Cl_2$ and shake gently to dissolve. Then, add 40.1 g Na_2EDTA and shake gently to dissolve, and make up to 1 L with DI water.

- Preparation of 1M hydrazine (N_2H_4) solution

In to 25 mL volumetric flask, add approximately 10 mL DI water, 0.80 mL pure, anhydrous (98%) N_2H_4 and make up to 25 mL using DI water

The plating solution was prepared at least one day prior to deposition to form stable metal complexes. The temperature of the plating bath was gradually increased to 60°C and hydrazine reducing agent was added just prior to immersion of the supports. The plating solution was renewed every 90 minutes.

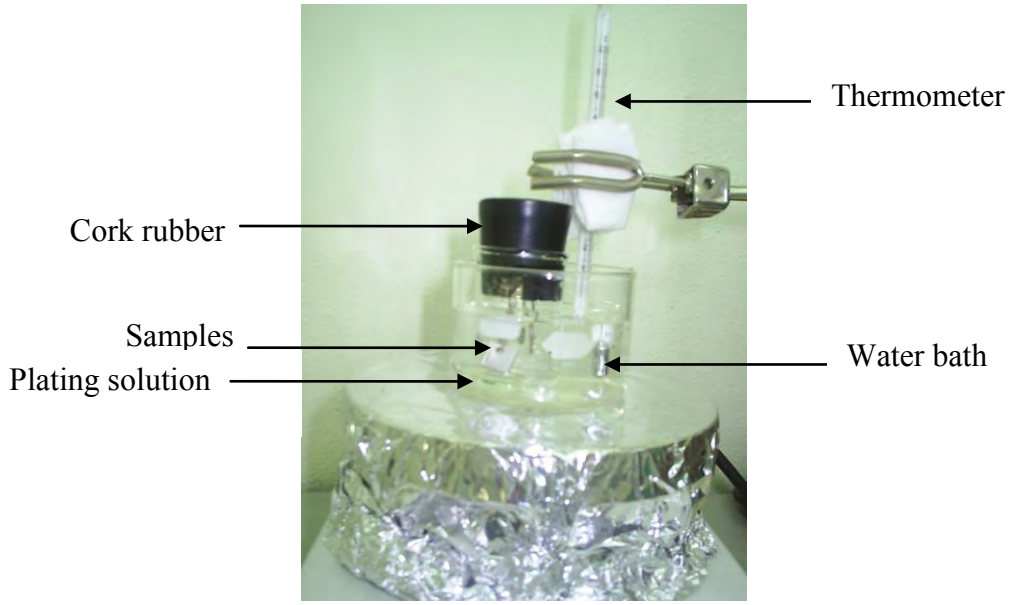

Figure 3.2 Palladium plating deposition.

3.2.4 Intermetallic diffusion characterization

In order to investigate the effectiveness in reducing the intermetallic diffusion of the diffusion barriers, the specimens of palladium membranes with and without diffusion barriers were heated in helium atmosphere with a ramp rate of 4 °C/minute. When the temperature reached 600°C, they were then heated in pure hydrogen. After annealing in hydrogen for 24 hours, the membranes were cooled down to 400°C, in helium before further cooling down to room temperature in order to prevent hydrogen

embrittlement in membranes [39]. The cross-sectional annealed specimens were then prepared for SEM-EDS investigation by mounting with phenolic resin powder, curing at 180°C and applying 30 kN of compression force in a Smithells II mounting press. Grinding and polishing were done on Metaserv 2000 grinder-polisher. The grinding was also carried out with SiC paper of 300, 600, 800, 1200 and 2000 grit. Polishing was done with a suspension of 3 μm-grade diamond. Surface characterizations were performed using Scanning Electron Microscope (SEM) (JEOL model JSM 5800LV) equipped with Electro Dispersive Spectrometer (EDS) for both qualitative and quantitative analyses.

3.2.5 Hydrogen permeation testing

The most effective film of each diffusion barrier in reducing intermetallic diffusion was selected for hydrogen permeation testing. Disk-shaped 316L porous stainless steel with a thickness of 1 mm and an average pore size of 0.2 μm was used as the substrate. The palladium membranes with and without the Zr-based intermetallic diffusion barriers were subjected to helium flux measurement until no more helium flux was detected from the outlet of the permeation cell, indicating that palladium membranes were dense and covered completely on the porous stainless steel area. The permeation for all runs was done under atmospheric pressure. The dense palladium membrane disk was heated in helium at a rate of about 4°C/min before subjecting to hydrogen at 350°C. Dense palladium membranes should not allow helium permeation through the permeation cell, shown in Figure 3.3. The pressure of the feed gas was monitored at 1-3 atm and the temperature of the reactor was varied from 350 to 500°C. The gas permeation rate was measured by a soap-bubble capillary flow meter. The diagram of apparatus set up for hydrogen permeation flux testing was shown in Figure 3.4.

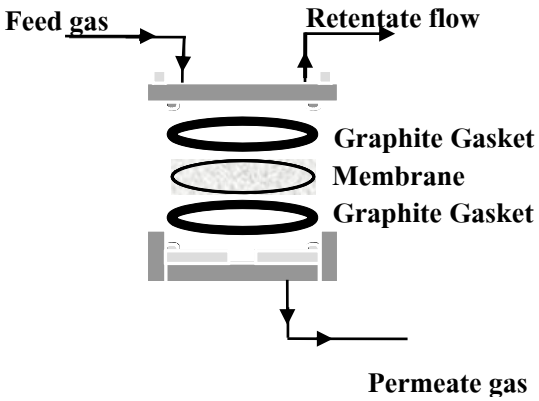

Figure 3.3 The permeation cell

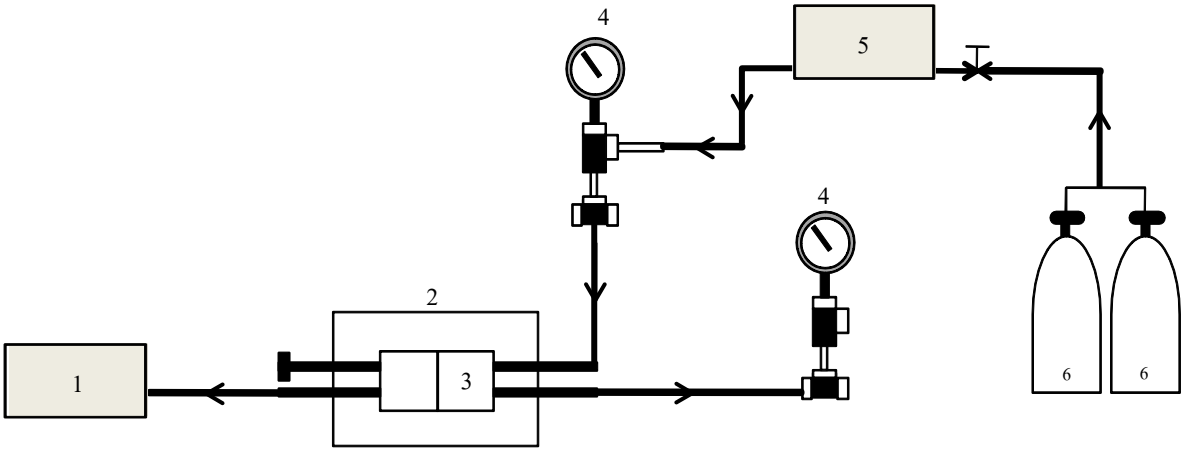

Figure 3.4 The gas permeation set up

1. Digital flow meter	2. Furnace	3. Permeation cell
4. Pressure gauge	5.Gas controller	6. Gas cylinder

CHAPTER IV

RESULTS AND DISCUSSION

4.1 Preparation of Stainless Steel Substrate

316L nonporous stainless steel supports were preliminary polished to obtain the smooth surface for coating. Figure 4.1 shows SEM micrographs of nonporous stainless steel surface before and after polishing. It is evident that the surface becomes smoother after polishing. However, the unpolished porous stainless steel supports was applied due to their uniform pore size and smooth surface as shown in Figure 4.2 and the polishing could change their pore structure. Before thin film deposition, the supports were cleaned thoroughly to remove grease, oil, dirt, corrosion products and others, existing on the surface. Without this step, the films could not be successfully deposited.

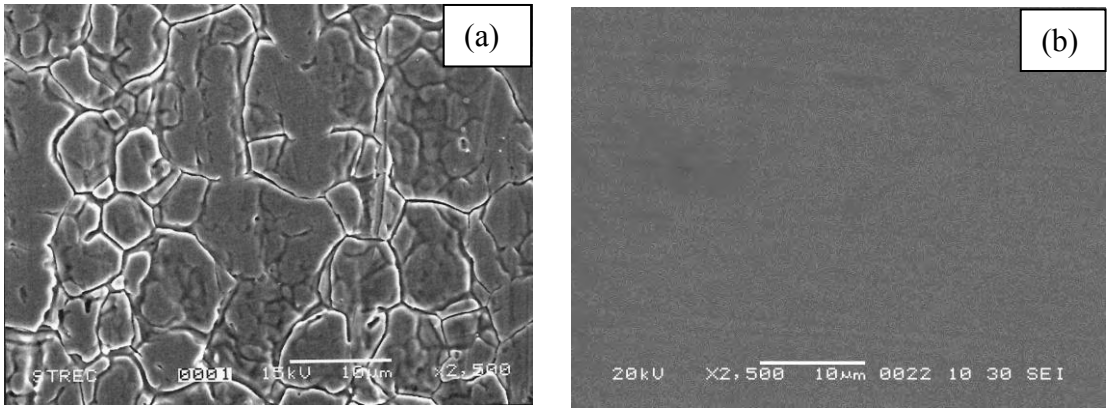

Figure 4.1 SEM micrographs of surface morphology of nonporous stainless steel (a) before and (b) after polishing.

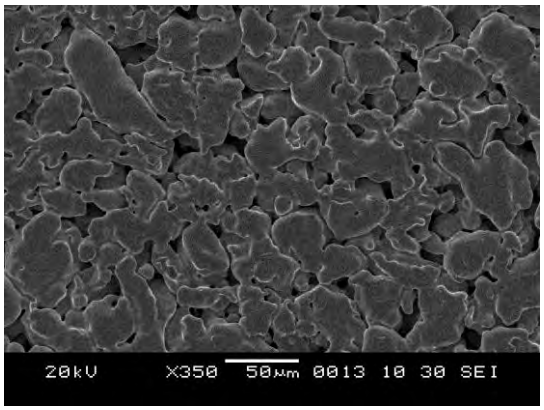

Figure 4.2 SEM micrograph of surface morphology of porous stainless steel without polishing.

4.2 Preparation and Characterization of Intermetallic Diffusion Barriers

4.2.1 Zr thin film

By magnetron sputtering, a typical thin film deposition method, giving layers of a few microns thick, the Zr thin films obtained were uniform, in color of silver with smooth surface as shown in Figure 4.3. Thus the layers are so thin that they do not change the macroscopic roughness of the support. Figure 4.4 shows cross-sectional SEM image of 0.17 μm, Zr thin film obtained from 5 minutes deposition time. The thickness of the deposited films (0.17 to 2 μm) was found to increase linearly with the deposition time as shown in Figure 4.5. The X-ray diffraction patterns of (a) 316 L stainless steel support and (b) Zr thin films on 316L stainless steel were shown in Figure 4.6. The Zr films exhibit dominant peaks of Zr(002) and Zr(100) planes with very small peaks of Zr(200) and Zr(004) planes of a hexagonal structure [40,41].

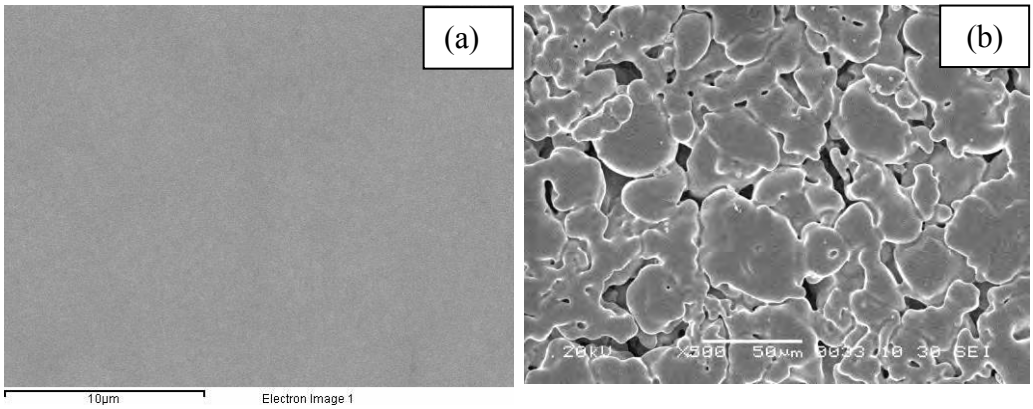

Figure 4.3 SEM micrographs of surface morphology of Zr thin film deposited on (a) nonporous stainless steel and (b) porous stainless steel.

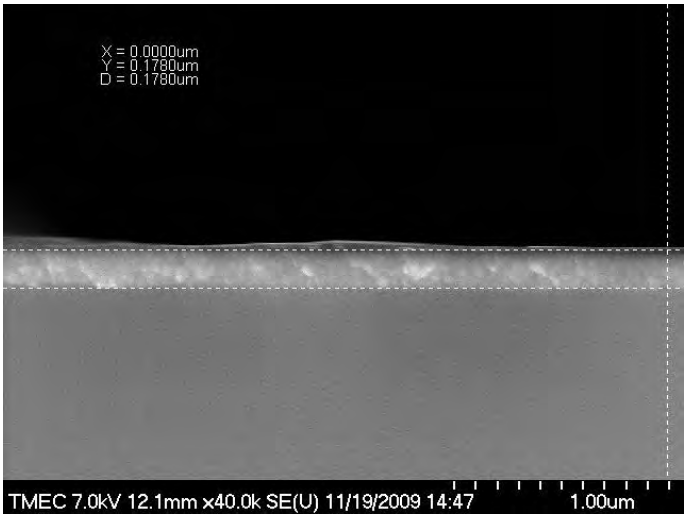

Figure 4.4 Cross-sectional SEM image of the Zr thin film with deposition time 5 minutes.

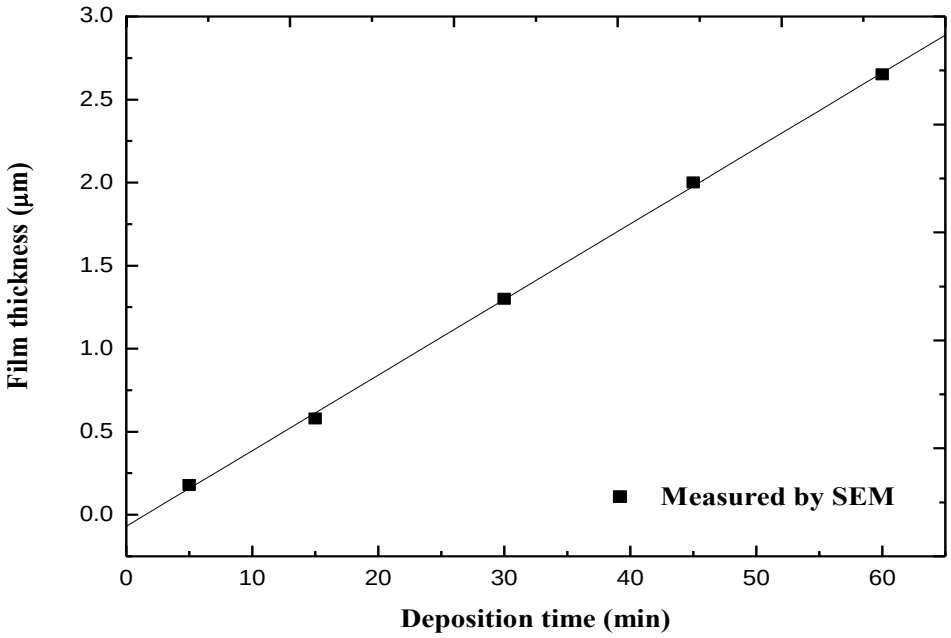

Figure 4.5 Film thickness as a function for deposition time of Zr thin films.

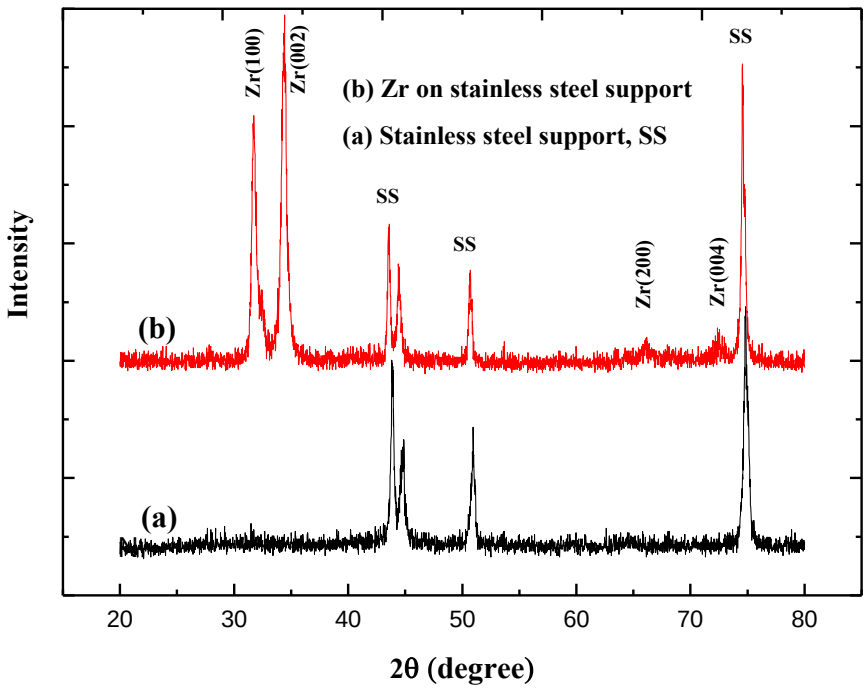

Figure 4.6 XRD patterns of Zr thin film on 316L stainless steel substrate.

4.2.2 ZrO_2 thin film

ZrO_2 thin films have been deposited by various techniques [17, 18, 42, 43]. Reactive magnetron sputtering has offered good control over deposition rate and film composition, and minimizes target poisoning. However, this technique gives relatively low deposition rate of oxide thin films. It was found that, nanocrystalline Zr could be easily oxidized in air yielding an only stable form of zirconium oxide, namely ZrO_2 [18]. Therefore, to obtain thicker film, the zirconium films were annealed in air.

Zr thin films were prepared on glass slides and 316L stainless steel supports and annealed in air at 400, 500 and 600ºC for 1 hour. At 400ºC, the thin films changed from dark to opal translucent because not all of Zr metal combined with oxygen at the surface. However, the films became transparent after annealing at 500 and 600ºC, indicating that ZrO_2 was formed on the surface, confirmed by x-ray diffraction. The XRD patterns in Figure 4.7 of (a) 316 L stainless steel support, (b), ZrO_2 thin films on 316L stainless steel annealed at 400ºC show peak broadening of monoclinic phase $ZrO_2(\bar{1}11)_M$, and strong hexagonal phases, Zr(002) and Zr(100). For (c) and (d), ZrO_2 thin films on 316L stainless steel annealed at 500 and 600ºC showed the monoclinic phase of $ZrO_2(1\bar{1}1)_M$ [43] which dominates with high intensity and small peaks of tetragonal phases, $ZrO_2(101)_T$ and $ZrO_2(002)_T$. It is evident that at 500 and 600ºC the samples were crystallized in a mixture of monoclinic and tetragonal phases. The oxidized films became transparent at 500 and 600ºC with the maximum thickness of 0.5 μm as shown in Figure 4.8. However, after annealing in air to 600ºC, film cracking and delaminating occurred as shown in Figure 4.9. F.Martin et al. [43] also found that the films annealed at 600ºC cracked and peeled off from the substrate. These phenomena were not due to lattice mismatch of ZrO_2 on the stainless steel but due to the growth of an interfacial oxide layer from the stainless steel at the interface. Therefore, ZrO_2 thin films were prepared by annealing at 500ºC for 1 hour in air to prepare ZrO_2 thin films.

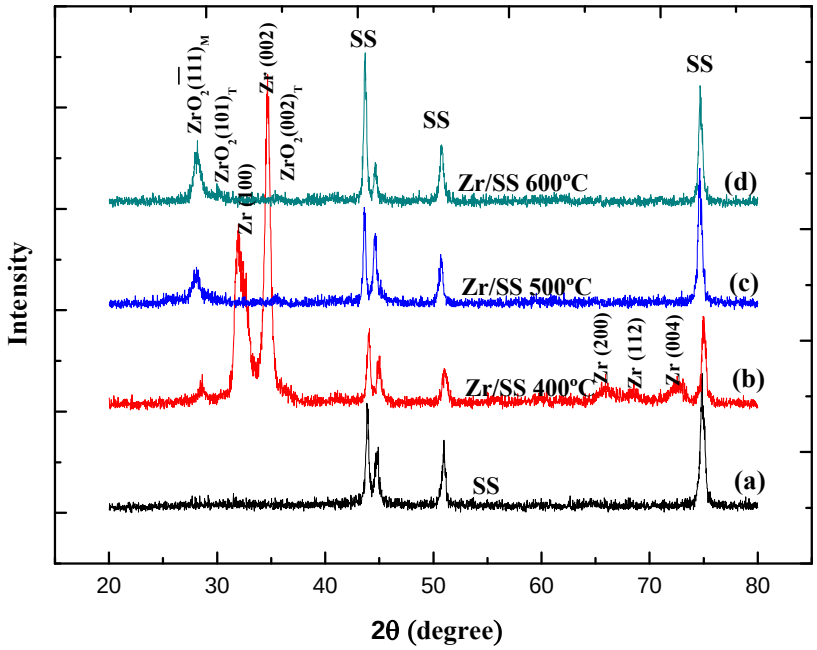

Figure 4.7 XRD patterns of ZrO_2 thin film on 316L stainless steel substrate at various annealing temperature.

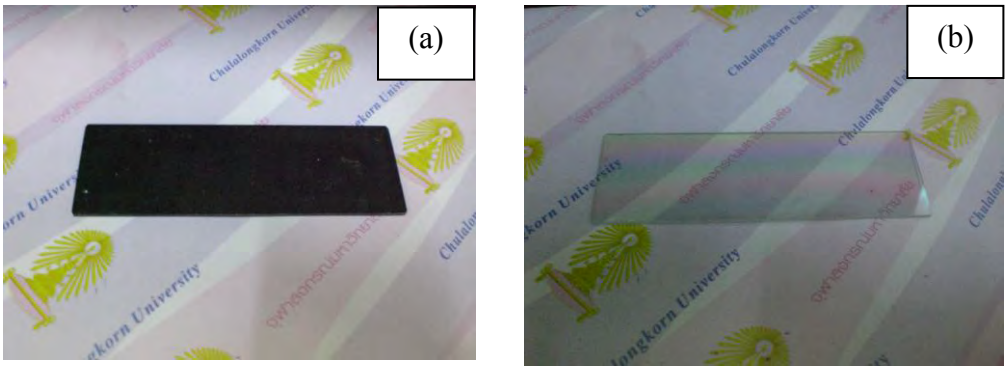

Figure 4.8 ZrO_2 thin films on glass substrates (a) before and (b) after annealing in air at 500ºC for 1 hour.

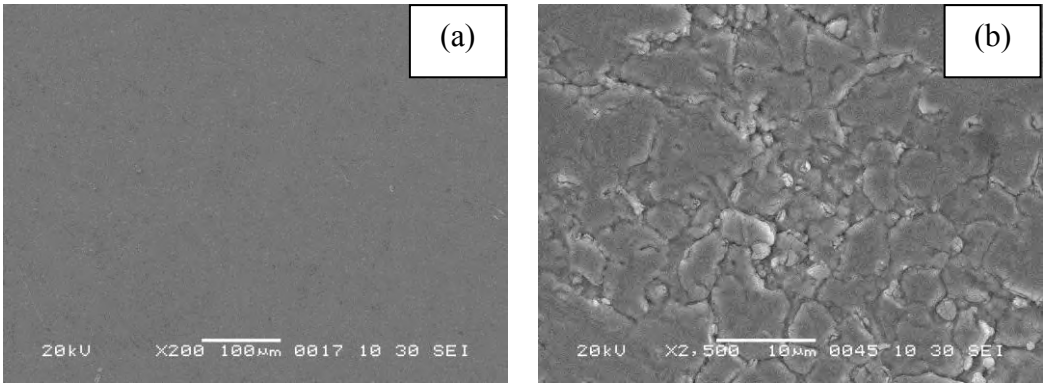

Figure 4.9 ZrO_2 thin film on stainless substrates (a) before and (b) after annealed in air at 600ºC for 1 hour.

Figure 4.10 shows EDS spectrum for an elemental analysis of the prepared ZrO_2 thin film yielding the atomic percent Zr:O of 33.91:66.09, close to 1:2, confirming the formation of ZrO_2 thin films. The ZrO_2 thin films deposited on porous and nonporous stainless steel have uniform and smooth surface as shown in Figure 4.11.

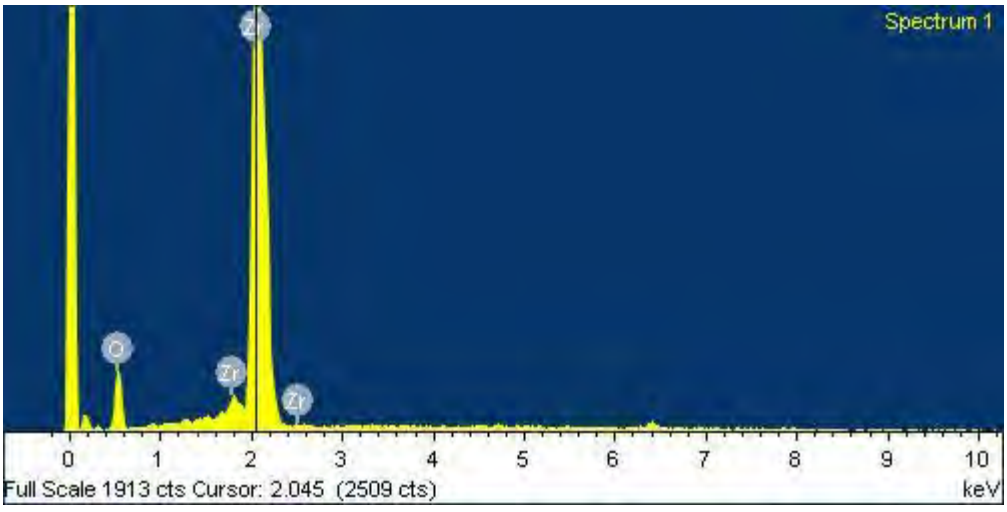

Figure 4.10 EDS spectrum of ZrO_2 thin film.

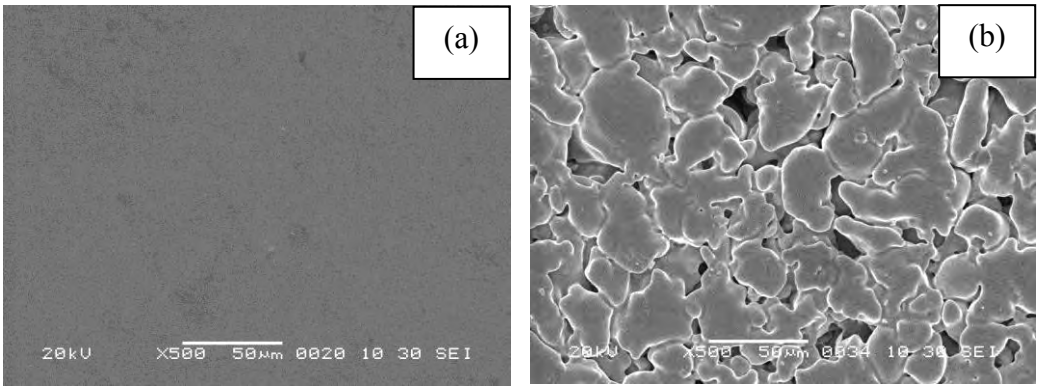

Figure 4.11 ZrO_2 thin film deposited on (a) nonporous stainless steel and (b) porous stainless steel.

4.2.3 ZrN thin film

XRD patterns of the deposited ZrN films at nitrogen flow rates of 1-3 sccm were shown in Figure 4.12. It can be seen that all specimens have (111) and (311) preferred orientations. An additional crystallographic plane, (200) can be found at N_2 flow rate of 2 and 3 sccm. All diffraction peaks pertain to crystal planes of ZrN phase with NaCl-type structure. [44] Table 4.1 summaries the composition of ZrN films at different flow rates. The deposited film obtained from nitrogen flow rate of 1 sccm had grey color with non-stoichiometric N/Zr ratio of 0.58. Lighter gold color with near-stoichiometric N/Zr ratio of 1.04 was obtained at the nitrogen flow rate of 2 sccm. The deposited film with nitrogen flow rate of 3 sccm had dark brown color with non-stoichiometric, N/Zr ratio of 1.64. Therefore, the ZrN films were prepared at nitrogen flow rate of 2 sccm to form near-stoichiometric $ZrN_{1.04}$ films. EDS analysis of ZrN film was shown in Figure 4.13. The amounts of reactive gas constituents incorporated into growing films depended on whether a compound had been formed on the target surface [45]. When nitrogen partial pressure became sufficiently high, the reaction was initiated at the target surface. At low nitrogen partial pressure, no compound was formed on the target surface, and hence the composition of the growing films was mainly governed by the direct impingement of species from the

reactive gas and the target. The reactivity was low for N_2 impinging directly from the gas on the growing film, and the species originating from the target determined the composition of the coatings. The optimum group parameters for growing ZrN thin film were summarized in Table 4.2. The deposited thin films on porous and nonporous stainless steel had uniform and smooth surface as shown in Figure 4.14. Cross-sectional SEM image of 0.25 µm, ZrN thin film obtained from 7.5 minutes deposition time is shown in Figure 4.15. The thickness of the deposited films (0.25 to 2 µm) was found to increase linearly with the deposition time as shown in Figure 4.16.

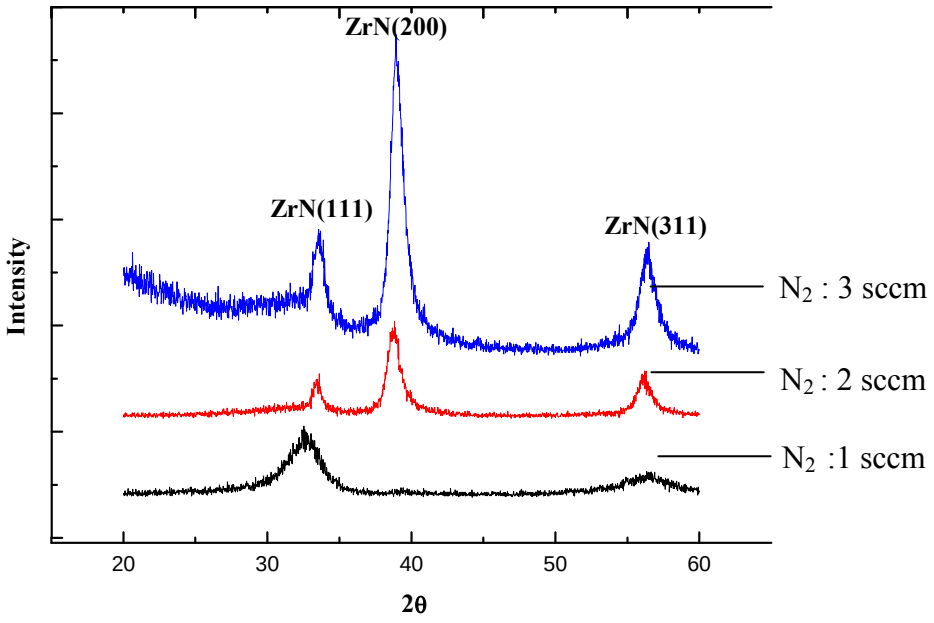

Figure 4.12 XRD patterns of ZrN thin film at different N_2 flow rate.

Table 4.1 Atomic percent of elements in ZrN thin film with different N_2 flow rate

N_2 Flow rate	1 SCCM			2 SCCM			3 SCCM		
Element	Zr	N	N/Zr	Zr	N	N/Zr	Zr	N	N/Zr
Atomic%	63.33	36.67	0.58	48.91	51.09	1.04	37.80	62.20	1.64

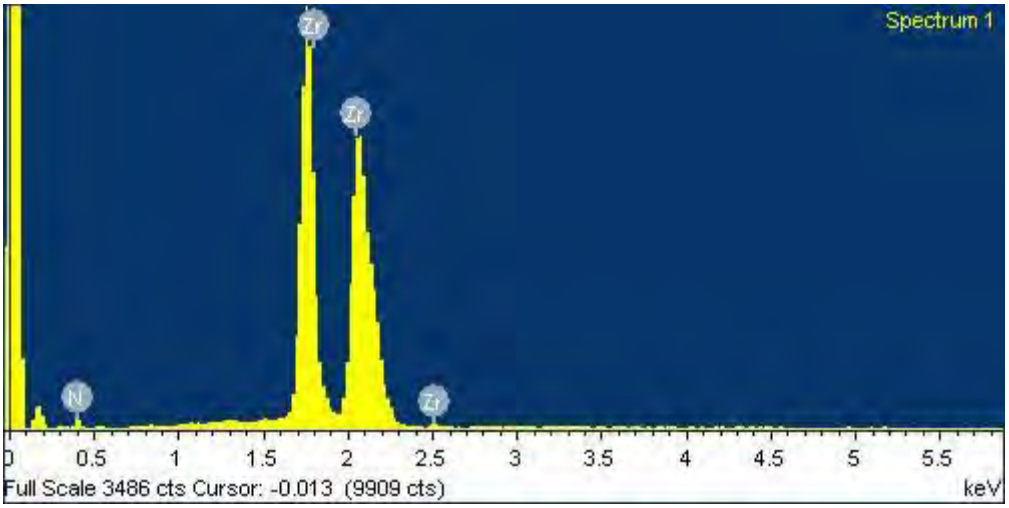

Figure 4.13 EDS spectrum of ZrN film.

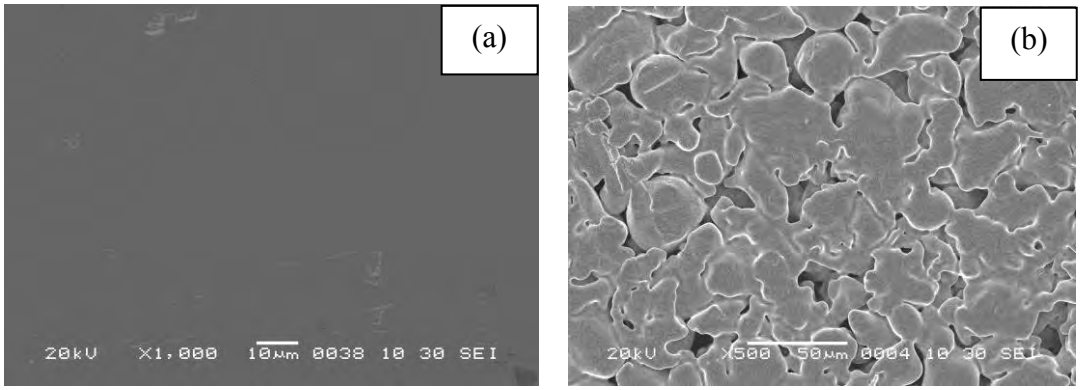

Figure 4.14 Surface morphology of ZrN thin films deposited on (a) nonporous stainless steel and (b) porous stainless steel.

Table 4.2 Main deposition parameter of ZrN thin film

Parameter	ZrN film
Substrate to target distance	7 cm
Base pressure	6 x 10^{-6} mbar
Total gas pressure	2.7 x10^{-3} mbar
Argon flow rate	4 sccm
Nitrogen flow rate	2 sccm
Argon partial pressure	2 x 10^{-6} mbar
Nitrogen partial pressure	4 x 10^{-6} mbar
Magnetron Voltage	415 V
Magnetron Current	700 mA
Power consumption	290.5 W
Deposition time	7.5-60 min

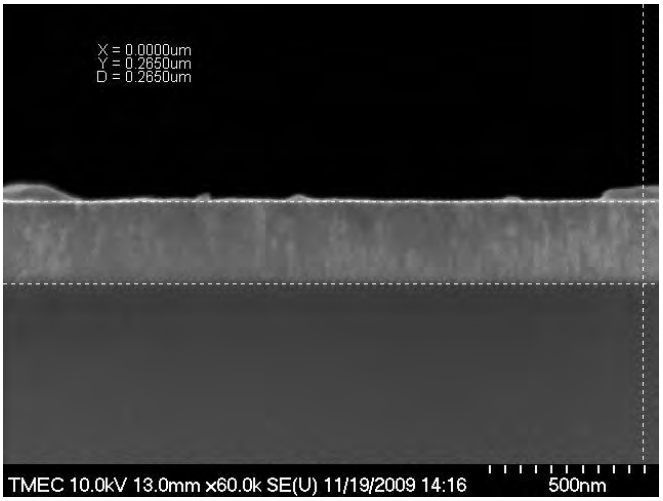

Figure 4.15 Cross-sectional SEM image of the ZrN thin film with deposition time 7.50 minutes.

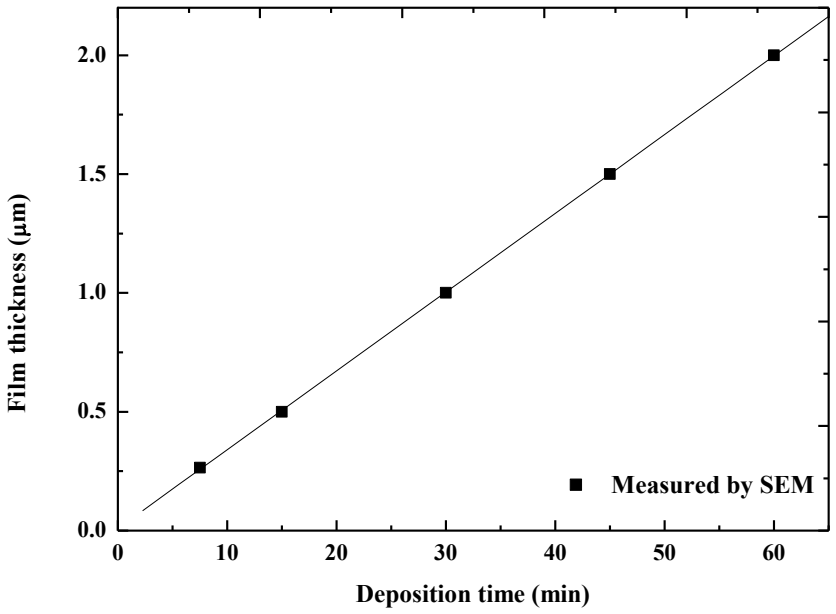

Figure 4.16 Film thickness as a function of deposition time for ZrN thin films.

4.3 Preparation of Palladium Membrane

4.3.1 Surface activation

Prior to electroless plating, the support was activated by nucleating palladium seeds onto substrate surface, in order to initiate the autocatalytic process of electroless deposition of Pd metal. During the activation step, colloidal particles of Sn(II) were adsorbed on the supporting surface. These particles acted as catalytic sites for palladium reduction during the activating step, due to the redox reaction as illustrated in equation 4.1 and 4.2

$$2SnCl_2 + 3H_2O \longrightarrow 2Sn(OH)_{1.5}Cl_{0.5} + 3HCl \quad 4.1$$

$$Pd^{2+} + Sn^{2+} \longrightarrow Pd^{0} + Sn^{4+} \quad 4.2$$

At the end of the activation step, palladium spots and Sn(IV) seeds were spread over the supporting surface and became catalytically active for the deposition

of palladium metal. SEM micrographs of the stainless steel surface after surface activation are shown in Figure 4.17. There are a large number of seeds with relatively uniform particles of dark brown color on the supporting surface, confirming that the surface was effectively activated. Ma et at. [46] suggested that the preseeded palladium nuclei at the activating stage reduced the induction period of the autocatalytic process at the beginning.

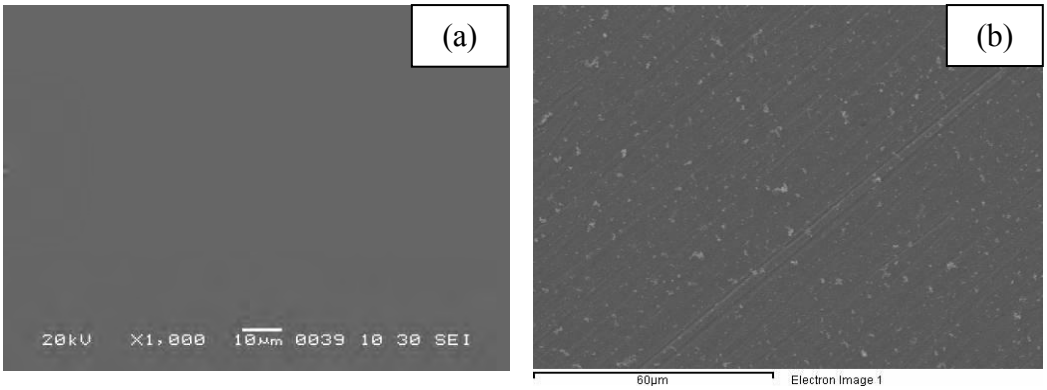

Figure 4.17 SEM micrographs of the stainless steel before (**a**) and after (**b**) surface activation.

4.3.2 Palladium electroless plating

Palladium deposition occurs according to the following oxidation-reduction reactions [47]

$$2Pd(NH_3)_4^{2+} + 4e^- \longrightarrow 2Pd^0 + 8NH_3 \qquad E^0 = 0.0\ V$$
$$N_2H_4 + 4OH^- \longrightarrow 4H_2O + N_2 + 4e^- \qquad E^0 = 1.12\ V$$
$$2Pd(NH_3)_4^{2+} + N_2H_4 + 4OH^- \longrightarrow 2Pd^0 + 4H_2O + N_2 + 8NH_3 \qquad E^0 = 1.12\ V \qquad (4.3)$$

During the immersion of stainless steel disk in the plating solution, bubbling gases produced by the redox reaction were observed. It was explained [47] that the reaction occurred on the surface of the support, and preferentially around the palladium seeds. The occurrence was initiated by the reaction of hydrazine with

hydroxide ion forming nitrogen gas and water with simultaneous release of electrons. The electrons were transferred across the palladium islands and used for reducing Pd^{2+} complex into palladium metal. The palladium metal was deposited onto nuclei resulting in the growth. Nitrogen and ammonia gases were concomitantly evolved as bubbles during the plating process. The use of excessive amount of hydrazine hydrate resulted in precipitation of a great deal of palladium powder in the plating bath.

The thickness of palladium layer can simply be determined by weighing. The stainless steel disk was weighed before and after palladium plating at different plating time. The calculation for the thickness of palladium layer was done using the following equation:

$$\text{Pd thickness } (\mu m) = \left(\frac{\text{plated disk weight} - \text{initial disk weight}}{\text{disk surface area x palladium density}} \right) \text{ x } 10^4$$

It was assumed that the gained weight of the disk came only from palladium plated on the entire disk surface. The reliability of the weighing method in determining the palladium layer thickness was assessed by SEM micrographs. It can be seen that the palladium layer thickness obtained by weighing is in the range determined by SEM as illustrated in Table 4.3. For example, SEM micrographs of the cross-section of palladium membranes with Zr film (0.5 μm) in Figure 4.18 gave palladium membrane thickness of about 36.3 μm close to the value of 34.07 μm obtained from weighing.

Table 4.3 Palladium layer thickness on stainless steel disks

Underlying Surface	Disk weight (g)		Palladium layer thickness (μm)	
	Before plating	After plating	Weighing	SEM
plain stainless steel	0.8163	0.8573	21.07	21.92
Zr	0.7733	0.8396	34.07	36.30
ZrO_2	0.8643	0.9333	35.46	36.60
ZrN	0.8153	0.9718	52.51	52.80

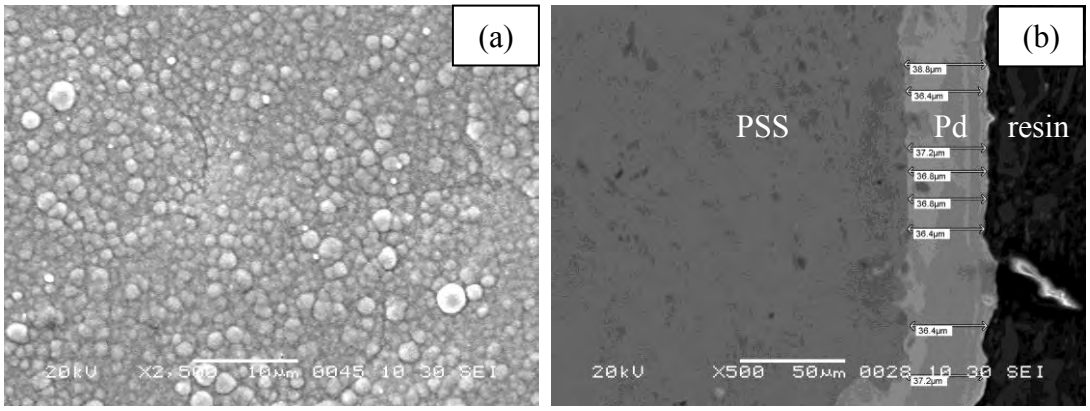

Figure 4.18 SEM micrographs of (a) palladium membrane surface morphology on porous stainless steel and (b) cross-section of palladium membrane with Zr (0.5 μm) diffusion barrier.

4.4 Investigation of Intermetallic Diffusion

The efficacies in preventing the intermetallic diffusion of the palladium membranes with and without the diffusion barriers were assessed by annealing in hydrogen at 450°C, 500°C, and 600°C for 24 hours. The elemental compositions at the interface between the palladium layers and the stainless steel supports were determined by SEM-EDS line-scan of the cross-section.

4.4.1 No diffusion barriers

The SEM-EDS line scan of palladium membranes without any protective diffusion barriers as shown in Figure 4.19 clearly demonstrated the intermetallic diffusion of Fe, Cr and Ni from the stainless steel supports to the palladium layers. More Fe and Cr were accumulated in the palladium layers than Ni, due to their relative amounts in the stainless steel supports, Fe >Cr >Ni. The amount of each metal element diffused into the palladium layer increased with increasing temperatures, especially at 600°C. In addition, hydrogen had been found to increase the rate of the intermetallic diffusion [48].

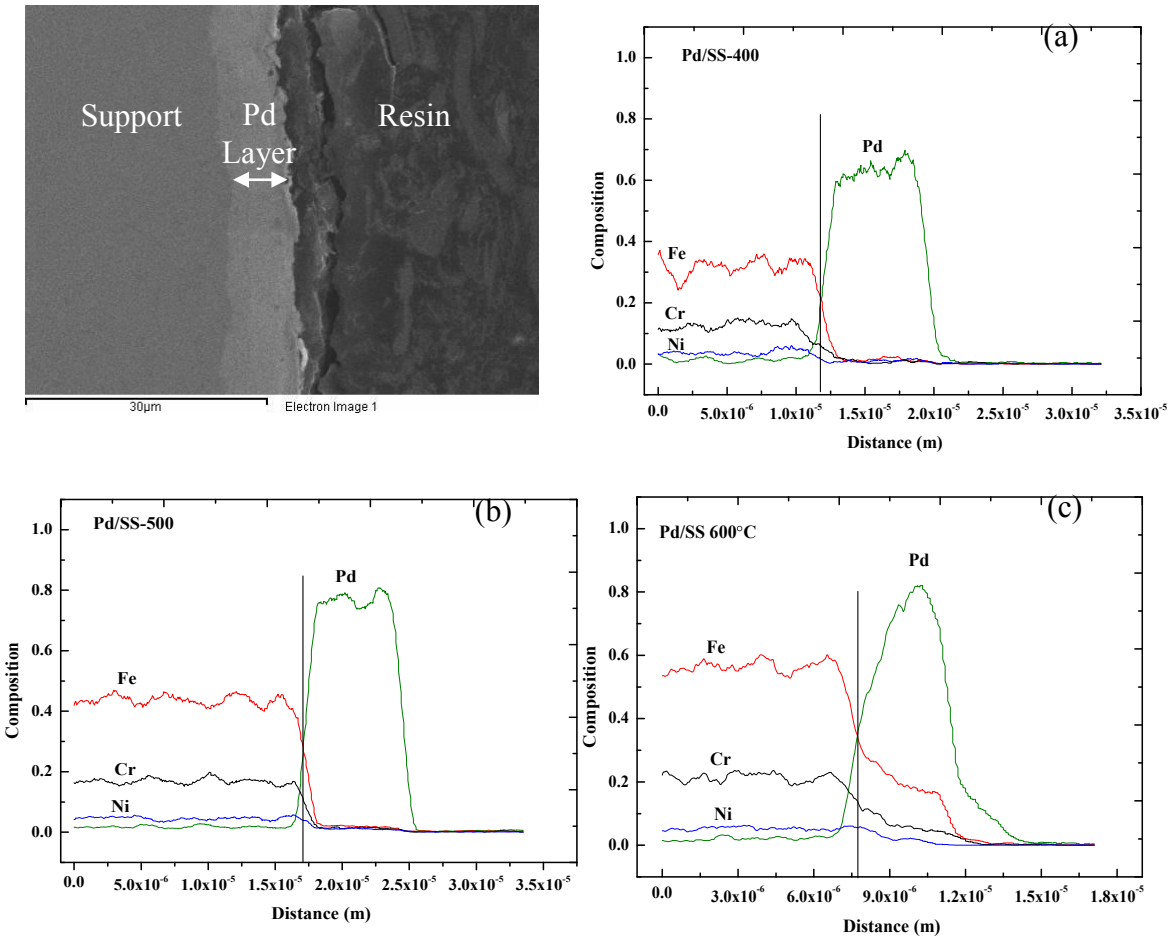

Figure 4.19 SEM-EDS line-scan micrographs of palladium membrane supported on stainless steel exposed in hydrogen at (a) 400°C, (b) 500°C, and (c) 600°C.

4.4.2 Intermetallic diffusion barriers

With the resolution of SEM-EDS line scan, it was difficult to quantitatively determine the compositions of the metal penetration into the thin layers of the intermetallic diffusion barriers. The effectiveness of the diffusion barrier was thus assessed from the cross-sectional SEM-EDS line scan micrographs.

4.4.2.1 Zr thin films

At 400ºC, it was found that Zr, 0.17 µm thick could not inhibit the intermetallic diffusion but with Zr, 0.35, 0.5, and 1 µm thick, the metals could not cross Zr/Pd interface into palladium layer. Thus, the minimum thickness of 0.35µm could prevent the intermetallic diffusion at 400ºC, as shown in Figure 4.20. SEM and SEM-EDS line-scan micrographs of the cross-section of Zr barrier, 0.35 µm thick were shown in Figure 4.21.

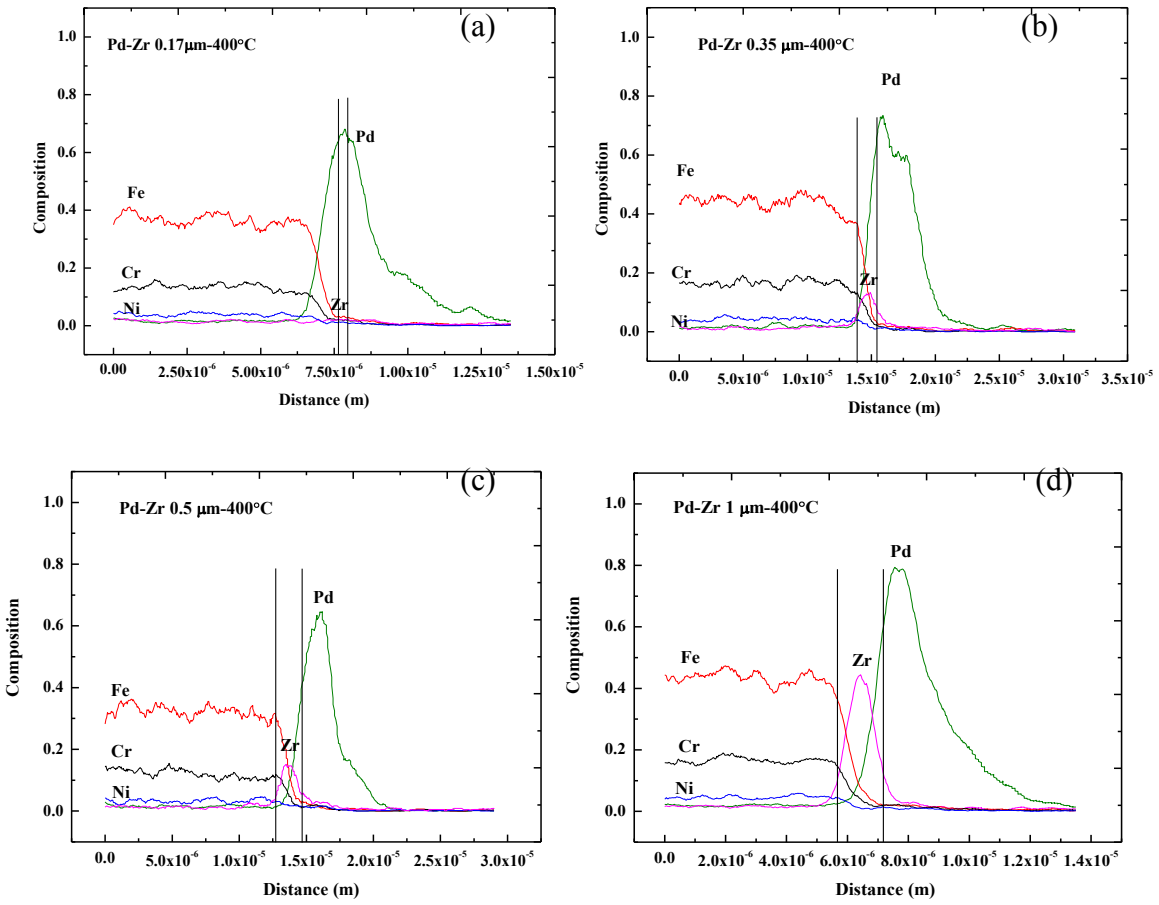

Figure 4.20 SEM-EDS line-scan micrographs of supported palladium membrane with different thickness of Zr diffusion barriers (a) 0.17µm, (b) 0.35 µm, (c) 0.5 µm, and (d) 1 µm on stainless steel substrates exposed in hydrogen at 400°C.

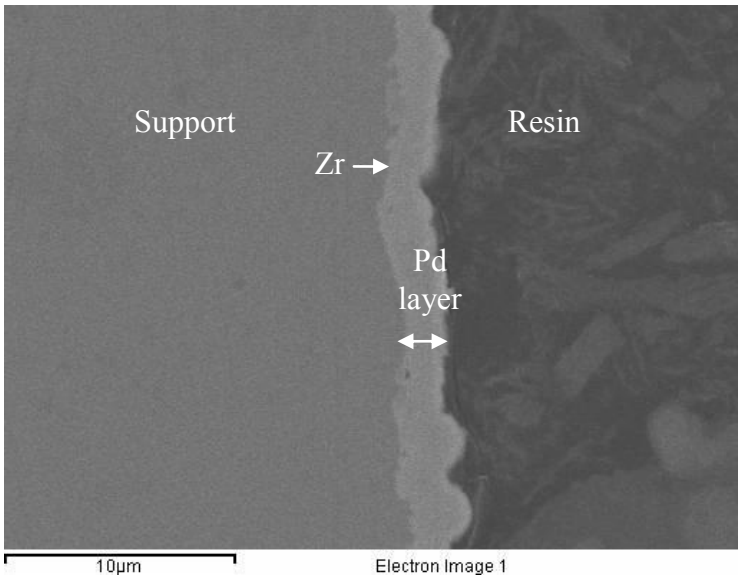

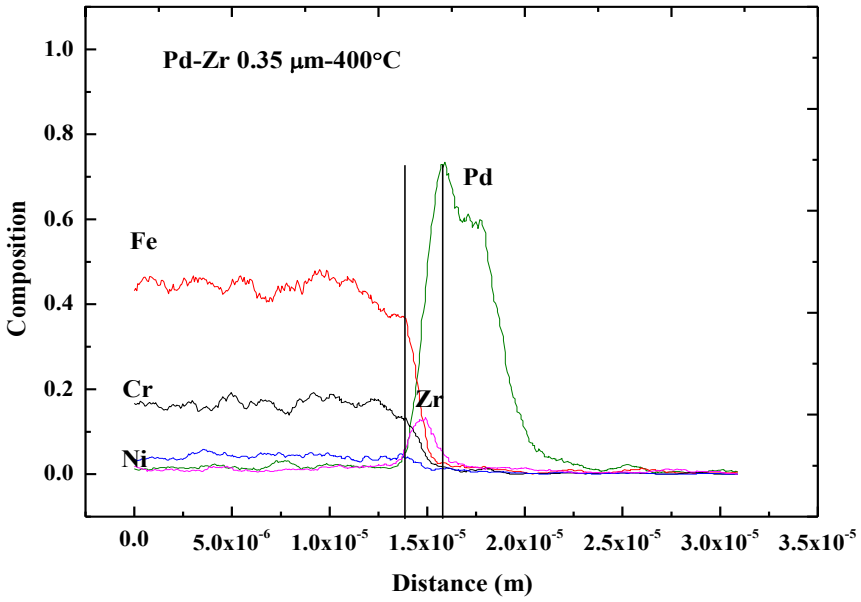

Figure 4.21 SEM and SEM-EDS line-scan micrographs of supported palladium membrane with Zr diffusion barrier, 0.35 µm on stainless steel substrates exposed in hydrogen at 400°C.

At 500ºC, Fe and Cr could diffuse through the zirconium layer, 0.17 µm thick. With Zr 0.35, 0.5 µm thick, although more Fe and Cr diffused into zirconium layer than Zr, 1 µm thick, they did not get across to the palladium layer, as shown in Figure 4.22. Thus, the minimum thickness of 0.35 µm could prevent the intermetallic diffusion at 500ºC. SEM and SEM-EDS line-scan micrographs of the cross-section of Zr barrier, 0.35 µm thick were shown in Figure 4.23.

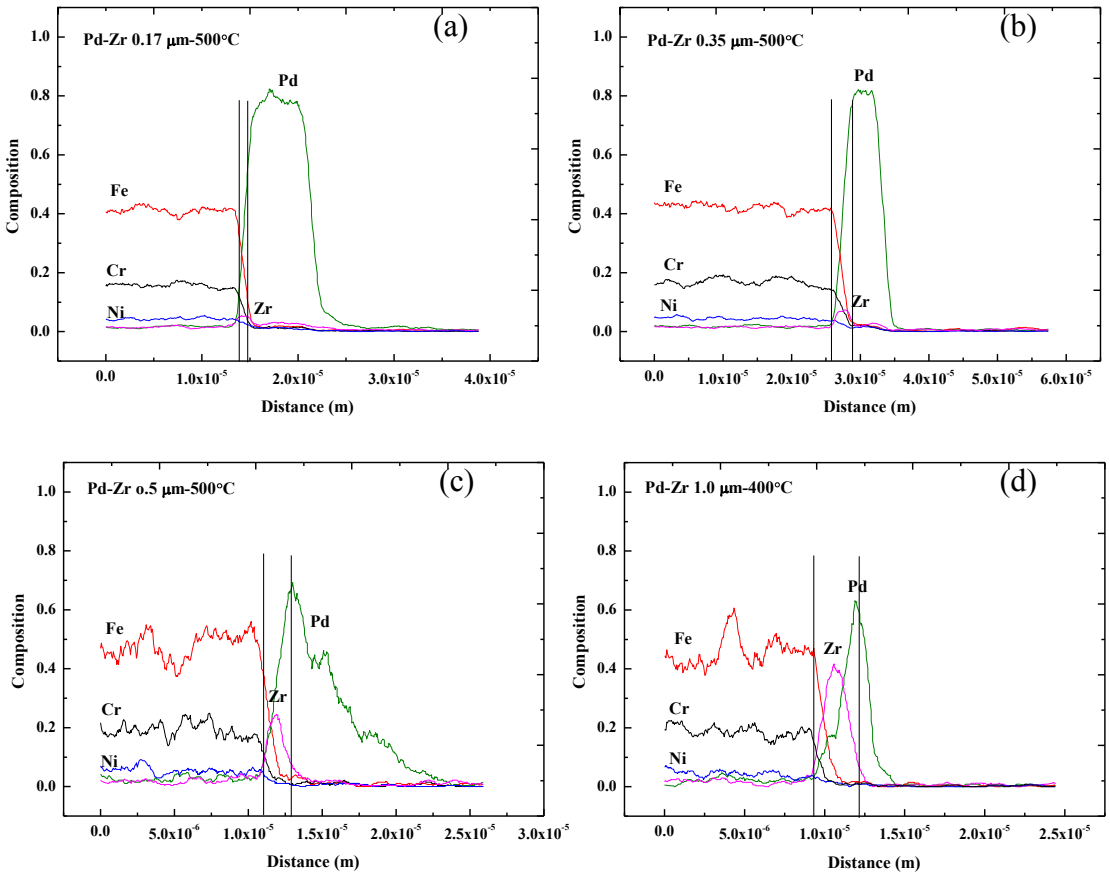

Figure 4.22 SEM-EDS line-scan micrographs of supported palladium membrane with different thickness of Zr diffusion barriers (a) 0.17µm, (b) 0.35 µm, (c) 0.5 µm, and (d) 1 µm on stainless steel substrates exposed in hydrogen at 500°C.

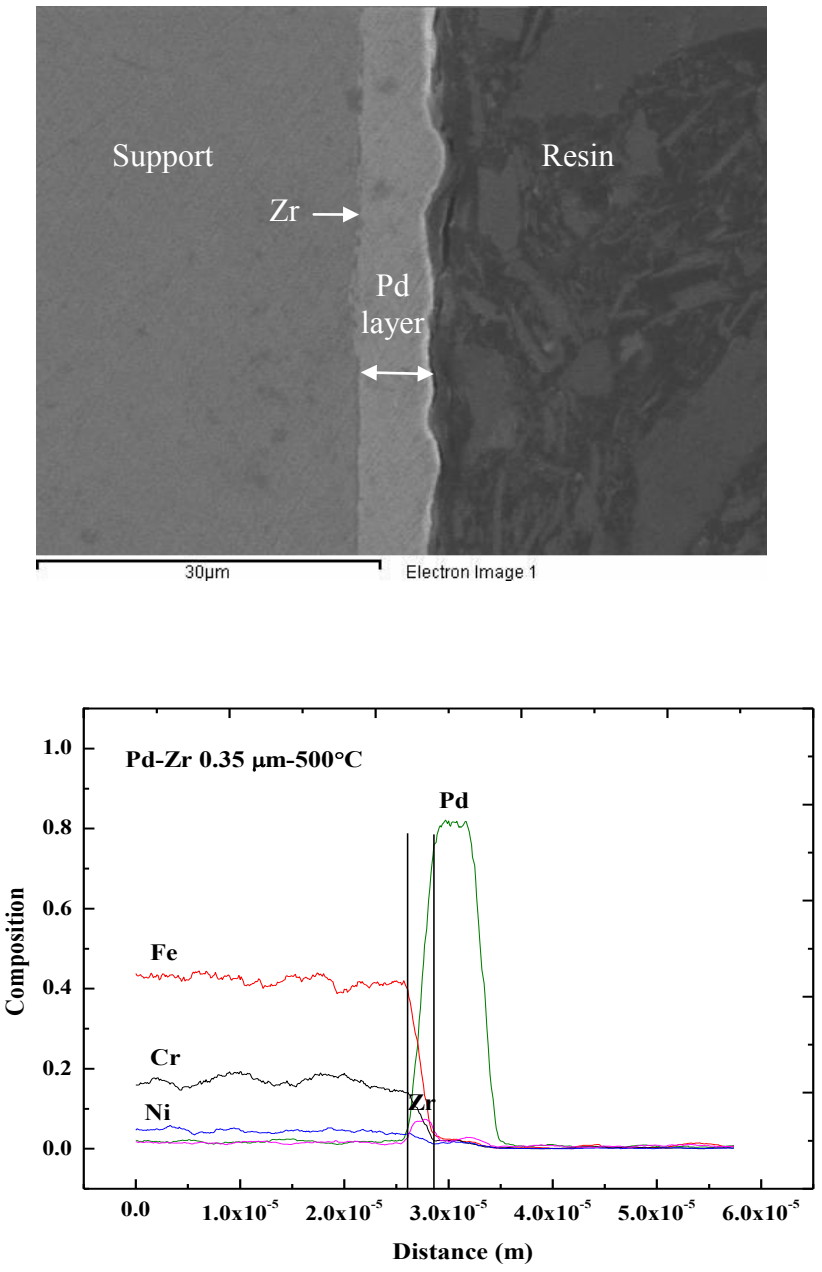

Figure 4.23 SEM and SEM-EDS line-scan micrographs of supported palladium membrane with Zr diffusion barrier, 0.35 µm on stainless steel substrates exposed in hydrogen at 500°C.

At 600°C, all metals diffused across the zirconium layer, 0.17 and 0.35 µm thick. More Fe and Cr diffused into Zr, 0.5 µm thick than Zr, 1 µm thick but did not reach the palladium layer, as shown in Figure 4.24. Thus, the thickness of at least 0.5 µm was required at 600ºC. SEM and SEM-EDS line-scan micrographs of the cross-section of Zr barrier, 0.5 µm thick were shown in Figure 4.25.

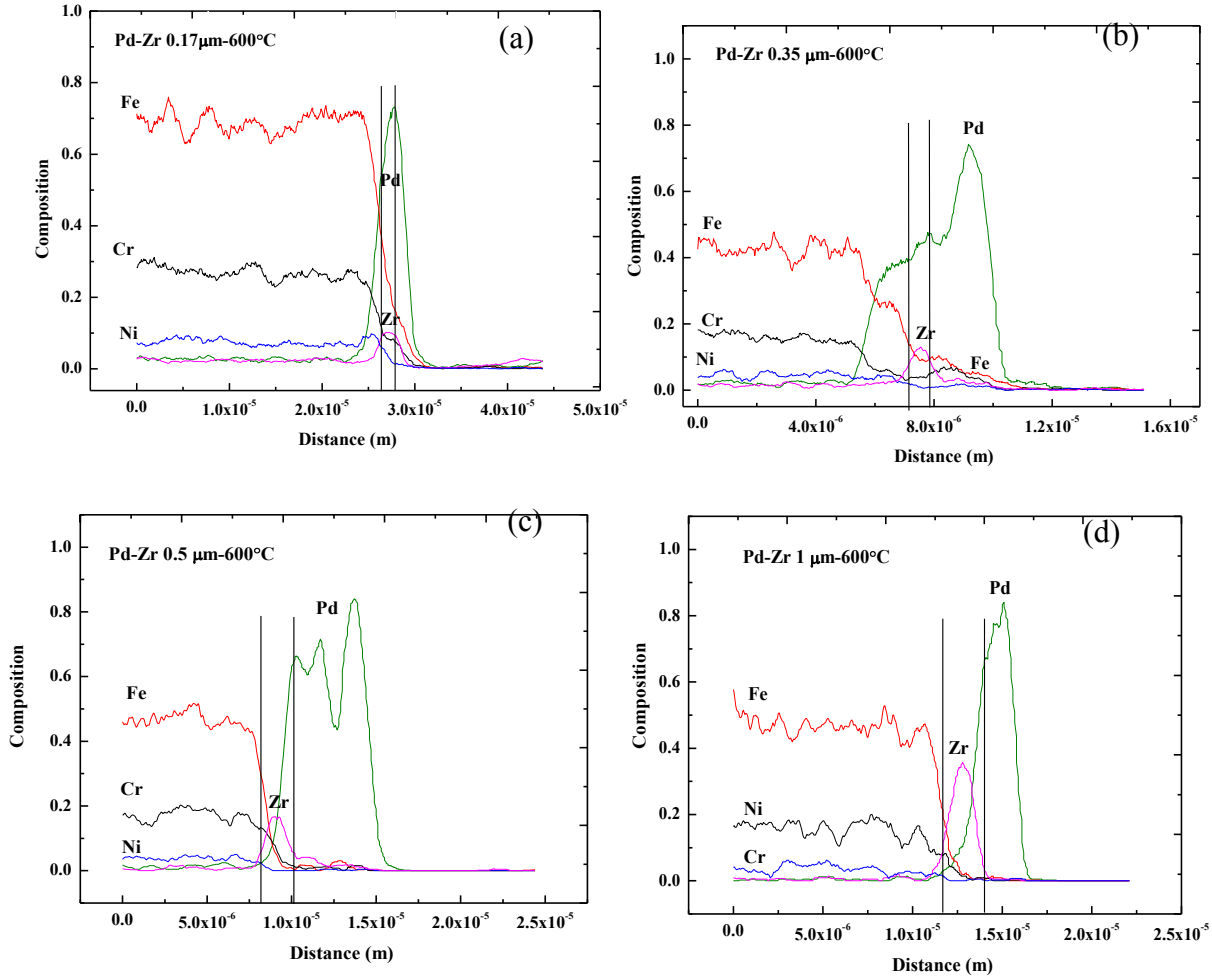

Figure 4.24 SEM-EDS line-scan micrographs of supported palladium membrane with different thickness of Zr diffusion barriers (a) 0.17µm, (b) 0.35 µm, (c) 0.5 µm, and (d) 1 µm on stainless steel substrates exposed in hydrogen at 600°C.

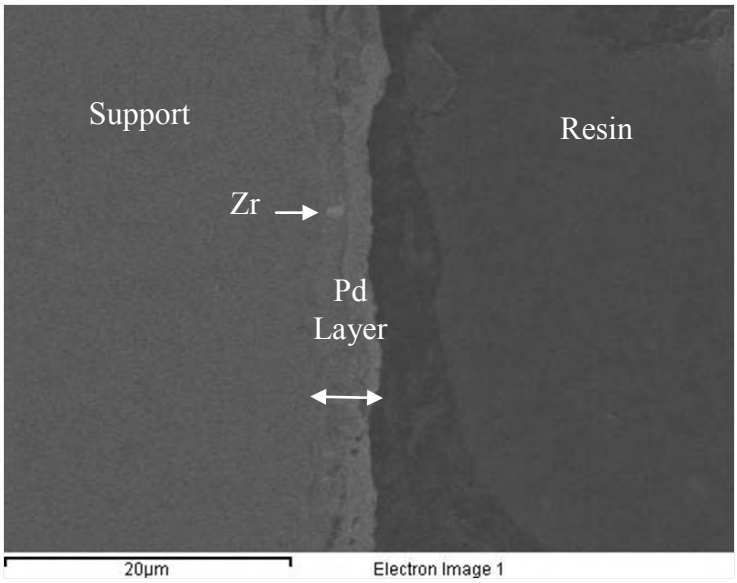

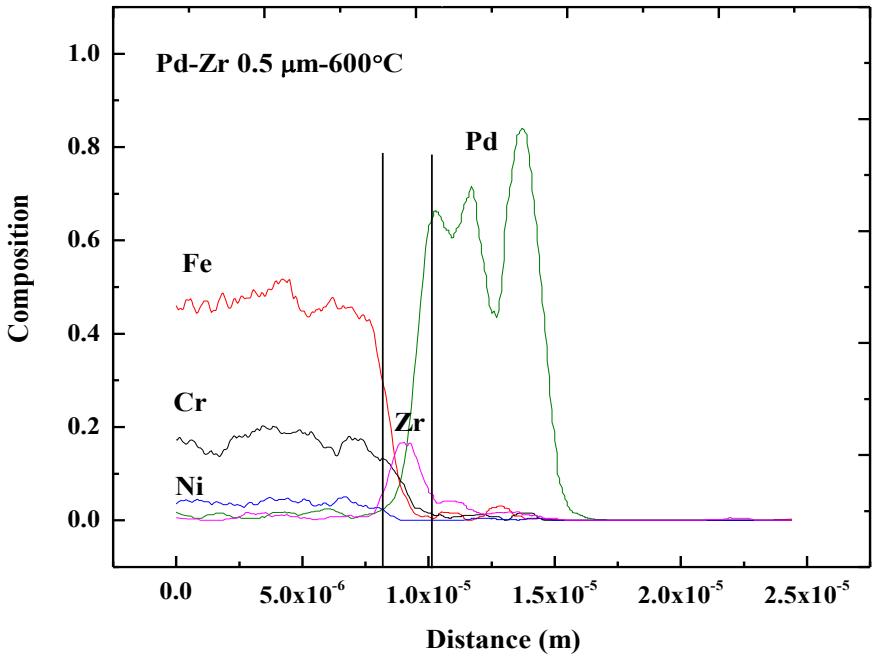

Figure 4.25 SEM and SEM-EDS line-scan micrographs of supported palladium membrane with Zr diffusion barrier, 0.5 µm on stainless steel substrates exposed in hydrogen at 600°C.

4.4.2.2 ZrO_2 thin films

At 400ºC, no metals penetrated across the interface between zirconium and palladium layers for ZrO_2 barrier, 0.17, 0.35, 0.5 and 1 µm thick, as shown in Figure 4.26. The results indicated that ZrO_2 film with the minimum thickness of 0.17 µm is effective in preventing the intermetallic diffusion at 400ºC. SEM and SEM-EDS line-scan micrographs of the cross-section of ZrO_2 barrier, 0.17 µm thick were shown in Figure 4.27.

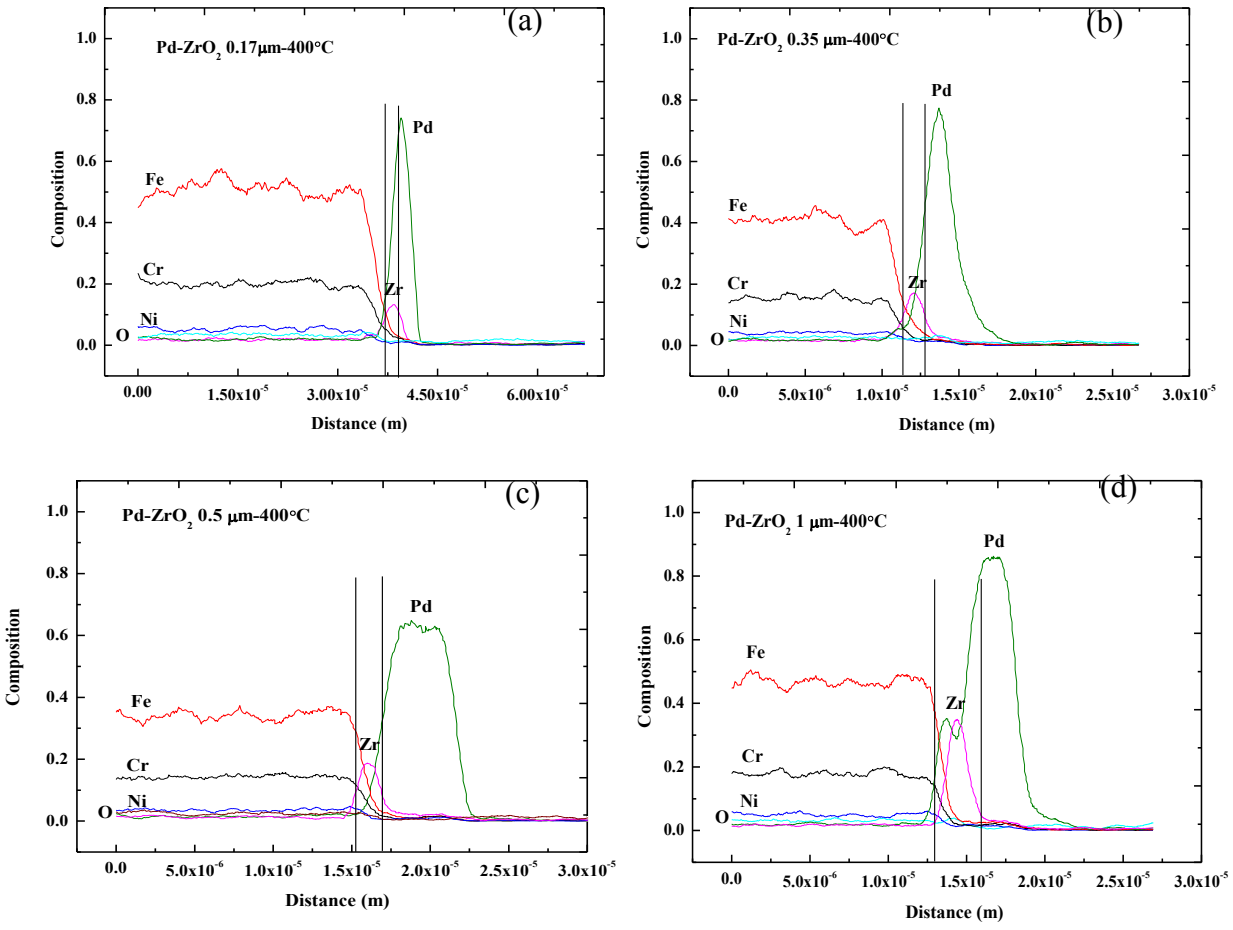

Figure 4.26 SEM-EDS line-scan micrographs of supported palladium membrane with different thickness of ZrO_2 diffusion barriers (a) 0.17µm, (b) 0.35 µm, (c) 0.5 µm, and (d) 1 µm on stainless steel substrates exposed in hydrogen at 400°C.

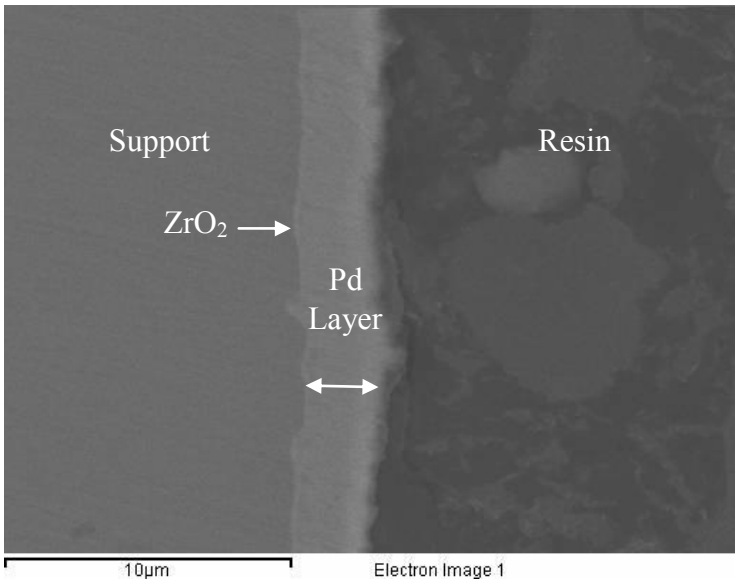

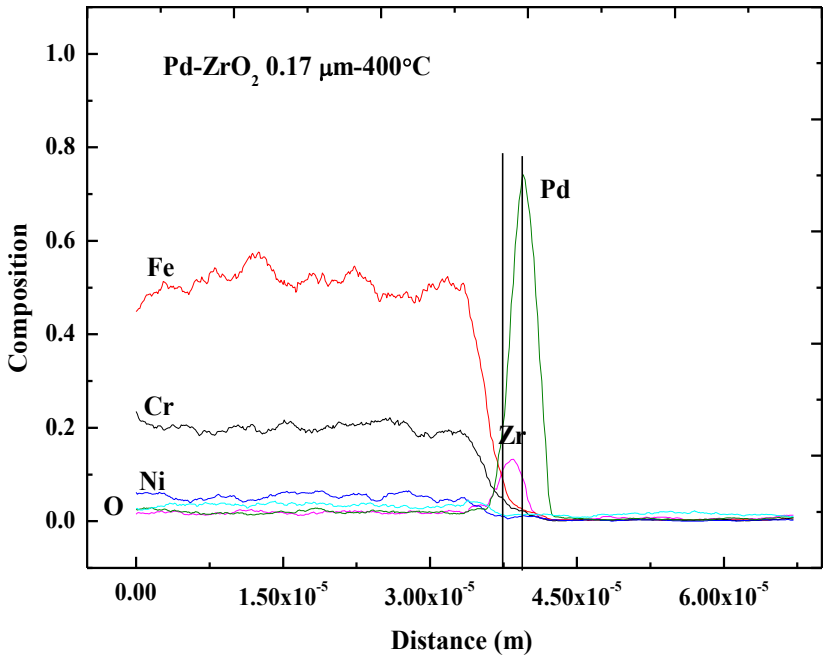

Figure 4.27 SEM and SEM-EDS line-scan micrographs of supported palladium membrane with ZrO_2 diffusion barrier, 0.17 µm on stainless steel substrates exposed in hydrogen at 400°C.

At 500ºC, the metals could diffuse into ZrO_2 barrier, 0.17, 0.35, 0.5 and 1 µm thick but did not reach palladium layer, as shown in Figure 4.28. Thus, the minimum of effective thickness is 0.17 µm at 500ºC. SEM and SEM-EDS line-scan micrographs of the cross-section of ZrO_2 barrier, 0.17 µm thick were shown in Figure 4.29.

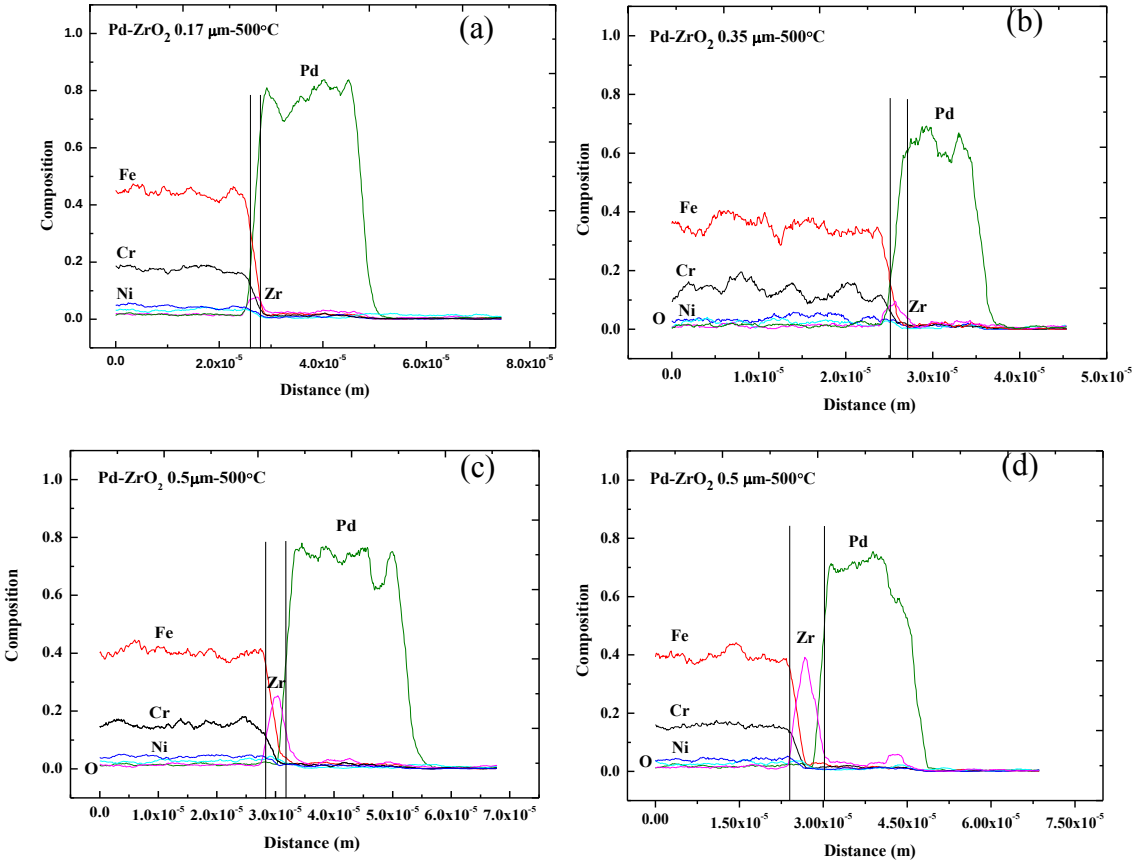

Figure 4.28 SEM-EDS line-scan micrographs of supported palladium membrane with different thickness of ZrO_2 diffusion barriers (a) 0.17µm, (b) 0.35 µm, (c) 0.5 µm, and (d) 1 µm on stainless steel substrates exposed in hydrogen at 500°C.

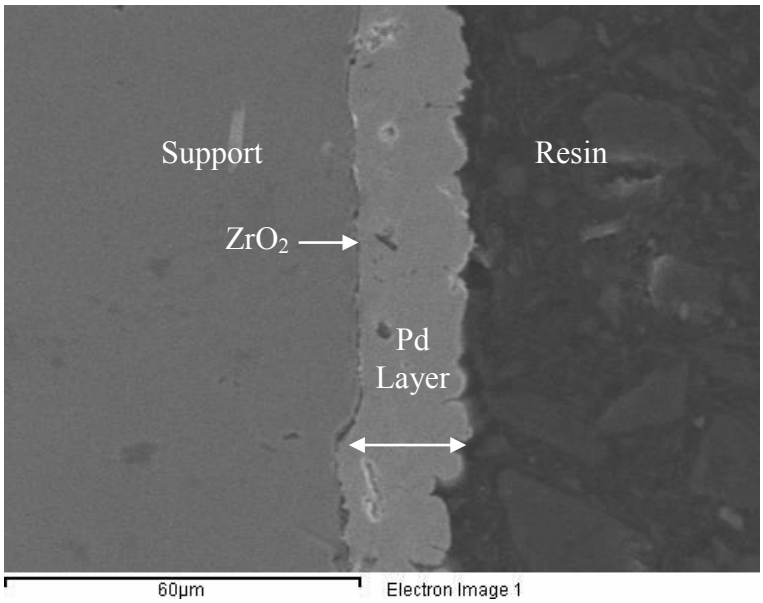

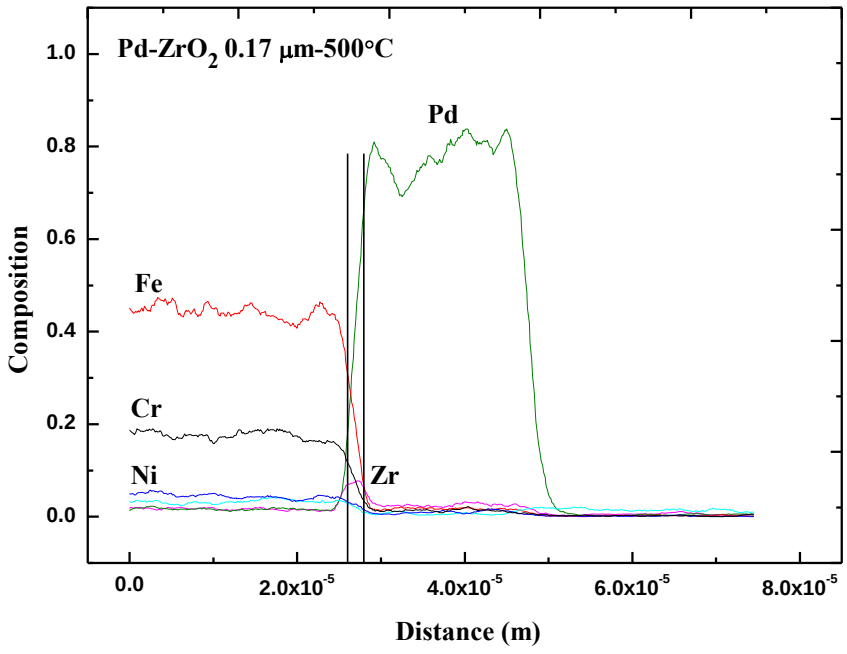

Figure 4.29 SEM and SEM-EDS line-scan micrographs of supported palladium membrane with ZrO_2 diffusion barrier, 0.17 µm on stainless steel substrates exposed in hydrogen at 500°C.

At 600ºC, the metals could not penetrate across the barrier at all thicknesses. The minimum thickness of 0.17 µm could prevent the intermetallic diffusion, as shown in Figure 4.30. Therefore, ZrO_2 with 0.17 µm thick could be used as the effective intermetallic diffusion barrier at 600ºC. SEM and SEM-EDS line-scan micrographs of the cross-section of ZrO_2 barrier, 0.17 µm thick were shown in Figure 4.31.

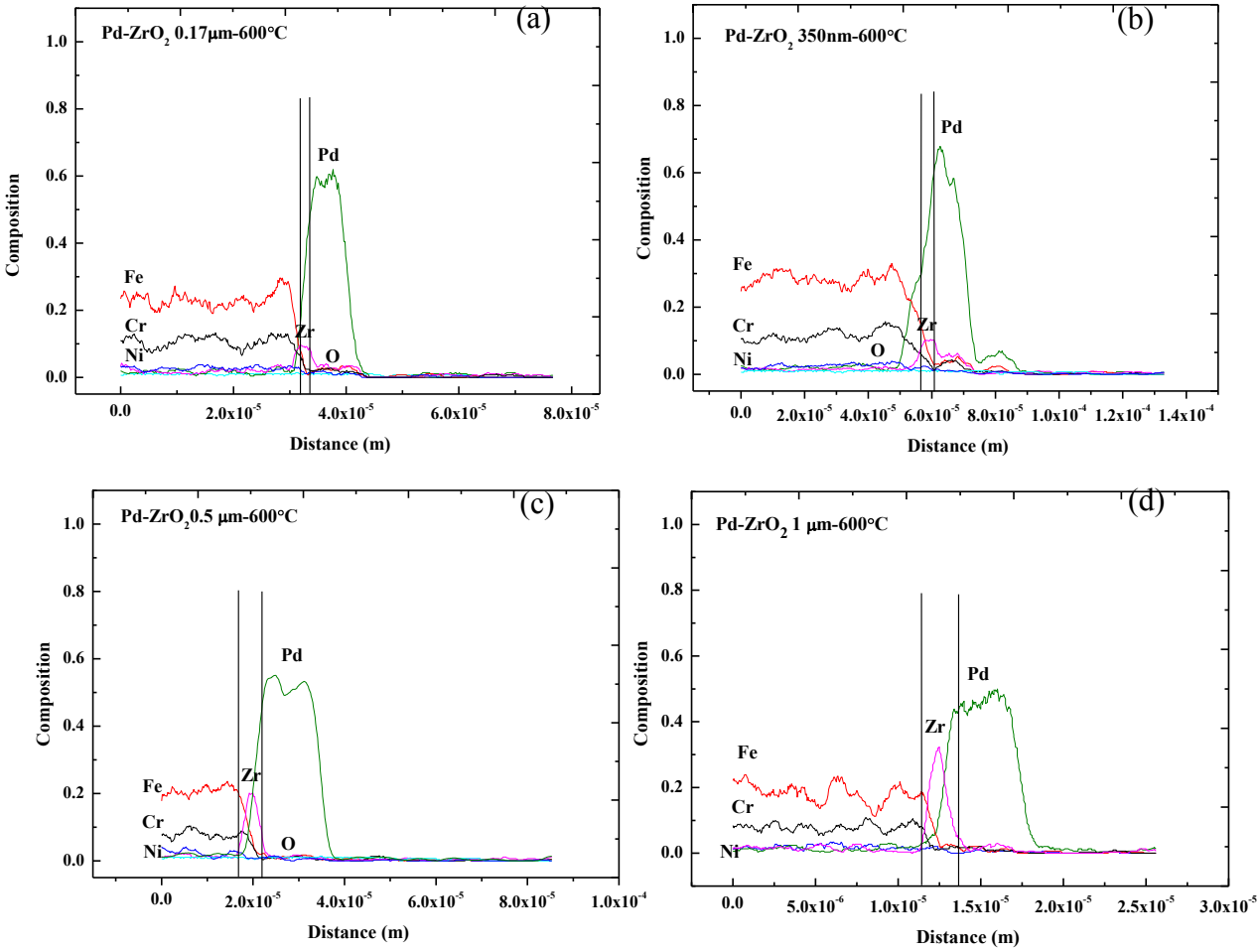

Figure 4.30 SEM-EDS line-scan micrographs of supported palladium membrane with different thickness of ZrO_2 diffusion barriers (a) 0.17µm, (b) 0.35 µm, (c) 0.5 µm, and (d) 1 µm on stainless steel substrates exposed in hydrogen at 600°C.

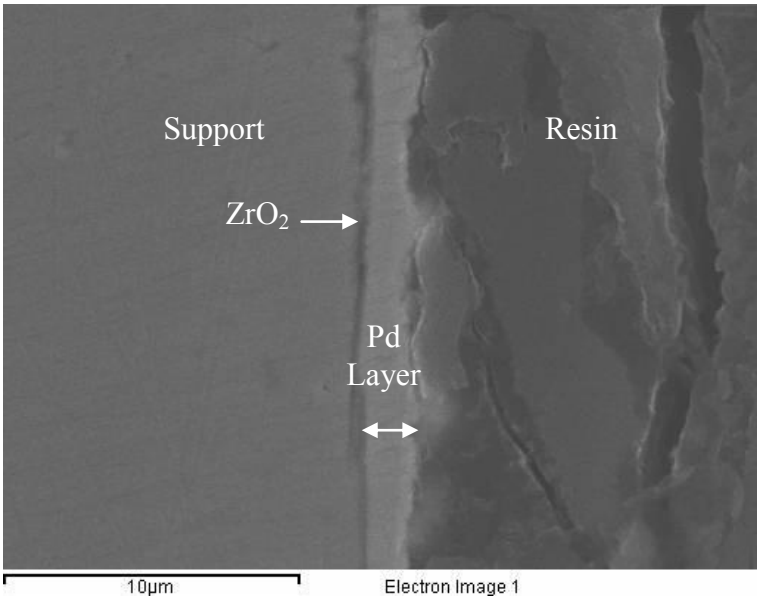

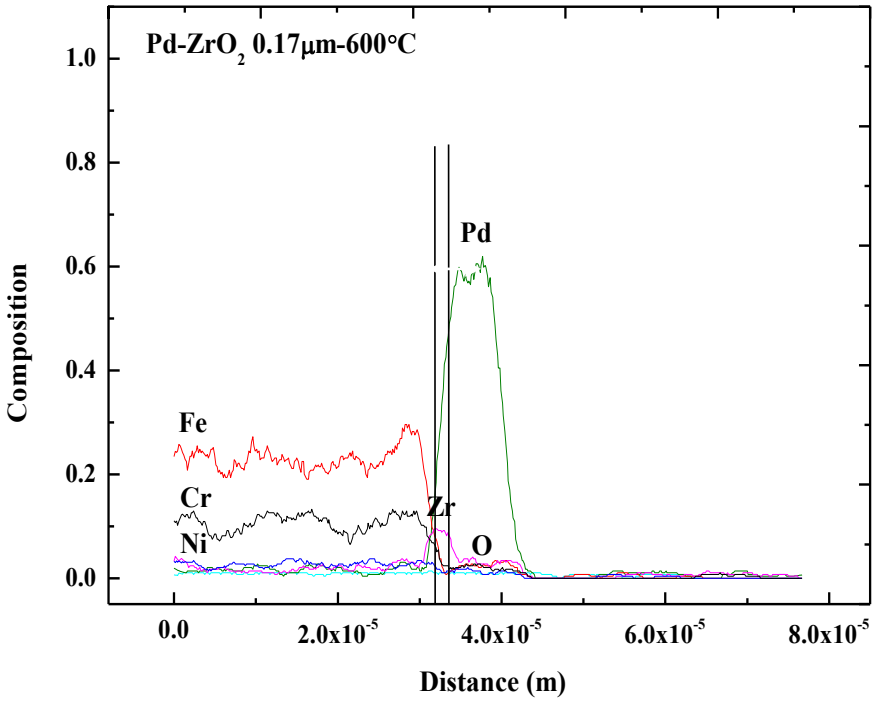

Figure 4.31 SEM and SEM-EDS line-scan micrographs of supported palladium membrane with ZrO_2 diffusion barrier, 0.17 µm on stainless steel substrates exposed in hydrogen at 600°C.

4.4.2.3 ZrN thin films

At 400 ºC, the metal could not migrate into the palladium layer with ZrN barrier, 0.25 0.5, 1 and 1.5 µm thick as shown in Figure 4.32. The results illustrated that ZrN film with the minimum thickness of 0.25 µm has efficiency in preventing intermetallic diffusion at 400 ºC. SEM and SEM-EDS line-scan micrographs of the cross- section of ZrN barrier, 0.25 µm thick were shown in Figure 4.33.

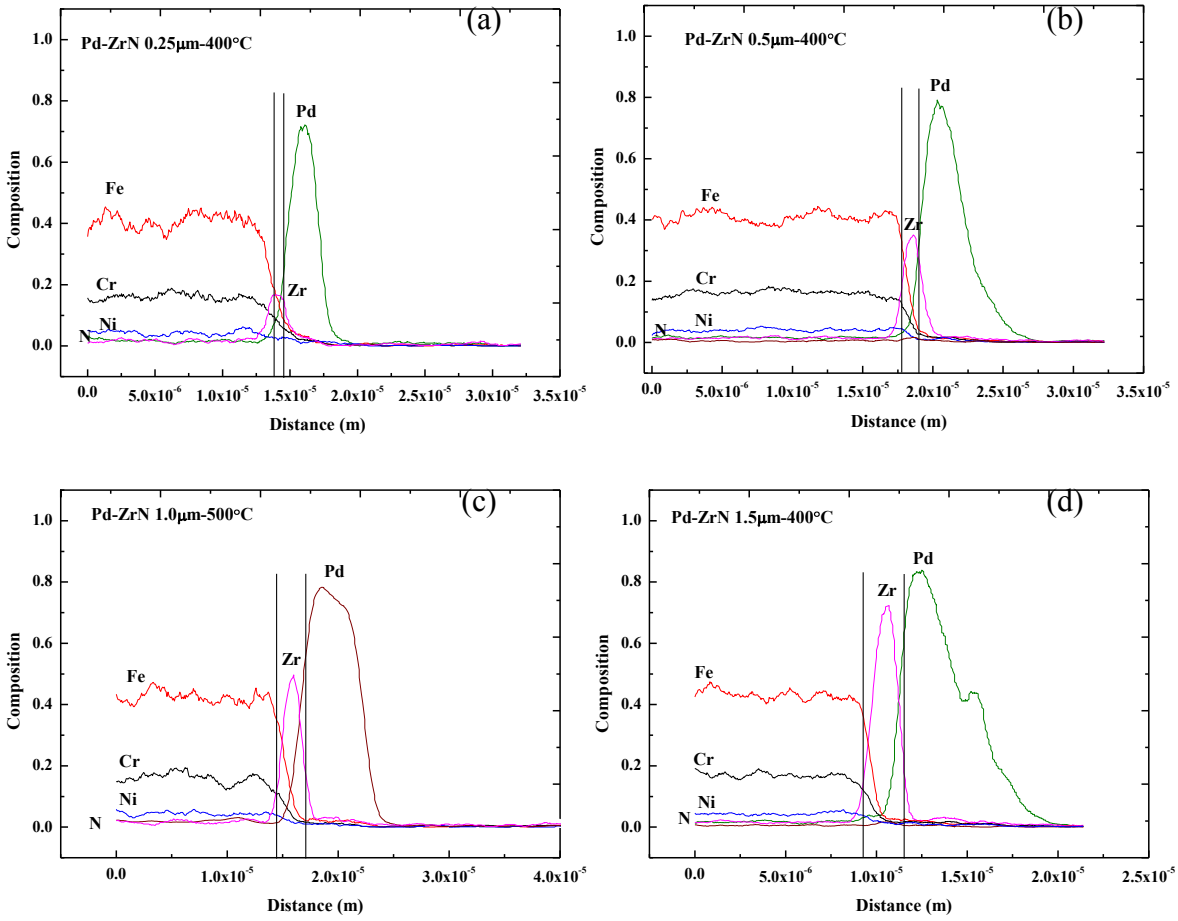

Figure 4.32 SEM-EDS line-scan micrographs of supported palladium membrane with different thickness of ZrN diffusion barriers (a) 0.25µm, (b) 0. 5 µm, (c) 1 µm, and (d) 1.5 µm on stainless steel substrates exposed in hydrogen at 400°C.

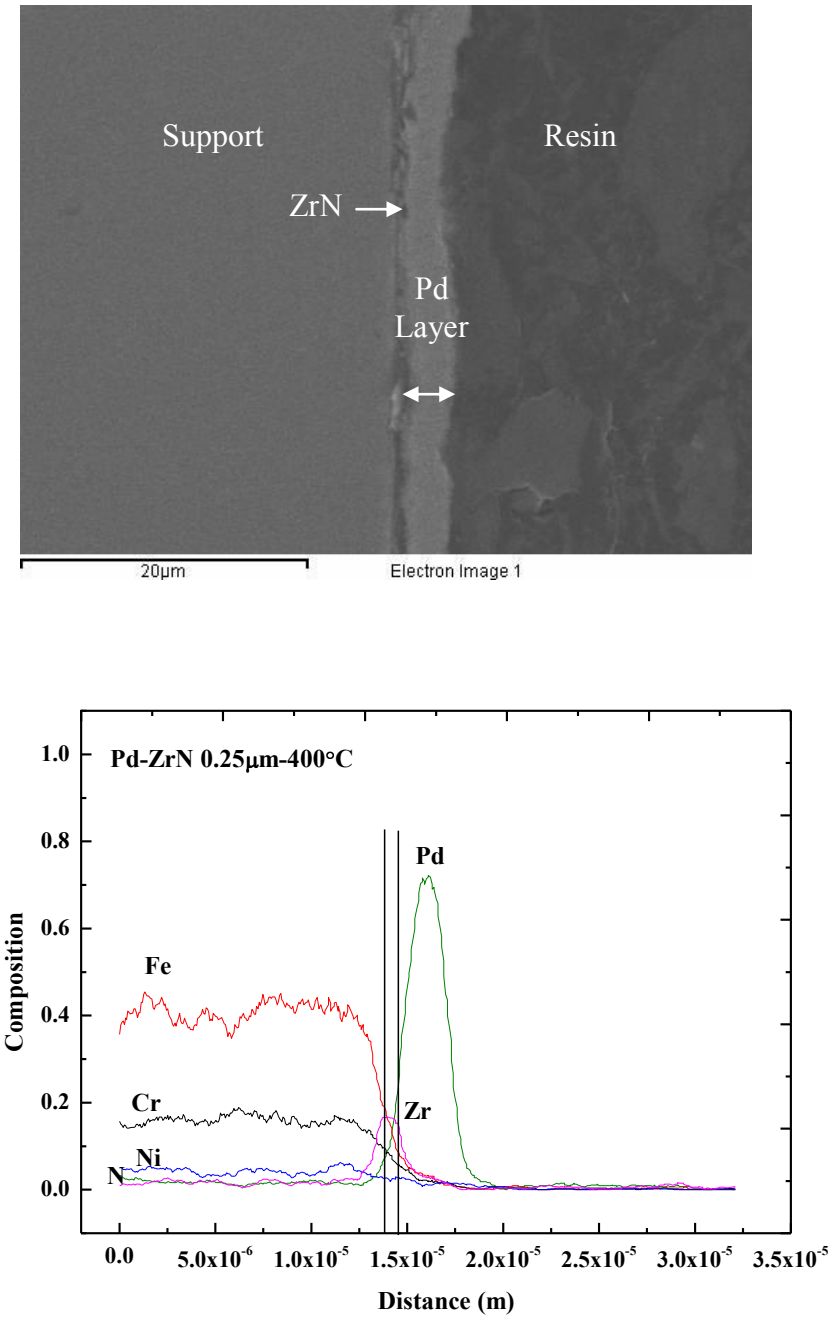

Figure 4.33 SEM and SEM-EDS line-scan micrographs of supported palladium membrane with ZrN diffusion barrier, 0.25 µm on stainless steel substrates exposed in hydrogen at 400°C.

At 500ºC, the metals diffusion into the barrier increased in the order, 1.5 < 1 < 0.5 < 0.25 µm, as shown in Figure 4.34. However, no metals diffused across the ZrN barriers. Thus, the minimum thickness ZrN of 0.25 µm is effective in preventing intermetallic diffusion when exposed in hydrogen at 500 ºC. SEM and SEM-EDS line-scan micrographs of the cross-section of ZrN barrier, 0.25 µm thick were shown in Figure 4.35.

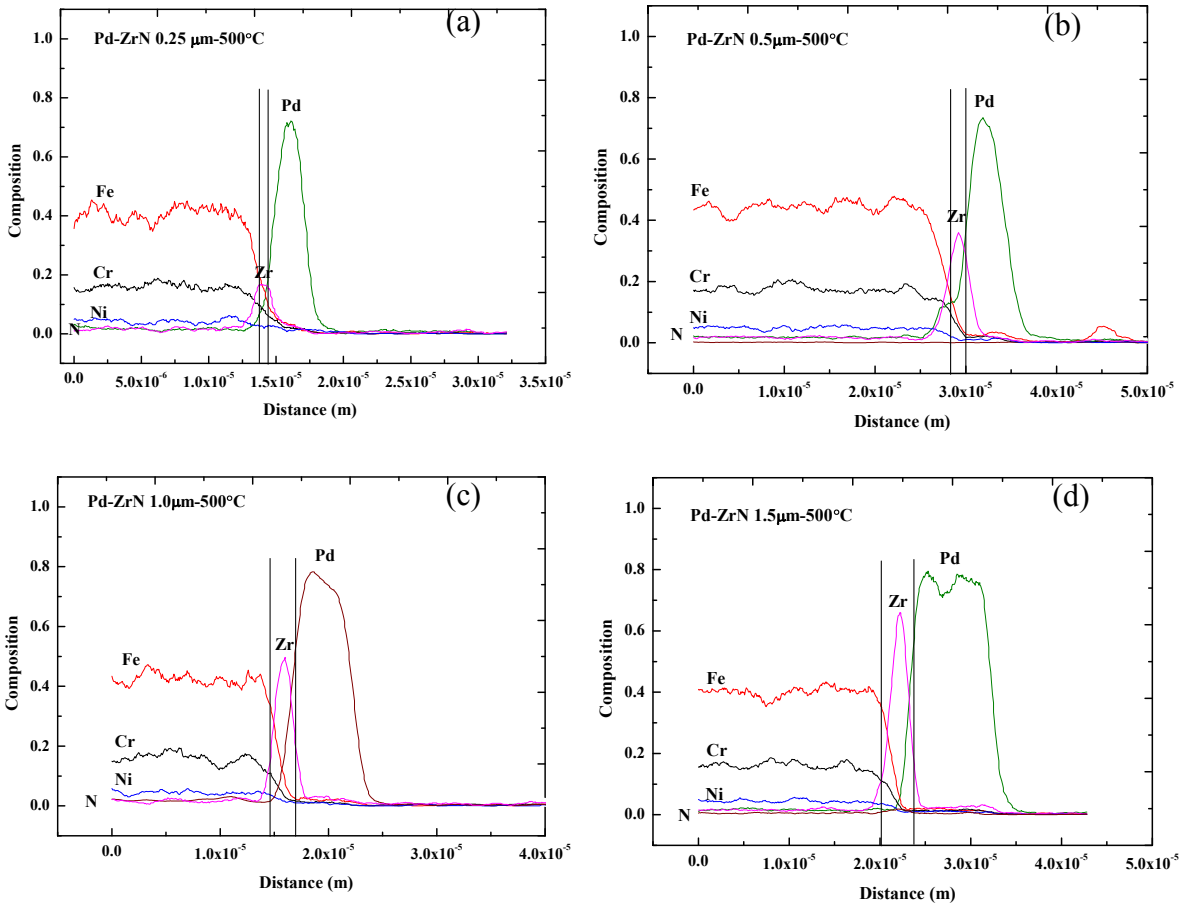

Figure 4.34 SEM-EDS line-scan micrographs of supported palladium membrane with different thickness of ZrN diffusion barriers (a) 0.25 µm, (b) 0.5 µm, (c) 1 µm, and (d) 1.5 µm on stainless steel substrates exposed in hydrogen at 500°C.

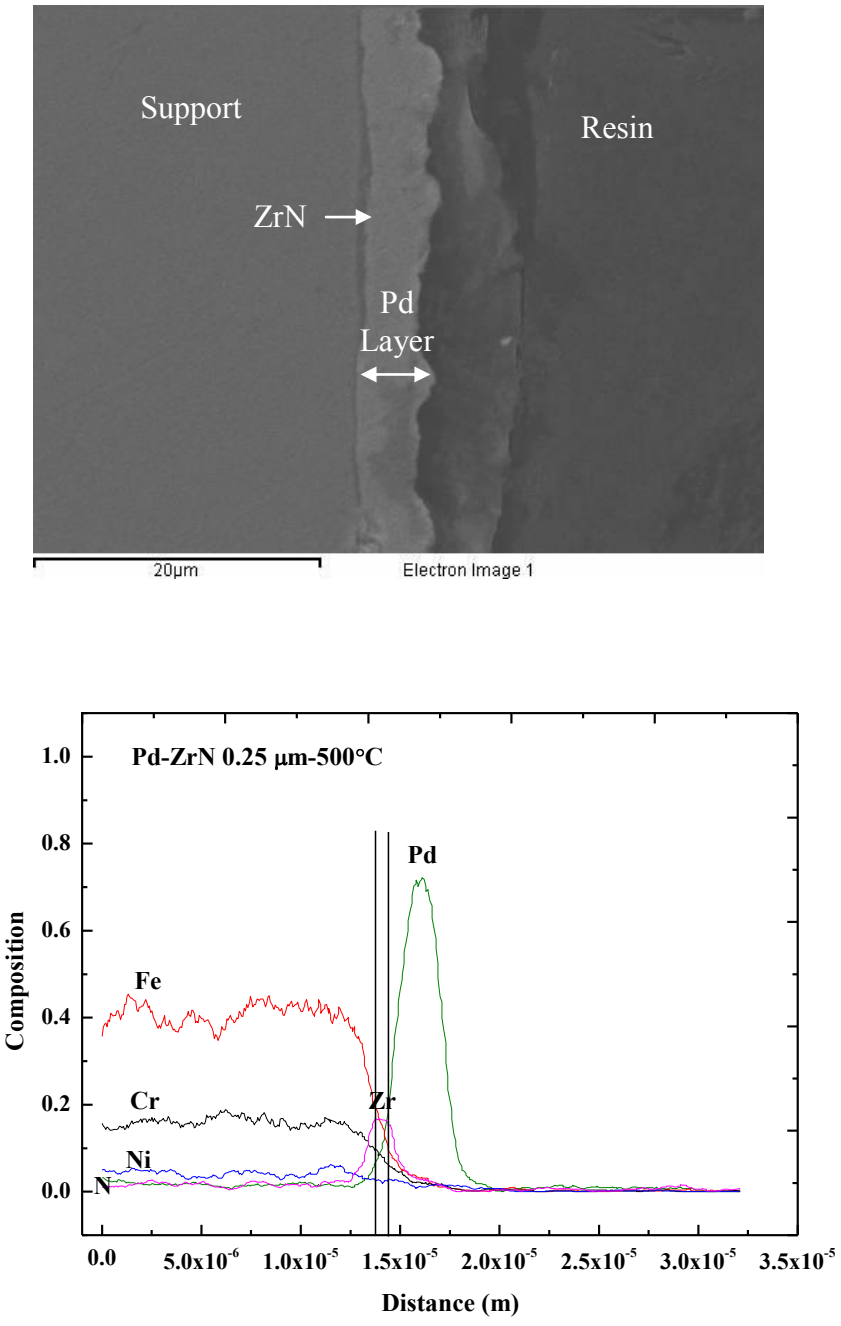

Figure 4.35 SEM and SEM-EDS line-scan micrographs of supported palladium membrane with ZrN diffusion barrier, 0.25 µm on stainless steel substrates exposed in hydrogen at 500°C.

At 600 ° C, Fe and Cr could diffuse across ZrN, 0.25µm thick but could not with the barrier, 0.5, 1 and 1.5 µm thick, as shown in Figure 4.36. Thus, the thickness of at least 0.5 µm was required as the intermeatllic diffusion at 600ºC. SEM and SEM-EDS line-scan micrographs of the cross-section of ZrN barrier, 0.5 µm thick were shown in Figure 4.37.

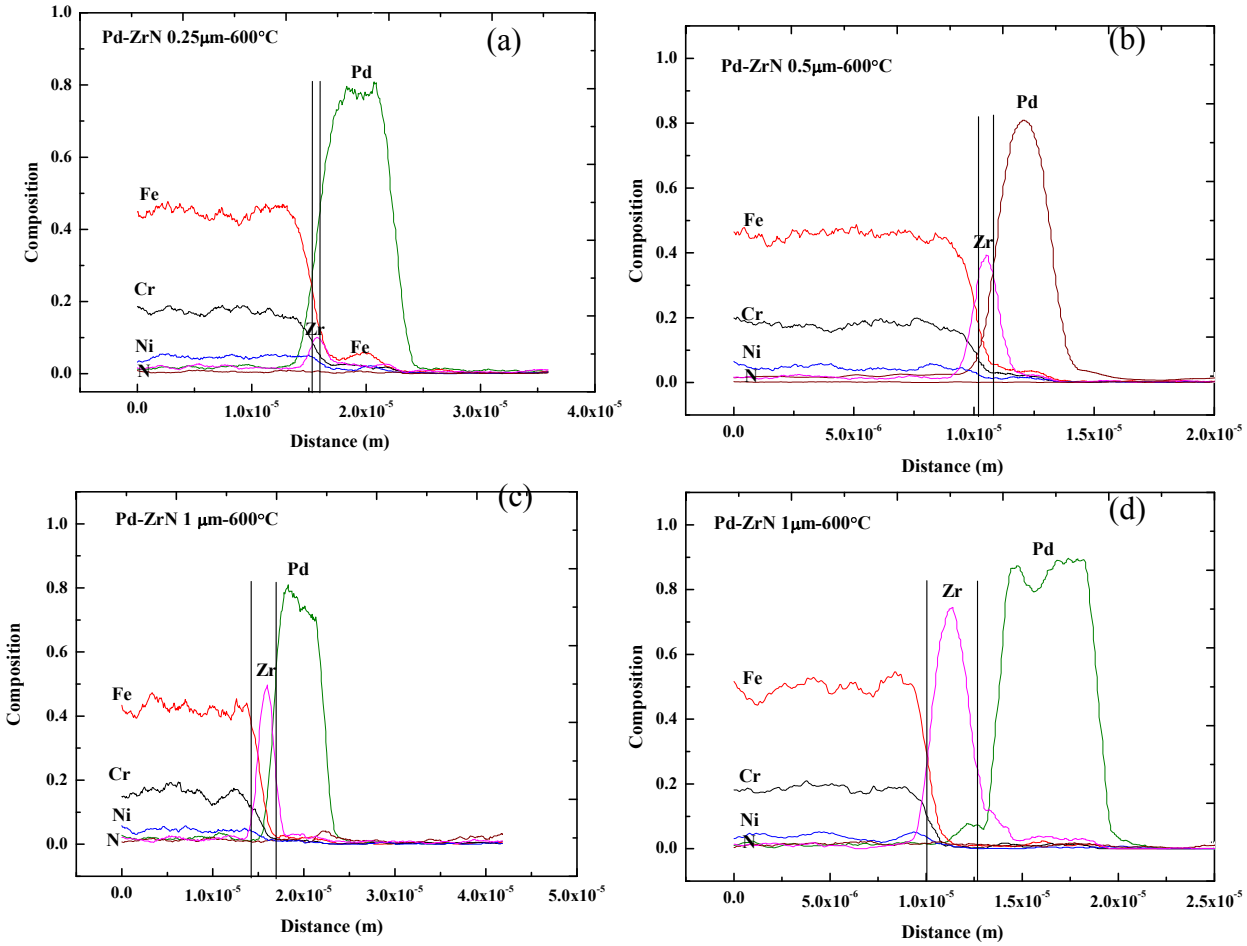

Figure 4.36 SEM-EDS line-scan micrographs of supported palladium membrane with different thickness of ZrN diffusion barriers (a) 0.25µm, (b) 0.5 µm, (c) 1 µm, and (d) 1.5 µm on stainless steel substrates exposed in hydrogen at 600°C

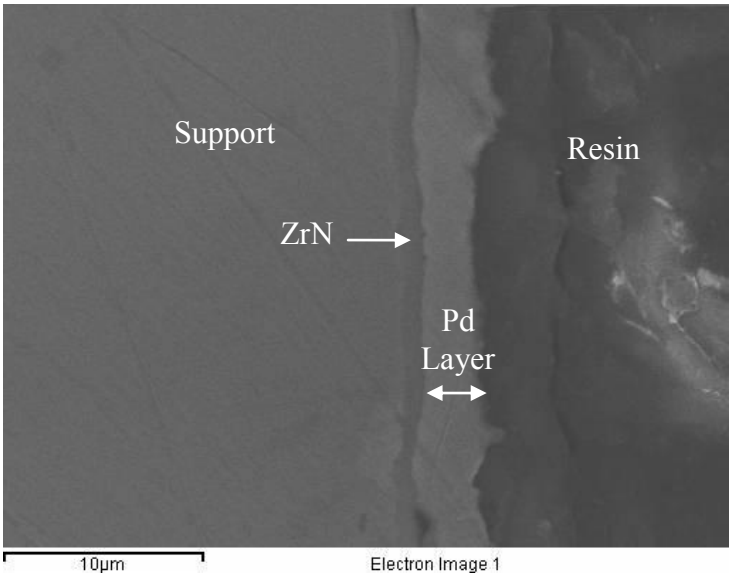

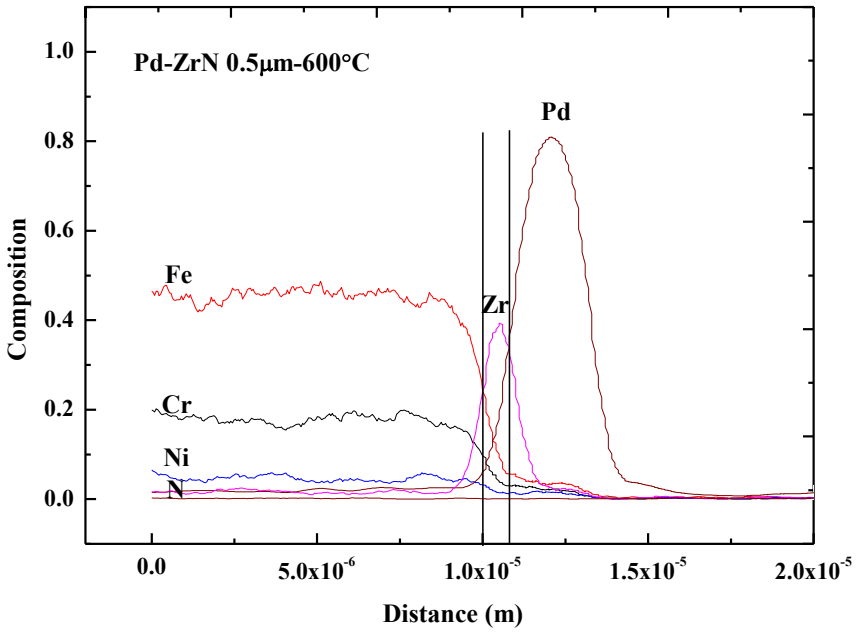

Figure 4.37 SEM and SEM-EDS line-scan micrographs of supported palladium membrane with ZrN diffusion barrier, 0.5 µm on stainless steel substrates exposed in hydrogen at 600°C.

The results showed that all forms of intermetallic diffusion barrier could prevent the diffusion at varying degrees as shown in Table 4.4. At 400 and 500°C, Zr barrier, 0.35 μm thick, and ZrN barrier, 0.25 μm thick could be used as the diffusion barrier but the minimum thickness of 0.5 μm was required at 600°C for both films. However, ZrO_2 films with the thickness of at least 0.17 μm could prevent the metals migration for all temperatures. Their shielding abilities seem to depend on temperature at least in the range of conditions tested 400-600°C for 24 hours, confirmed by more accumulation of metals in the palladium layers with increasing temperature. Thick barriers are also more efficacies in reducing intermetallic diffusion than thin barriers because of longer distance for metal migration and structure stability. To obtain the effective barriers, hydrogen permeation testing was carried out to determine the performance of the prepared films.

Table 4.4 Intermetallic diffusion prevention of Zr-based diffusion barriers at 400-600°C

Film	Zr		ZrO_2	ZrN	
Temp (°C)	0.35 μm	0.5 μm	0.17μm	0.25 μm	0.5 μm
400	✓	✓	✓	✓	✓
500	✓	✓	✓	✓	✓
600	X	✓	✓	X	✓

4.5 Hydrogen permeation

316L porous stainless steel disks, 1 mm thick and an average pore size of 0.2 μm were used as the substrates for hydrogen permeation test. The most suitable barriers in preventing intermetallic diffusion were selected to determine the efficiencies in gas separation, i.e., Zr, 0.5 μm, ZrO_2, 0.17 and 0.5 μm, and ZrN, 0.5 μm. The dense palladium membrane disks with and without diffusion barriers were heated in helium at the rate of about 4°C/min before subjecting to hydrogen at the temperature higher than 300°C due to the cracking effect of the palladium layer by

hydrogen at the temperature below 300°C, known as hydrogen embrittlement [49,50]. Figure 4.38 shows the photographs of an embrittled palladium membrane caused by contamination in gas line during helium flux testing at room temperature.

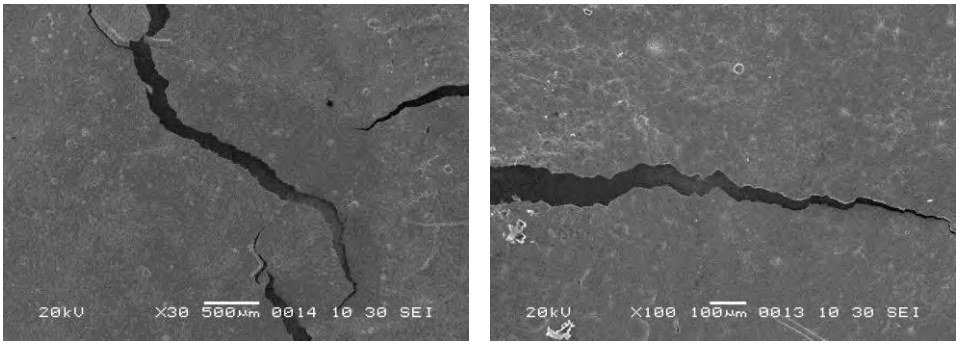

Figure 4.38 SEM image of the crack on palladium due to H_2 embrittlement.

The hydrogen permeation flow rate measured after the required temperature and pressure were reached. The data are in Appendix. The hydrogen permeation flux was calculated as follows

$$H_2 \text{ flux } (m^3/m^2h) = \left(\frac{\text{flow rate of hydrogen gas at permeate side (mL/min)}}{\text{activated surface area of palladium } (cm^2)} \right) \text{ x } 0.6$$

Figure 4.39 shows the plots of the hydrogen permeation flux of palladium membrane with different temperatures and pressures for various diffusion barriers. The hydrogen flux was initially low, then increased with temperature before reaching a steady state. It was clearly indicated that hydrogen flux depended on both pressure and temperature.

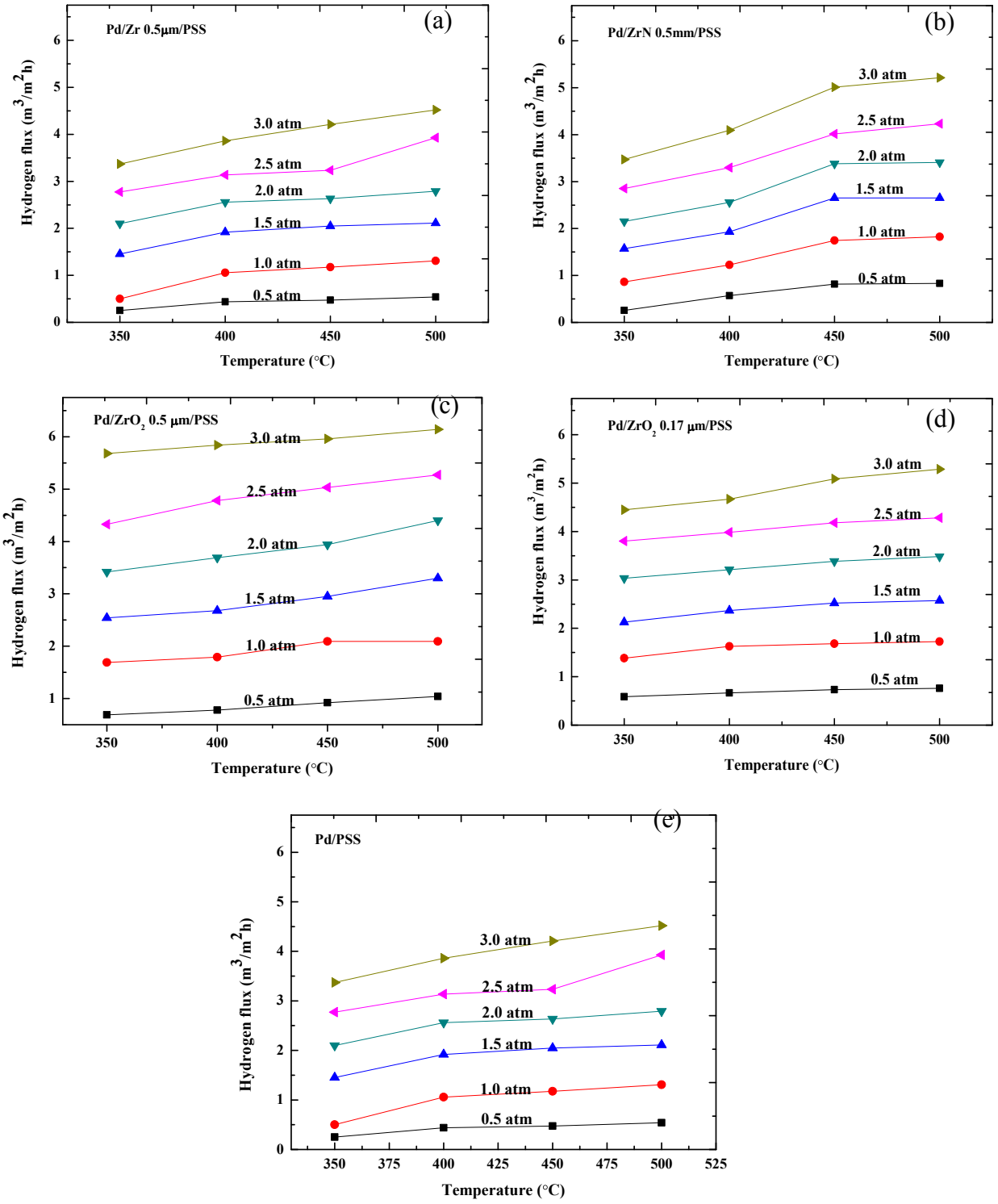

Figure 4.39 Variation of hydrogen flux at different temperatures and pressures for palladium membrane with different barriers: (a) Zr 0.5 μm, (b) ZrO_2 0.17 μm, (c) ZrO_2 0.5 μm, (d) ZrN 0.5 μm and (e) without diffusion barrier.

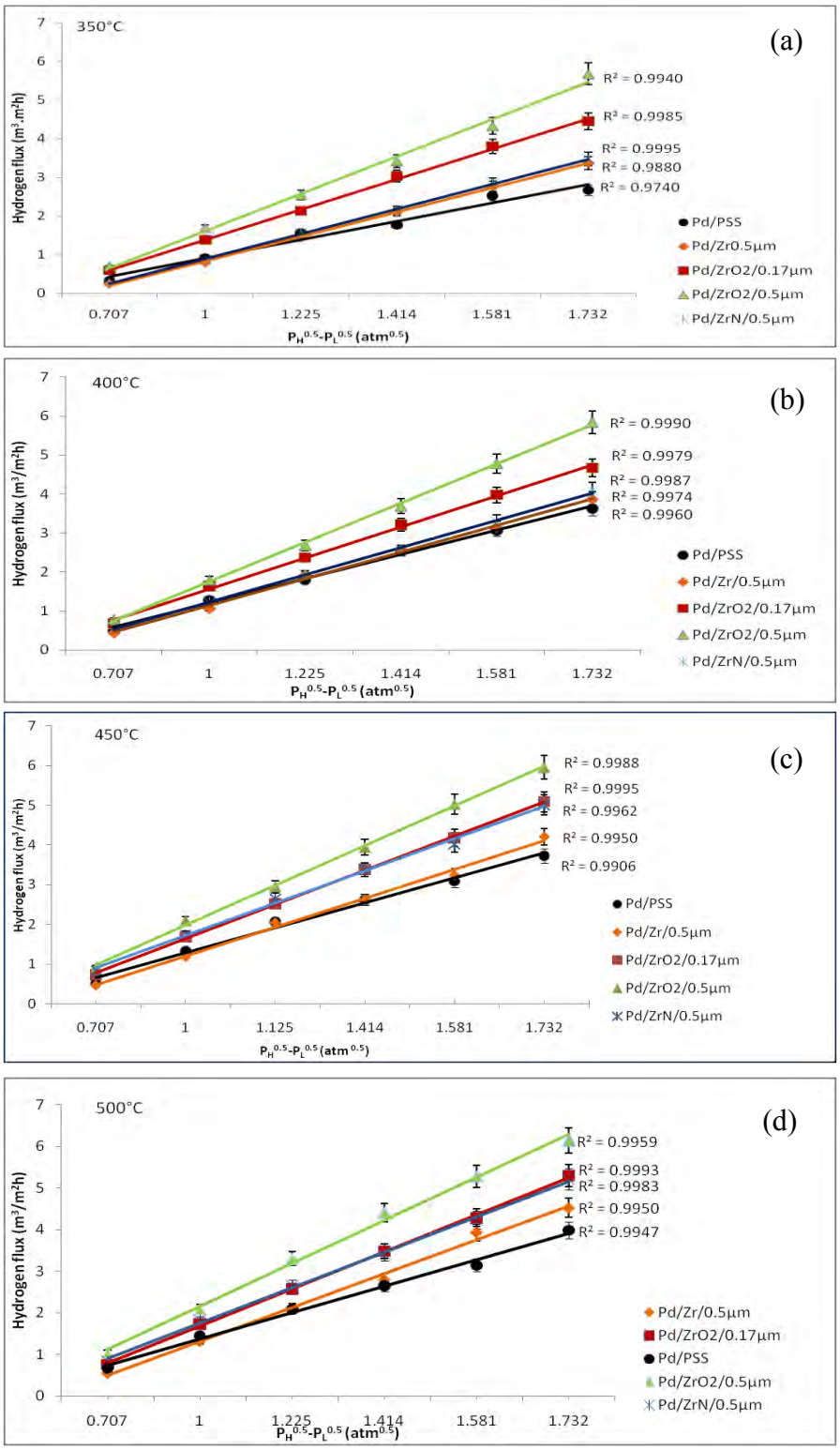

Figure 4.40 Sievert law plots of palladium membrane on different diffusion barriers at (a) 350°C, (b) 400°C, (c) 450°C, and (d) 500°C.

Figure 4.40 shows Sievert law plots of palladium membrane on different diffusion barriers at 350-500°C. The linear relationship between hydrogen permeation flux and the square root of pressure difference ($P_H^{0.5}$-$P_L^{0.5}$) indicates that the hydrogen permeation flux follows the Sieverts' law [51,52], confirming the hydrogen diffusion through palladium membrane as the rate determining step. It was found that at 400 and 450°C, Zr films gave hydrogen permeation flux as low as that obtained from palladium membrane without the diffusion barriers. The hydrogen permeation flux of palladium membrane with diffusion barriers increased in the order, Zr 0.5 μm < ZrN 0.5 μm < ZrO_2 0.17 μm < ZrO_2 0.5 μm.

Hydrogen permeance with various diffusion barriers were shown in table 4.5. It was found that palladium membranes with diffusion barriers give higher hydrogen permeance than palladium membrane without the barrier. Without the barriers, the intermetallic diffusion decreased active sites for gas diffusion of palladium membranes, leading to low hydrogen permeance. Similar results were obtained in the study of Edlund et al., [48] for the intermetallic diffusion between palladium coating-metal layer and the vanadium base-metal layer. They found that hydrogen increased the rate of intermetallic diffusion, and flux decline was correlated to the degree of intermetallic diffusion. When hydrogen dissociates and dissolves in a metal, the hydrogen atoms reside in octahedral or tetrahedral sites in the host metal lattice (in this case, palladium and vanadium). In so doing, the hydrogen atoms perturb the surrounding lattice, causing an overall expansion of the metal lattice by as much as a few percent. The dissolved hydrogen atoms become point defects in the crystal structure and introduce local strain gradients in the metal. The lattice expansion with associated local strain gradients is expected to favor vacancy formation in the metal, thus diffusion of Fe, Cr and Ni increases the rate of intermetallic diffusion in palladium membrane with or without diffusion barriers. In this study, the dissolution of hydrogen atoms into metals, palladium and zirconium increased the concentration of lattice defect sites and also increased the mobility of the defects. Furthermore, the point defects diffuse very rapidly through the palladium membrane and the Zr diffusion barriers, causing the interdiffusion between the palladium membrane and stainless steel supports, leading to a decrease in the active area of palladium

membrane for hydrogen permeation. However, the metal oxides are thermodynamically stable with respect to reaction with hydrogen, the coating metal, and the base metal under anticipated operating conditions [48]. Zirconium oxide meets these requirements and has been shown to effectively prevent the intermetallic diffusion and gives higher hydrogen permeation flux. Moreover, ZrO_2 has monoclinic phase at low temperature and fluorite-type structure with atomic packing factor less than Zr (hexagonal structure) and ZrN (NaCl type structure). Thus, the interstitial vacancies in ZrO_2 lead to higher hydrogen permeation than in Zr and ZrN.

The results were shown in Table 4.5, the hydrogen permeance obtained from palladium membranes with the same thickness of 0.5 μm increased in the order, Zr < ZrN < ZrO_2. Hydrogen permeance obtained from ZrO_2, 0.5 μm thick is higher than 0.17 μm thick because thick film could prevent intermetallic diffusion better than thin film. Thus, the hydrogen permeance increased in the order, Zr 0.5 μm < ZrN 0.5 μm < ZrO_2 0.17 μm < ZrO_2 0.5 μm.

Table 4.5 Hydrogen permeance with various diffusion barriers

Temp (°C)	Hydrogen permeance $m^3(STP)/(m^2.h.atm^{0.5})$				
	No barrier (palladium 35μm)	Zr 0.5 μm (palladium 34μm)	ZrO_2 0.17μm (palladium 35μm)	ZrO_2 0.5 μm (palladium 33μm)	ZrN 0.5 μm (palladium 38μm)
350	0.4771	0.6587	0.7846	0.9640	0.6462
400	0.6228	0.6855	0.7979	1.0008	0.6992
450	0.6263	0.7272	0.8610	1.0088	0.8147
500	0.6353	0.8123	0,8923	1.0316	0.8539

CHAPTER V

CONCLUSION AND RECOMMENDATIONS

5.1 Conclusion

To prevent intermetallic diffusion and prolong the membranes life-time, Zr-based intermediate layers, i.e., zirconium (Zr), zirconium oxide (ZrO_2) and zirconium nitride (ZrN) were applied as diffusion barriers between palladium membranes and stainless steel substrates. The dc magnetron sputter deposition technique was used to deposit Zr thin films, about 0.17-2 μm thick. To obtain ZrO_2 films of the same thickness, Zr films were oxidized in air at 500°C for 1 hour. ZrN thin films were grown by dc reactive magnetron sputtering at nitrogen flow rate of 2 sccm with the thickness ranging from 0.25 to 2 μm. Phase structure, elemental composition and surface morphology of the prepared films were characterized by XRD, EDS and SEM. XRD patterns, indicated that the structure of the prepared Zr, ZrO_2 and ZrN films are hexagonal, a mixture of monoclinic and tetragonal, and NaCl-type structure, respectively. EDS analysis of the ZrO_2 and ZrN films confirmed the near-stoichiometric structure. SEM micrographs indicated that the prepared films were uniform with smooth surface because the layers are so thin that they do not change the macroscopic roughness of the supports. SEM-EDS line scan was used to investigate palladium membranes with and without the diffusion barriers under hydrogen atmosphere at 400-600°C for 24 hours. It was found that at 400 and 500°C, Zr films, 0.35 μm thick, and ZrN films, 0.25 μm thick could be used as the diffusion barriers but the minimum thickness of 0.5 μm was required at 600°C for both films. However, ZrO_2 films with the thickness of at least 0.17 μm could inhibit the metals migration for all temperatures. The effectiveness of the diffusion barriers was found to increase in the order $Zr < ZrN < ZrO_2$.

The hydrogen permeation testing was carried out at 350-500°C and 0.5-3 atm. It was found that the hydrogen permeation flux obtained from palladium membrane with the diffusion barriers was higher than that without. The hydrogen permeation flux with the diffusion barriers increased in the order, Zr 0.5 μm < ZrN 0.5 μm < ZrO_2 0.17 μm < ZrO_2 0.5 μm. It is obvious that ZrO_2 not only effective in preventing the intermetallic diffusion but also promote hydrogen permeation. Thus, it can be concluded that ZrO_2 thin film is the most suitable intermetallic diffusion barrier for stainless steel supported palladium membranes used for hydrogen separation process.

5.2 Recommendations

- Prepare ZrO_2 layer by sol-gel method and compare its diffusion preventing efficacy.
- Test the palladium membrane selectivity and the life time with the Zr-based intermetallic diffusion barriers.

REFERENCES

[1] Li, A.; Grace, J.R.; and Lim, C.J. Preparation of thin Pd-based composite membrane on planar metallic substrate Part II. Preparation of membranes by electroless plating and characterization. **Journal of membrane science** 306(2007): 159-165.

[2] Wang, W.; Pan, X; Zhang, X.; Yang, W.; and Xiong, G. The effect of co-existing nitrogen on hydrogen permeation through thin Pd composite membranes. **Separation and Purification Technology** 54(2007): 262-271.

[3] Sato, I.; Takaki, M.; Arima, T.; Furuya, H.; Idemitsu, K.; Inagaki, Y.; Momoda, M.; and Namekawa, T. Oxidation behavior of modified SUS316 (PNC316) stainless steel under low oxygen partial pressure. **Journal of Nuclear Materials** 304(2002): 21-28.

[4] Robert, E.B.; and Peter, C.H. Measurement of diffusive and surface transport resistances for deuterium in palladium-coated zirconium membranes. **Journal of Nuclear Materials** 189(1992): 183-192.

[5] Knapton, A.G. Palladium Alloys for Hydrogen Diffusion Membranes A REVIEW OF HIGH PERMEABILITY MATERIALS. **Platinum Metals Review** 21(1977): 44-50.

[6] Bruce, R.L.; Omar, I.; Way, J.D.; David, E.; and Kent, C. Un-supported Palladium Alloy Membranes for the Production of Hydrogen. **Inorganic Membranes for Energy and Environmental Applications** (2009): 203-219.

[7] Ma, Y.H. Composite Pd and Pd/Alloy Membranes. **Inorganic Membranes for Energy and Environmental Applications** (2008): 241-254.

[8] Palladium Membrane Purification [Online]. 2006 Available from: http://pureguard.net/cm/Library/Palladium_Membrane_Purification.html [2010, March 1]

[9] Samingprai, S. **Dry Reforming of Methane Using Dense Palladium Membrane Supported on Porous Stainless Steel** Doctor of Philosophy's Thesis, Program of Petrochemistry, Faculty of Science, Chulalongkorn University, 2006.

[10] Diffusion: the Phenomena (1) (Interdiffusion) [Online]. 2006 Available from: http://www.fen.bilkent.edu.tr/~bengu/chem201/FinalCourseNotes/Chapter_05_avi_erman.ppt [2010, March 1]

[11] Diffusion in Solids [Online]. 2005 Available from: http://dmseg5.case.edu/classes/emse201/overheads/Diffusio1.pdf [2010, March 1]

[12] Diffusion [Online]. 2005 Available from: http://www.matsceng.ohio-state.edu/mse205/lectures/chapter5/chap5.pdf [2010, March 1]

[13] Non-steady State Diffusion [Online]. 2005 Available from: http://www.matsceng.ohiostate.edu/mse205/lectures/chapter5/chap5.pdf [2010, March 1]

[14] Zirconium [Online]. 2002 Available from: http://en.wikipedia.org/wiki/Zirconium [2010, March 1]

[15] Čyvienė, J.; and Dudonis, J. Zr, ZrN and Zr/Al Thin Films Deposition Using Arc Evaporation and Annealing. **Acta Physica Polonica A** 114(2008): 769-776.

[16] Solids and Crystal Structure [Online]. 2005 Available from: http://www.chem.ufl.edu/~itl/2045/lectures/lec_h.html

[17] Zirconium Oxide [Online]. 2000 Available from: http://www.designinsite.dk/htmsider/m1014.htm [2010, March 1]

[18] Chen, I.; Yeh, S.; Chiou, S.; Gan, D.; and Shen, P. Condensation of tetragonal zirconia polycrystals by reactive sputtering. **Thin Solid Films** 491 (2005): 339-346.

[19] Pamu, D.; Sudheendran, K.; Krishna, M.; Raju, K.; and Bhatnagar, A. Ambient temperature stabilization of crystalline zirconia thin films deposited by direct current magnetron sputtering. **Thin Solid Films** 517(2009): 1587-1591.

[20] Zirconium Oxide [Online]. 2000 Available from: http://www.keramverband.de/brevier_engl/3/4/2/3_4_2_3.htm [2010, March 1]

[21] William, D. S.; Michale, E.G.; Ming-Show, W.; Paul, J.R.; and Keith, O.L. **Hard and Protective Materials**, IOP Publishing, 1996.

[22] Arias, D.F.; Arango, Y.C.; and Devia, A. Study of TiN and ZrN thin films grown by cathodic arc technique. **Applied Surface Science** 253 (2006): 1683-1690.

[23] NaCl Type Structure [Online]. 2000 Available from: http://www.tf.uni-kiel.de/matwis/amat/def_en/kap_2/basics/b2_1_6.html

[24] Rointan, F.B. **Coatings Science, Technology and Applications** New Jersey: Noyes Pubbilcation, 1994.

[25] John, V. **Introduction to Surface and Thin Film Processes** New York: Cambridge University, 2001.

[26] Brain, C. **Glow Discharge Processes: Sputtering and Plasma Etching** New York: John Wiley and Sons, 1980.

[27] Behrisch, R.; and Wittmaack, K. **Sputtering by Particle Bombardment III: Characteristics of Sputtered Particles, Technical Applications** Berlin: Springer-Verlag, c1991.

[28] X-Ray Diffraction (XRD) [Online]. 2002 Available from: http://prism.mit.edu/xray/BasicsofXRD.ppt [2010, March 1]

[29] Scanning Electron Microscopy **(**SEM) **[**Online]. 2005 Available from: https://wiki.usask.ca/bio_tech_doc/index.php/How_an_SEM_works [2010, March1]

[30] Yeh, S.W.; Hsieh, T.Y.; Huang, H.L.; Gana, D.; and Shen, P. Annealing induced oxidation and transformation of Zr thin film prepared by ion beam sputtering deposition. **Materials Science and Engineering A** 452-453 (2007): 313–320.

[31] Zhang, K.; Gao, H.; Rui, Z.; Liu, P.; Li, Y.; and Lin, Y.S. High-Temperature Stability of Palladium Membranes on Porous Metal Supports with Different Intermediate Layers. **Industrial & Engineering Chemistry Research** 48(2009): 1880-1886.

[32] Soo, Y. L.; Chen, P.J.; Huang ,S.H.; Shiu, T.J.; Tsai, T.Y.; Chow, Y. H.; Lin, Y.C.; Weng ,S.C.; Chang, S.L.; Wang, G.; Cheung, C.L.; Sabirianov, R.F.; Mei, W.N.; Namavar, F.; Haider, H.; Garvin, K.L.; Lee, H.Y.; and Chu, P.P. Local structures surrounding Zr in nanostructurally stabilized cubic zirconia: Structural origin of phase stability. **Journal of Applied Physics** 104(2008): 113-535.

[33] Larijani, M.; Tabrizi, N.; Norouzian, S.; Jafari, A.; Lahouti, S.; Hosseini, H. H.; and Afshari, N. Structural and mechanical properties of ZrN films prepared by ion beam sputtering with varying N_2/Ar ratio and substrate temperature. **Vacuum** 81(2006): 550-555.

[34] Takeyama, M.B.; Itoi, T.; Aoyagi, E.; and Noya, A. High performance of thin nano-crystalline ZrN diffusion barriers in Cu/Si contact systems. **Applied Surface Science** 190(2002): 450-454.

[35] Nam, S.E.; and Lee, K.H. Preparation and Characterization of Palladium Alloy Composite Membranes with a Diffusion Barrier for Hydrogen Separation. **Industrial & Engineering Chemistry Research** 44 (2005): 100-105.

[36] Zahedi, M.; Afra, B.; Dehghani-Mobarake, M.; and Bahmani, M. Preparation of a Pd membrane on a WO_3 modified Porous Stainless Steel for hydrogen separation. **Journal of Membrane Science** 333(2009): 45-49.

[37] Gao, H.; Lin, J.Y.S.; Li, Y.; and Zhang, B. Electroless plating synthesis, characterization and permeation properties of Pd–Cu membranes supported on ZrO_2 modified porous stainless steel. **Journal of Membrane Science** 265(2005): 142-152.

[38] Era, H.; Ide, Y.; Nino, A.; and Kishitake, K. TEM study on chromium nitride coatings deposited by reactive sputter method. **Surface & Coating Technology** 194(2005): 265-270.

[39] Ryi, S.K.; Park, J.S.; Kim, S.H.; Cho, S.H.; Kim, D.W.; and Um, K.Y. Characterization of Pd-Cu-Ni ternary alloy membrane prepared by magnetron sputtering and Cu-reflow on porous nickel support for hydrogen separation. **Separation and Purification Technology** 50 (2006): 82-91.

[40] Liu, C.P.; and Yang, H.G. The Texture and electrical properties of Zr and ZrN_x thin films deposited by DC sputtering. **Material Research Society Symposium Proceedings** 721 (2002): J4-9.

[41] Pulzara, A.; Pineda P.; Arias D.;Aranfo J.; and Devia A. ZrN Hard Coating by PAPVD. **Revista Colombiana De Fīsica** 34(2002): 95-99.

[42] Steiner, P.; Sander, I.; Siegwart, B.; and Hüfner, S. Oxidation of Zr and thin (0.2–4 nm) Zr films on Ag: an ESCA investigation. **Fresenius' Journal of Analytical Chemistry** 329(1987): 272-277.

[43] Martin, F.; Ayouchi, R; Ruiz, C.; Ramos-Barrado, J.R.; and Leinen, D. Compositional and structural characterization of zirconia films with reticular structure obtained by spray pyrolysis. **Surface and Interface Analysis** 34(2002): 719-723.

[44] Ruan, J.; Lii, D.; Lu, H.; Chen, J.; and Huang, J. Investigation of substrate bias effects on the reactively sputtered ZrN diffusion barrier films. **Ceramics International** 35(2009): 1999-2005.

[45] Ruan, J.; Lii, D.; Lu, H.; Chen, J.; and Huang, J. Microstructural and electrical characteristics of reactively sputtered ZrNx thin films. **Journal of Alloys and Compounds** 478(2009): 671-675.

[46] Mardilovich, P.P.; Ma, Y.H.; and Rei, M.H. Defect-free palladium membranes on porous stainless-steel support. **American Institute of Chemical Engineers Journal** 44(2004): 310-322.

[47] Yeung, K.L.; Christiansen, S.C.; and Varma, A. Palladium composite membranes by electroless plating technique Relationships between plating kinetics, film microstructure and membrane performance. **Journal of Membrane Science** 159(1999): 107-122.

[48] Edlund, D.J.; and McCarthy, J. The relationship between intermetallic diffusion and flux decline in composite-metal membranes: implications for achieving long membrane lifetime. **Journal of Membrane Science** 107 (1995): 147-153.

[49] Huang, Y.; and Dittmeyer, R. Preparation and characterization of composite palladium membranes on sinter-metal supports with a ceramic barrier against intermetallic diffusion. **Journal of Membrane Science** 282 (2006): 296-310.

[50] Jaroenporn, C. **Cr-Base Intermetallic Diffusion Barrier for Stainless Steel Supported Palladium membrane** Master's Thesis, Program of Petrochemistry and Polymer Science, Faculty of Science, Chulalongkorn University, 2007.

[51] Samingprai, S.; Tantayanon, S. and Ma, Y.H. Chromium oxide intermetallic diffusion barrier for palladium membrane supported on porous stainless steel. **Journal of Membrane Science** 347(2010): 8-16.

[52] Lin, A.; Grace, J.R.; and Lim, C.J. Preparation of thin Pd-based composite membrane on planar metallic substrate Part II. Preparation of membranes by electroless plating and characterization. **Journal of Membrane Science** 306 (2007): 159-165.

APPENDIX

APPENDIX

1. Hydrogen flow rate of palladium membrane with Zr, 0.5 µm thick

Temp (°C)	Zr 0.5µm	Flow rate (mL/min) at different pressure (atm)					
		0.5	1.0	1.5	2.0	2.5	3.0
350°C	1	0.59	1.58	2.91	4.21	5.54	6.72
	2	0.61	1.57	2.90	4.16	5.54	6.76
	3	0.65	1.55	2.88	4.18	5.50	6.67
	Avg	0.62	1.57	2.90	4.18	5.52	6.71
	SD	0.03	0.02	0.02	0.03	0.02	0.05
400°C	1	0.87	2.09	3.81	5.11	6.23	7.68
	2	0.86	2.12	3.76	5.12	6.26	7.65
	3	0.88	2.11	3.90	5.07	6.25	7.74
	Avg	0.87	2.11	3.82	5.10	6.25	7.69
	SD	0.01	0.01	0.07	0.03	0.01	0.05
450°C	1	0.97	2.33	4.07	5.22	6.51	8.43
	2	0.95	2.38	4.06	5.29	6.42	8.39
	3	0.91	2.32	4.12	5.23	6.40	8.34
	Avg	0.94	2.34	4.08	5.25	6.45	8.39
	SD	0.03	0.03	0.03	0.04	0.06	0.04
500°C	1	1.12	2.60	4.23	5.55	7.94	9.05
	2	1.07	2.60	4.20	5.55	7.80	8.97
	3	1.04	2.62	4.19	5.58	7.74	8.98
	Avg	1.08	2.61	4.21	5.56	7.83	9.00
	SD	0.038	0.012	0.019	0.020	0.100	0.044

2. Hydrogen flow rate of palladium membrane with ZrO_2 0.17 µm thick

Temp (°C)	ZrO_2 0.17µm	Flow rate (mL/min) at different pressure (atm)					
		0.5	1.0	1.5	2.0	2.5	3.0
350°C	1	1.16	2.74	4.22	6.04	7.64	8.88
	2	1.17	2.77	4.25	6.03	7.56	8.85
	3	1.18	2.76	4.24	6.05	7.52	8.85
	Avg	1.17	2.76	4.24	6.04	7.57	8.86
	SD	0.01	0.02	0.02	0.01	0.06	0.02
400°C	1	1.33	3.24	4.7	6.41	7.94	9.3
	2	1.32	3.25	4.72	6.39	7.93	9.31
	3	1.33	3.24	4.73	6.38	7.93	9.3
	Avg	1.33	3.24	4.72	6.39	7.93	9.30
	SD	0.01	0.01	0.02	0.02	0.01	0.01
450°C	1	1.46	3.36	5.01	6.70	8.28	10.17
	2	1.46	3.35	5.05	6.83	8.37	10.22
	3	1.46	3.34	5.01	6.68	8.33	10.02
	Avg	1.46	3.35	5.02	6.74	8.33	10.14
	SD	0.00	0.01	0.03	0.08	0.05	0.11
500°C	1	1.50	3.42	5.13	7.01	8.57	10.27
	2	1.52	3.44	5.15	6.90	8.46	10.79
	3	1.53	3.44	5.11	6.90	8.57	10.54
	Avg	1.52	3.43	5.13	6.94	8.54	10.54
	SD	0.01	0.01	0.02	0.06	0.06	0.26

3. Hydrogen flow rate of palladium membrane with ZrO_2 0.5 µm thick

Temp (°C)	ZrO_2 0.5µm	Flow rate (mL/min) at different pressure (atm)					
		0.5	1.0	1.5	2.0	2.5	3.0
350°C	1	1.36	3.36	5.05	6.76	8.57	11.24
	2	1.39	3.36	5.05	6.83	8.65	11.43
	3	1.39	3.39	5.08	6.86	8.65	11.30
	Avg	1.38	3.37	5.06	6.82	8.62	11.32
	SD	0.018	0.014	0.015	0.048	0.043	0.098
400°C	1	1.54	3.56	5.33	7.39	9.68	11.63
	2	1.56	3.55	5.32	7.35	9.51	11.56
	3	1.55	3.56	5.33	7.33	9.36	11.72
	Avg	1.55	3.56	5.33	7.36	9.52	11.64
	SD	0.01	0.00	0.01	0.03	0.16	0.08
450°C	1	1.83	3.95	5.87	7.86	10.00	11.98
	2	1.83	4.03	5.85	7.89	10.00	11.86
	3	1.83	4.06	5.89	7.80	10.05	11.79
	Avg	1.83	4.01	5.87	7.85	10.02	11.87
	SD	0.00	0.06	0.02	0.05	0.03	0.10
500°C	1	2.07	4.19	6.60	8.76	10.54	12.24
	2	2.08	4.11	6.58	8.82	10.49	12.22
	3	2.08	4.17	6.55	8.72	10.43	12.22
	Avg	2.08	4.16	6.58	8.77	10.49	12.23
	SD	0.01	0.04	0.03	0.05	0.06	0.01

4. Hydrogen flow rate of palladium membrane with ZrN 0.5 µm thick

Temp (°C)	ZrN 0.5µm	Flow rate (mL/min) at different pressure (atm)					
		0.5	1.0	1.5	2.0	2.5	3.0
350°C	1	0.55	1.74	3.13	4.29	6.91	0.55
	2	0.53	1.71	3.13	4.29	6.91	0.53
	3	0.46	1.72	3.13	4.29	6.91	0.46
	Avg	0.51	1.72	3.13	4.29	6.91	0.51
	SD	0.05	0.01	0.00	0.00	0.00	0.00
400°C	1	1.11	2.39	3.86	5.12	6.58	7.94
	2	1.14	2.42	3.87	5.00	6.51	8.13
	3	1.16	2.51	3.80	5.16	6.62	8.42
	Avg	1.14	2.44	3.84	5.10	6.57	8.16
	SD	0.03	0.06	0.04	0.08	0.06	0.24
450°C	1	1.65	3.48	5.23	6.74	8.45	10.00
	2	1.61	3.46	5.33	6.76	8.38	10.05
	3	1.62	3.49	5.29	6.70	8.46	9.98
	Avg	1.63	3.48	5.29	6.73	8.43	10.01
	SD	0.02	0.01	0.05	0.03	0.04	0.03
500°C	1	1.67	3.63	5.33	6.74	7.97	10.17
	2	1.63	3.67	5.27	6.83	8.10	10.20
	3	1.66	3.60	5.24	6.79	7.94	10.79
	Avg	1.65	3.63	5.28	6.79	8.00	10.39
	SD	0.02	0.04	0.05	0.05	0.09	0.35

5. Hydrogen flow rate of palladium membrane without barrier

Temp (°C)	No barrier	Flow rate (mL/min) at different pressure (atm)					
		0.5	1.0	1.5	2.0	2.5	3.0
350°C	1	0.68	1.83	3.12	3.41	5.03	5.33
	2	0.69	1.84	3.09	3.59	5.06	5.32
	3	0.67	1.83	3.10	3.58	5.03	5.29
	Avg	0.68	1.84	3.10	3.52	5.04	5.31
	SD	0.01	0.01	0.02	0.10	0.02	0.02
400°C	1	1.00	2.57	3.59	5.05	6.15	7.30
	2	0.98	2.56	3.59	5.09	6.17	7.19
	3	0.95	2.52	3.60	5.03	6.04	7.19
	Avg	0.98	2.55	3.59	5.06	6.12	7.23
	SD	0.02	0.03	0.00	0.03	0.07	0.06
450°C	1	1.03	2.66	4.13	5.24	6.04	7.43
	2	1.01	2.68	4.17	5.24	6.23	7.42
	3	1.00	2.64	4.11	5.18	6.19	7.44
	Avg	1.02	2.66	4.14	5.22	6.15	7.43
	SD	0.01	0.02	0.03	0.04	0.10	0.01
500°C	1	1.33	2.89	4.14	5.24	6.28	7.83
	2	1.35	2.83	4.16	5.31	6.24	7.94
	3	1.33	2.86	4.08	5.26	6.23	8.03
	Avg	1.33	2.86	4.12	5.27	6.25	7.93
	SD	0.01	0.03	0.04	0.03	0.02	0.10

6. Hydrogen flux of palladium membrane with and without diffusion barrier

Barrier	Temp (°C)	* Flux (m^3/m^2h) at $P_{HP}^{1/2} - P_{LP}^{1/2}$					
		0.707	1	1.125	1.414	1.581	1.732
No barrier	350°C	0.33	0.92	1.56	1.77	2.53	2.67
	400°C	0.49	1.28	1.80	2.54	3.07	3.63
	450°C	0.51	1.33	2.07	2.62	3.09	3.73
	500°C	0.67	1.44	2.08	2.65	3.14	3.98
Zr 0.5 µm	350°C	0.25	0.50	1.45	2.10	2.77	3.37
	400°C	0.44	1.06	1.92	2.56	3.14	3.86
	450°C	0.47	1.18	2.05	2.63	3.24	4.21
	500°C	0.54	1.31	2.11	2.79	3.93	4.52
ZrO_2 0.5 µm	350°C	0.69	1.69	2.54	3.42	4.33	5.68
	400°C	0.78	1.79	2.68	3.69	4.78	5.84
	450°C	0.92	2.09	2.95	3.94	5.03	5.96
	500°C	1.04	2.09	3.30	4.40	5.27	6.14
ZrO_2 0.17 µm	350°C	0.59	1.38	2.13	3.03	3.80	4.45
	400°C	0.67	1.63	2.37	3.21	3.98	4.67
	450°C	0.73	1.68	2.52	3.38	4.18	5.09
	500°C	0.76	1.72	2.57	3.48	4.28	5.29
ZrN 0.5 µm	350°C	0.26	0.86	1.57	2.15	2.85	3.47
	400°C	0.57	1.22	1.93	2.56	3.30	4.09
	450°C	0.82	1.75	2.65	3.38	4.02	5.01
	500°C	0.83	1.82	2.65	3.41	4.23	5.21

* H_2 permeation flux (m^3/m^2h) = (flow rate of H_2 (mL/min)/active surface area) x 0.6

Active surface area = ¶R^2 (surface area of membrane disk) - ¶r^2 (surface area of graphite gaket)

= (3.14 *0.625 cm*0.625 cm) - (3.14*0.1 cm*0.1cm)

= 1.195

VITA

Miss Maslin Chotirach was born on August 30, 1984 in Songkhla, Thailand. She graduated with a Bachelor's degree of Science, Faculty of Science, Prince of Songkla University in 2007. She has continued her study in Master's degree, majoring in Petrochemistry and Polymer Science, Faculty of Science, Chulalongkorn University, Bangkok, Thailand since 2007 and finished her study in 2009.

Presentation at the 35th Congress on Science and Technology of Thailand (STT35) in the topic of "GROWTH AND CHARACTERIZATION OF ZIRCONIUM THIN FILMS AS INTERMETALLIC DIFFUSION BARRIERS FOR PALLADIUM MEMBRANES ON STAINLESS STEEL SUPPORTS"